The University of British Columbia

FACULTY OF GRADUATE STUDIES

PROGRAMME OF THE

FINAL ORAL EXAMINATION

FOR THE DEGREE OF

DOCTOR OF PHILOSOPHY

OF

RICHARD CARL CATTON

B.Sc., University of British Columbia

WEDNESDAY, AUGUST 30, at 3:30 P.M.

IN ROOM 225, CHEMISTRY BUILDING

COMMITTEE IN CHARGE

Chairman: I. McT. Cowan

J.W. Bichard

L.G. Harrison

W.C. Lin

R. Stewart

R.C. Thompson

External Examiner: J.E. Wertz
Department of Chemistry
University of Minnesota
Minneapolis, Minnesota

Research Supervisor: L.G. Harrison

ELECTRON SPIN RESONANCE STUDIES OF REACTION INTERMEDIATES IN METALLIC HALIDES

ABSTRACT

The object of this work was to produce and identify reaction intermediates in systems containing group I and group II halides treated with fluorine. The systems which are studies in detail are the NaCl and KCl/F_2 and $SrCl_2/F_2$ systems.

In accordance with predictions from kinetic studies, ESR has shown that treatment of vacuum-sublimed NaCl with F_2 at room temperature produces a defect containing an unpaired electron, and that the decay of this defect is retarded by Cl_2. The ESR spectrum indicates an anisotropic g-factor and unresolved hyperfine structure. In KCl a spectrum is obtained which is closely similar except that the hyperfine structure is partly resolved. The spectra appear consistent with interactions of the unpaired electron with Cl atoms, rather than with F or such impurities as O or Br, and can be accounted for adequately by a model of the defect as linear Cl_4^{3-}, i.e. an H-center or something very similar. For NaCl, the spectra indicate that the vacuum-sublimed material is sometimes partly oriented.

It is suggested that centers with one-electron deficiency are observable at such high temperatures in vacuum-sublimed material because this consists of essentially perfect crystals devoid of sites which

could accept a second electron from the centers.

The reaction of $SrCl_2$ powder or single crystal with fluorine at room temperature produces a defect, stable after removal of fluorine but located close to the reaction interface only, which has an electron spin resonance absorption. The ESR spectrum is consistent with a model of the defect as a chlorine atom desplaced from an anion site towards a neighbouring anion vacancy. The principal directions of the hyperfine tensor and g-tensor are two two-fold axes and a four-fold axis of the $SrCl_2$ lattice. The tensor components indicate that the unpaired electron is localized on the Cl atom, and suggest that the atom is subject to a strong crystal field determined chiefly by two nearest-neighbour cations which define a two-fold axis of the crystal. The unpaired electron is in an orbital mainly of p-character and aligned along a two-fold axis which is probably the one perpendicular to the line of the cations.

The single crystal spectrum, although having orientation-dependent line positions, has line shapes and intensities resembling those of a powder spectrum. This suggests a range of relative displacement of Cl atoms and neighbouring cations along a "reaction coordinate" which is probably a four-fold axis of the crystal.

GRADUATE STUDIES

Field of Study: Chemistry

Topics in Physical Chemistry	J.A.R. Coope W.C. Lin
Seminar in Chemistry	K.B. Harvey
Topics in Chemical Physics	C.A. McDowell W.C. Lin C.E. Brion
Chemical Thermodynamics	J.R. Sams
Topics in Inorganic Chemistry	W.R. Cullen R.C. Thompson N.L. Paddock H.C. Clark
Spectroscopy and Molecular Structures	K.B. Harvey A.V. Bree
Chemistry of the Solid State	L.G. Harrison
Topic in Organic Chemistry	F. McCapra L.D. Hall D.E. McGreer

PUBLICATIONS

L.G. Harrison, R.J. Adams and R.C. Catton, ESR Studies of a Reaction Intermediate in Vacuum-sublimed NaCl and KCl, J. Chem. Phys., 45, 4023 (1966).

R.C. Catton and L.G. Harrison, ESR Studies of a Reaction Intermediate in Strontium Chloride, J. Chem. Phys. (in press, should appear about November, 1967).

ELECTRON SPIN RESONANCE STUDIES

OF

REACTION INTERMEDIATES

IN

METALLIC HALIDES

by

RICHARD CARL CATTON, JR.
B.Sc., UNIVERSITY OF BRITISH COLUMBIA, 1964

A THESIS SUBMITTED IN PARTIAL FULFILLMENT OF
THE REQUIREMENTS FOR THE DEGREE OF
DOCTOR OF PHILOSOPHY
in the Department of
CHEMISTRY

We accept this thesis as conforming to the
required standard

THE UNIVERSITY OF BRITISH COLUMBIA
AUGUST, 1967

In presenting this thesis in partial fulfilment of the requirements for an advanced degree at the University of British Columbia, I agree that the Library shall make it freely available for reference and Study. I further agree that permission for extensive copying of this thesis for scholarly purposes may be granted by the Head of my Department or by his representatives. It is understood that copying or publication of this thesis for financial gain shall not be allowed without my written permission.

Department of Chemistry

The University of British Columbia
Vancouver 8, Canada

Date August 1, 1967.

ABSTRACT

The object of this work was to produce and identify reaction intermediates in systems containing group I and group II halides treated with fluorine. The systems which are studied in detail are the NaCl and KCl / F_2 and $SrCl_2$ / F_2 systems.

In accordance with predictions from kinetic studies, ESR has shown that treatment of vacuum-sublimed NaCl with F_2 at room temperature produces a defect containing an unpaired electron, and that the decay of this defect is retarded by Cl_2. The ESR spectrum indicates an anisotropic g-factor and unresolved hyperfine structure. In KCl, a spectrum is obtained which is closely similar except that the hyperfine structure is partly resolved. The spectra appear consistent with interactions of the unpaired electron with Cl atoms, rather than with F or such impurities as O or Br, and can be accounted for adequately by a model of the defect as linear Cl_4^{3-}, i.e., an H center or something very similar. For NaCl, the spectra indicate that the vacuum-sublimed material is sometimes partly oriented.

It is suggested that centers with one-electron deficiency are observable at such high temperatures in vacuum-sublimed material because this consists of essentially perfect crystals devoid of sites which could accept a second electron from the centers.

The reaction of $SrCl_2$ powder or single crystal with fluorine at room temperature produces a defect, stable after removal of fluorine but located close to the reaction interface only, which has an electron spin resonance absorption. The ESR spectrum is consistent with a model of the defect as a chlorine atom displaced from an anion site towards a neigh-

bouring anion vacancy. The principal directions of the hyperfine tensor and g-tensor are two two-fold axes and a four-fold axis of the $SrCl_2$ lattice. The tensor components indicate that the unpaired electron is localized on the Cl atom, and suggests that the atom is subject to a strong crystal field determind chiefly by two nearest-neighbour cations which define a two-fold axis of the crystal. The unpaired electron is in an orbital mainly of p-character and aligned along a two-fold axis which is probably the one perpendicular to the line of the cations.

The single-crystal spectrum, although having orientation-dependent line positions, has line shapes and intensities resembling those of a powder spectrum. This suggests a range of relative displacement of Cl atoms and neighbouring cations along a "reaction co-ordinate" which is probably a four-fold axis of the crystal.

TABLE OF CONTENTS

LIST OF FIGURES

Page

LIST OF TABLES

ACKNOWLEDGEMENTS

I would like to express my sincerest thanks to my research director, Dr. L. G. Harrison, for his invaluable advice, guidance, and enlightening discussions throughout the course of this work.

I would also like to thank Dr. C. A. McDowell for the use of his ESR facilities; the departmental shops - especially Mr. S. Rak, the glass blower, and Mr. L. de Fehr, the illustrator; Mr. C. R. Byfleet for his informative discussions; Mr. A. Fowler and Mr. R. Wolfe for their assistance in writing programmes; and finally to the National Research Council for my studentships.

INTRODUCTION

A. Kinetics and Mechanisms of Reactions of Alkali Halides

Reaction mechanisms in solids, like those in the much more widely studied fluid phases, are likely to involve intermediates with unpaired electrons. Such free radicals have not dominated the field of solid state kinetics as they have that of gas phase kinetics because transport and nucleation, which are specific to the solid phase, have required prior attention. Nevertheless, such defects have been discussed in a number of studies (1-5), although the analogy to gas-phase mechanisms is commonly obscured by the conventional use of the terms "trapped electron" and "trapped hole", rather than "free radical", in the solid phase.

a) Room temperature NaCl / Cl_2 exchange reactions

Alkali halides were chosen for mechanistic studies of exchange reactions (in Dr. J.A. Morrison's laboratory at N.R.C. Ottawa and later in Dr. L.G. Harrison's laboratory here) since more is known about the structures of their ionic and electronic defects than is the case for any other class of solids. Thus there is some hope of obtaining precise information on the role of these defects in reaction mechanisms.

The first sodium chloride particles used in the study of the exchange reaction, $NaCl^{36}$/ Cl_2, were made by evaporating sodium chloride in dry nitrogen at atmospheric pressure (6). The experiments (7) showed that there was a rapid surface exchange at room temperature (like that found in oxygen-metallic oxide systems (8)), followed by a slower extension of the process into the bulk (which has been followed for a period of days). This indicated (9) that structural irregularities must be present at least in the surface layer itself and possibly over a larger region. In order to avoid surface disordering by adsorption of atmospheric gases

sodium chloride particles were later made by evaporation in vacuo (10^{-7} to 10^{-8} mm Hg). It was expected that the avoidance of surface contamination by vacuum evaporation would greatly reduce the rate of the exchange or even suppress it altogether. However, the exchange (10) was found to be much more rapid than in previous experiments and to involve the bulk of the solid in a process not kinetically seperable from surface exchange. Harrison, Hoodless, and Morrison (10) found that the rate of exchange obeys a power law of the form $C = \alpha t^n$ in which α is independent of specific surface. They postulated that the unusual rate law probably indicates the reaction is self-inhibited by the blocking of vacancies by chlorine atoms or molecules taken up from the gas phase. The defect structures thus formed should be similar to some of the trapped-hole defects which have been studied in X-irradiated alkali halides, known as V-centers, although other letters are used for some of them.

Harrison (11) devised a tentative mechanism of this type. The mechanism was very speculative since it was based on limited experimental evidence and since it is known to be difficult to produce V-centers in alkali chlorides by additive coloration (12).

Adams and Harrison (13), again using vacuum-sublimed sodium chloride, confirmed the t^n rate law and the lack of dependence of the rate of exchange on specific surface. They attempted to elucidate the role of defects in the reaction mechanism from the pressure and temperature dependence of the exchange rate, and from the exchange kinetics of sodium chloride samples into which electronic defects had been deliberately introduced by X-irradiation and fluorination. The kinetics of exchange were completely changed from a power law to a second order rate law of

the form:

$$[\ 1/(\ C_\infty - C\ ]\ -\ [\ 1/C_\infty] = K_o t$$

In the light of this more extensive evidence, mechanisms involving electronic defects were postulated to account for both observed rate laws. In both cases, the proposed kinetic schemes involved a "molecular" trapped hole defect and an "atomic" trapped defect. It was proposed that pretreatment, with fluorine or X-irradiation, produces an "atomic"defect (a single trapped hole, probably asociated with vacancies and hence mobile) which decays bimolecularly, rapidly in vacuo and more slowly after introducing chlorine. To explain the probable composition of the defect and its decay by the desorption of chlorine in terms of a chemical equation, Harrison's (14) chemical notation for V-centers was used. In this notation, the customary ion sign is omitted for an ion on its proper site. If these signs are replaced by suffixes (a) and (c) for anion and cation sites respectively, the V-centers acquire superscripts which represent the number of trapped positive holes. The untrapped hole is designated $X(a)^+$; X(a) is the halide ion; a^+ is an anion vacancy, c^- a cation vacancy, and ac a vacancy pair.

The postulated second order decay of the "atomic" defect can now be written (13):

$$2Cl(a)^+(ac_2)^- \longrightarrow Cl_2(g) + 4ac$$

It was proposed that the decay of the defects is retarded in the presence of chlorine by a reversible absorption of chlorine molecules which

also serves as a step in the exchange:

$$2Cl(a)^{+}(ac_2)^{-} + Cl_2(g) \rightleftharpoons [\ Cl(a)_2^{++}(c_2)^{--}\ ]_2$$

Harrison suggested that the possible presence of "atomic" defects merits further study by electron spin resonance (13).

Following these proposals, Adams and Catton using vacuum sublimed sodium chloride, treated with fluorine in situ in an electron spin resonance spectrometer, detected unpaired spins. A peak at $g = 2.017 \pm 0.005$ was found but was not intense enough for any weaker hyperfine lines to be visible. The peak grew after the fluorine was removed, reached a maximum, and then decayed rapidly. When chlorine was introduced the decay slowed down and a reasonable second-order plot was indicated in agreement with Harrison's prediction (13).

(This work, which was eventually published, together with the later studies reported in this thesis, under the names of Harrison, Adams and Catton (15), is given here as introductory material because it was principally the work of Adams as a brief postdoctoral project. The present author assisted in the experiments but was not yet registered as a graduate student.)

b) Room temperature oxidation by chlorine and fluorine

If a solid alkali halide is exposed to a more electronegative halogen, one expects that electrons will be removed from the anion band to leave positive holes. These positive holes may be trapped in various ways: (i) by electrostatic attraction to point imperfections (e.g. cation vacancies in the bulk); (ii) by covalent bond formation in a small group of halogen atoms to form trapped hole centers which can usually be detec-

ted by U.V. spectroscopy (e.g. V-centers or H-centers); (iii) at growing halogen nuclei, leading to completion of the simple halogen displacement reaction. The following discussion will deal mainly with oxidation reactions which produce V-centers as a product.

Spectroscopic work, using single crystals of alkali halides, on the systems KI/Cl_2 (16), $NaCl/F_2$ (17), and KBr/Cl_2 (18) in all cases gave U.V. absorption bands which appeared to correspond to known bands produced in the same alkali halides by X-irradiation or treatment with the parent halogen.

In the case of the $NaCl/F_2$ reaction (Adams (17)), polished crystals gave a large V band at 2150 Å, which indicates a V_3 center, supposed by Seitz to contain one trapped hole, (and which therfore should have an unpaired electron) and very little chlorine was produced. For a similar crystal with a scratch across it the reaction took place to a greater extent with the formation of a lot of chlorine (both in the gas phase and trapped in the crystal) and a small V band at 2270 Å, indicating a V_2 center which Seitz postulated to contain two trapped holes. In the polished crystal, the growth of the V_3 center followed a sigmoid rate curve and the accelerating region of the sigmoid curve was usually parabolic (16).

The KBr/Cl_2 reaction, studied by Catton (18), was analogous to the latter type of behaviour observed in the $NaCl/F_2$ system. The production of V-centers in this system occured only after nucleation had taken place. The V-band observed at 2700 Å was suggested as representing a "molecular center". This band was comparable with the known (19,20,21) V_2 band observed in U.V. studies of KBr doped with Br_2 at high tempera-

tures.

The KI/Cl_2 system studied by Bird (16) produced little I_2; the principal products were V-centers which were regarded as various forms of molecular or atomic iodine dissolved in the lattice. The absorption peaks were at 2800 Å, which was believed to be an "atomic" center, and at 3600 Å, ascribed to a "molecular" center. These two peaks were also observed by Mollwo (19), and Hersh (20) in KI doped with I_2. The 2800 Å band was associated by Seitz with his V_3 model and the 3600 Å band with his model of a V_2 center (22). Hersh, however, suggested (20) that both peaks may arise from I_3^- (a linear triatomic molecule-ion) which is in disagreement with Bird who said they arise from different centers (23). It should be noted that an electrically neutral structure of I_3^- would contain two cation vacancies and, except for the covalent bonds of I_3^-, would correspond to Seitz's model of a "V_2 center" (24).

Baijal (24), doing electrical conductivity work on pressed pellets of KI during reaction with chlorine, found that after an initial increase in conductance two types of reactions were observed.

For initially low resistance pellets (high initial cation vacancy concentration), a mechanism involving the trapping of positive holes at isolated cation vacancies was postulated. After the initial rise of conductivity (due to an excess of cation caused by the formation of $I(a)_2^{2+}(c)^-$), there is a decay of the conductivity which is either first or second order. The first order decay was explained by the recombination of vacancies with the grain boundaries or dislocations yielding iodine. The second order decay, which occurs in unusually low resistance pellets, was explained by the joining together of the two defects of eq-

ual concentration. Baijal also found that with high resistance pellets

$$2I(a)^{+} + 2(c)^{-} \longrightarrow I(a)_2^{++}(c)_2^{--}$$

or

$$I(a)_2^{++}(c)^{-} + c^{-} \longrightarrow I(a)_2^{++}(c)_2^{--}$$

(rarely the case) sigmoid rate curves were obtained. These curves were explained in terms of the formation and growth of nuclei of the reaction products. Sigmoid rate curves of this type were also found by Morrison (25) for the KBr/Cl_2 system.

c) Production of colour centers by irradiation at low temperatures, and subsequent interactions

F-centers and V-centers are produced simultaneously in the same crystal by irradiation (26). This is the chief way of producing V-centers in alkali halides at low temperatures (most commonly liquid N_2 temperature). The type of mechanism involved in the production of these centers was first envisaged (27) as follows.

Initially in ionic crystals there are anion and cation vacancies. When these crystals are irradiated, there is excitation across the band gap and electrons are moved from the valence band to the conduction band leaving holes in the valence band. The processes which may then occur are that electrons from the conduction band may be trapped at anion vacancies forming F-centers, while positive holes in the valence band may be trapped at cation vacancies forming V-centers.

Such a mechanism is an oversimplification. It has been recognized that the concentrations of colour centers formed are usually greatly in excess of the initial vacancy concentrations. Thus in the formation of F-centers there must be a vacancy-creating step. For the trap-

ped-hole centers, structural studies in the last twelve years have shown that the trapping process may often involve covalent bonding without requiring the assistance of a vacancy.

The following account is not intended to be a comprehensive survey of the extensive literature on formation and destruction of colour centers, but rather to focus attention on a few aspects relevant to the present work.

A great deal of work has been done on the bleaching properties of the colour centers (28,29,30,31) but much less on the kinetics of their chemical interactions. It was shown (31,32,33) that at room temperature in KBr, KCl, and NaCl, of the known V-bands, the V_2 and the V_3 bands only were observed and that they have different bleaching characteristics (32).

The work done by Känzig (34,35,36), Wilkins (37), Cohen (38) and others on electron deficient or trapped hole defects, produced at low temperatures by irradiation, has mainly dealt with the structural determination of these centers but not with the kinetics or mechanisms of their chemical interactions.

Some general trends of reactivity have been published by Känzig (39) on the production of F, V_K and H centers at 20.3°K in KCl by irradiation. Känzig found that:

i) The F-center and V-center concentration grow rapidly at first which was attributed to the trapping of electrons at already existing traps (halide vacancies) while holes are "self-trapped" (by covalent bond formation to form Cl_2^-, the V_K center). When the electron traps are full the rate of growth then becomes smaller for it now depends on the

defects produced by X-irradiation.

ii) The H-centers grow slowly at the begining and faster as radiation damage proceeds which shows that they are not dependent on already existing traps.

Since the three centers were observed simultaneously at 20.3° K a mechanism for their production was proposed which agreed with their appearance and disappearance at various temperatures. The proposed mechanism (39) is like that of Varley (40) and was explained as follows.

An halide ion is multiply ionized by the X-irradiation and hence takes on a positive charge. This positive charge moves freely in the crystal but finally becomes neutralized and settles in an interstitial position forming an H-center. The electron remaining is trapped at the halide vacancy forming an F-center. In terms of a chemical equation using Harrison's (14) notation (see section A(a)).

$$X(a) \xrightarrow{\text{irradiation}} X^{n+} + (n+1)e^- + a^+$$

$$X^{n+} + ne^- + X(a) \longrightarrow X_2(a) \text{ (H-center)}$$

$$e^- + a^+ \longrightarrow a \text{ (F-center)}$$

The overall reaction is

$$\underset{\text{(anions on lattice sites)}}{2X(a)} \longrightarrow \underset{\text{(H-center)}}{X_2(a)} + \underset{\text{(F-center)}}{a}$$

with X^{n+} and conduction e^- as mobile intermediates. (Note that for an interstitial species like X^{n+}, just as for a gas-phase species, effective charge and ordinary ionic charge are identical; but because they are different in the crystal, (n+1) electrons are produced with X^{n+}. The

symbol a^+ necessitates $(n+1)e^-$ for charge-conservation. Thus there is no difficulty in using interstitials or gas molecules in Harrison's notation.) Another possible mechanism assumes that interstitial ions are already present. These become unstable at higher temperatures (about 42°K) and release electrons forming H-centers. The released electron was explained away by having it annihilate a V_K center. Annealing experiments support this mechanism only in KCl and NaCl. This is expected since the interstitial halide ions would be less stable in bromides and iodides because of their relatively large size. The chemical equations of this mechanism are:

$$X^- \text{ (interstitial)} \longrightarrow X + e^-$$

$$X + X(a) \longrightarrow X_2(a) \quad \text{(H-center)}$$

$$e^- + X(a)_2^+ \longrightarrow 2X(a) \text{ (anions on lattice sites)}$$

$$(V_K \text{ center})$$

The equation showing the production of the V_K center would be

$$X(a) \xrightarrow{\text{irradiation}} X(a)^+ + e^-$$

$$X(a)^+ + X(a) \longrightarrow X(a)_2^+$$

Experiments (41,42) have shown that the optical H band and the optical V_1 band are closely related. Thermal bleaching of the H band is connected with the growth of the V_1 band. Teegarden and Maurer (41) discovered that the optical H band can be generated in a KCl crystal containing V_1 centers by light absorbed in the V_1 band at 35°K. Känzig (39) found that H centers could also be produced by this method. Experiments

in KCl and KBr indicated that the H center on warming is transformed into a non-paramagnetic center which is presumably a V_1 center since through optical-excitation in the V_1 band it can be changed back into the H center at 20°K. The proposed mechanism envisages the V_1 center as a halogen molecule in a single anion site:

$$X_2(a) \longrightarrow e^- + X_2(a)^+ \quad (V_1 \text{ center})$$

$$e^- + \underset{(F \text{ center})}{a} \longrightarrow \underset{(F' \text{ center})}{a^-}$$

The H center releases an electron to form a X_2 molecule, the e^- is trapped nearby an F center to form an F' center which is neutral. On excitation with V_1 light the H center was reproduced; but the F center concentration did not increase.

More recently (1960) Känzig (43) found in studying low temperature (77°K) irradiated LiF that four main trapped hole centers were produced (the V_K, H, V_F, and V_t centers; see figure 1). The V_K center is a self-trapped hole (F_2^-) localized on two fluoride ions; the H center is chemically equivalent to an interstitial F atom; the V_F center is a hole trapped at a Li vacancy but the hole is localized on two fluoride ions so that the F_2^- molecule-ion has a bent bond; and the V_t center is a hole localized on three fluoride ions which form an isosceles triangle (F_3^{2-}).

Seitz proposed that the optical absorption band V_1 in NaCl, KCl and KBr might be due to a hole trapped at an alkali vacancy (44). The V_F center is a center of this type but its optical absorption band has not been identified. Känzig (39) pictures the V_1 center in KCl and KBr

as a non-paramagnetic center such as a X_2 molecule in a negative-ion vacancy (unless the absorption band of the center postulated as X_2 overlaps the V_1 band and is obscurred by it). The model of the V_t center (45) corresponds in a general way to Seitz's (26) model of the center that gives rise to the optical V_4 band in KCl and KBr but none of the absorption bands in X-irradiated LiF have been established to be the analogue of the V_4 band in KCl and KBr. Kingsley (46) studying the bleaching and symmetry properties of the V_4 center in X-irradiated KBr came to the conclusion that the V_4 center is a single hole trapped at a single alkali vacancy. He concluded that the V_4 center may be the antimorph of the F center whose paramagnetic resonance Känzig found in LiF (47). Therefore the Seitz's model for the V_1 center and Kingsley's model for the V_4 center are the same but the centers have different optical absorption bands so they cannot be the same center.

An investigation (47) was made of the generation and decay of the V_K, H, V_t and V_F centers found in irradiated LiF at 77°K as a function of the annealing temperature (see figure 2). The annealing experiments showed:

i) from 95-100°K the H centers are the most unstable and in decaying they emit electrons which annihilate V_K centers causing their concentration to drop.

$$F_2(a) \longrightarrow e + F(a)_2$$
$$e + F(a)_2^+ \longrightarrow 2F(a)$$

ii) from 110-130°K, neglecting V_K centers destroyed by H cen-

Figure 1 - Trapped hole centers

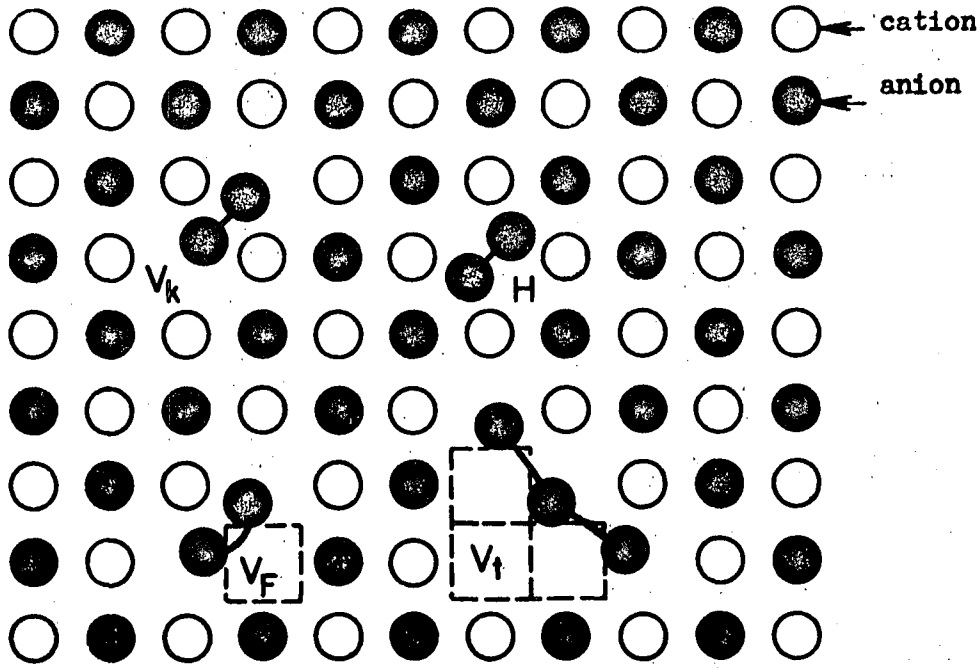

Figure 2 - Conc. of V-centers in LiF vs annealing temperature

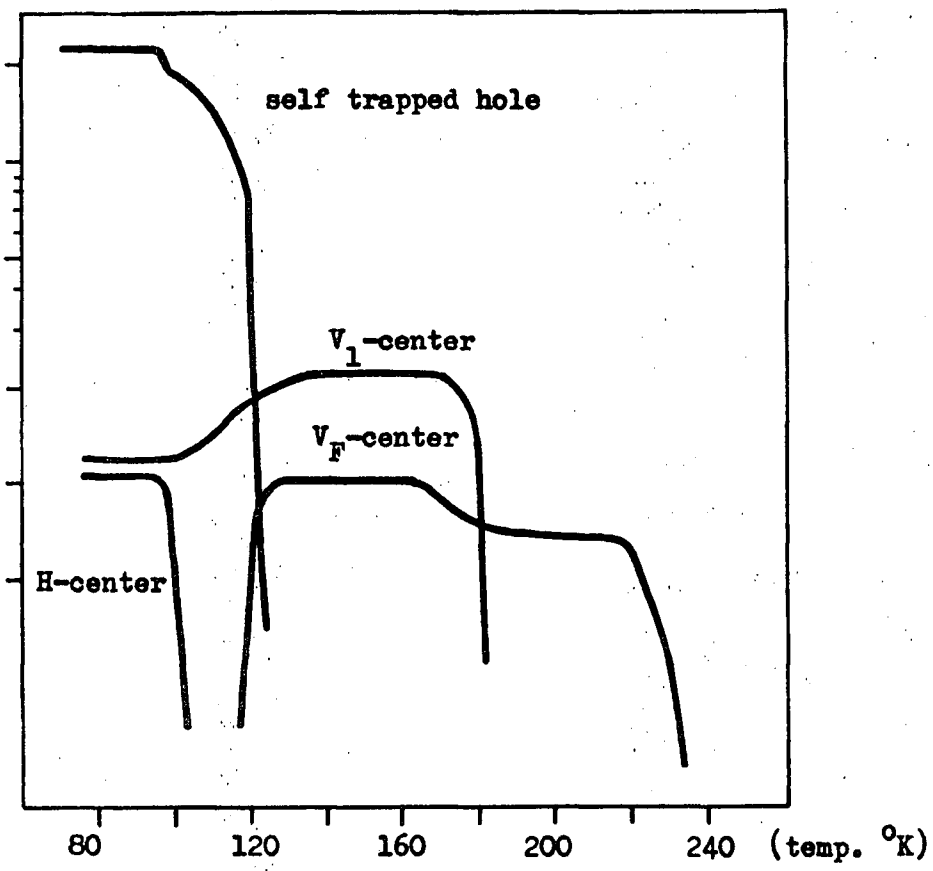

ters decaying, the decay of V_K centers is second order. This decay is associated with the increase of V_t and V_F centers which suggests that some of the migrating holes are trapped at vacancy aggregates and at Li vacancies.

iii) from 175-185°K the V_t and V_F centers decay together for a time which suggests that the V_t centers release holes which recombine with trapped electrons or transform F_2^- molecule-ions of V_F centers into F_2 molecules.

d) Summary of electron-deficient colour centers in alkali halides relevant to the present work

The objective of the present work is to use electron spin resonance as a means of obtaining information on colour centers acting as reaction intermediates. Hence the following table is intended primarily to summarize the situations in which unpaired electrons have been detected (by ESR)or postulated (on the basis of kinetic evidence). There are some unresolved conflicts, in which unpaired electrons are postulated but have not been observed by ESR. These are noted in the table. In general, it should be noted that no structure is yet definitely established for any of the V centers with the numerical subscripts (V_1, V_2, V_3, V_4) which produce the strongest U.V. absorptions in X-irradiated alkali halides, and that no ESR signal has been detected for any of these centers, although structures including unpaired electrons have been postulated for some of them on the basis of less direct evidence.

Table I

Sample	Method of production of defects	Electron-deficient centers detected by U.V. spectroscopy or postulated from indirect evidence	Centers detected or postulated as having unpaired electrons
NaCl crystal KCl crystal KBr crystal	irradiated (low temp)	V_1, V_2, V_3, V_4, V_K, H	V_K, H (structures determind by ESR)
LiF crystal	irradiated (low temp)	V_K, H	V_K, V_F, V_t, H (structures determined by ESR)
NaCl crystal	F_2 oxidation	V_2, V_3	V_3 according to Seitz's model; but no ESR absorption is known correlated with the V_3 optical absorption
KI crystal	Cl_2 oxidation	V_2, V_3	Assignments of structures very uncertain
KI powder	Cl_2 oxidation	$I(a)_2^{2+}(c)^-$ and $I(a)_2^{2+}(c_2)^{2-}$ postulated to explain observations on conductivity	None
KBr crystal	Cl_2	V_2	Assignments of structures very uncertain
NaCl vacuum KCl sublimed particles	F_2 oxidation	$Cl(a)^+(ac_2)^-$ and $Cl(a)_2^{2+}(c_2)^{2-}$ postulated to account for kinetic results; the former is Seitz's V_3 model	Seitz's V_3 model postulated; detected H-center (by ESR; this thesis)

B. Basic Theory of Electron Spin Resonance

a) Resonance condition

An unpaired electron in a paramagnetic species can exist in two spin states, $m_s = \pm 1/2$, which form a doubly degenerate state since they have the same energy. When the species is put into a magnetic field the degeneracy is lifted (i.e. the two states have different energies) and interaction with electromagnetic radiation of energy $h\nu$ equal to the gap between the two levels causes both absorption ($|-1/2\rangle \rightarrow |+1/2\rangle$) and emission ($|+1/2\rangle \rightarrow |-1/2\rangle$) to occur at the same time. Since an excess of the molecules are in the lower energy state ($|-1/2\rangle$) the net result is absorption.

The potential energy of a magnetic dipole (of the electron) with a magnetic moment $\underline{\mu}$ in a magnetic field H is expressed as:

$$E = -\underline{\mu} \cdot \underline{H} \quad \text{(where } \underline{\mu} \text{ and } \underline{H} \text{ are vectors)}$$

with the direction of the magnetic field H taken to be along the z axis the expression becomes

$$E = -\mu_z H_z$$

The spin operator in the magnetic field can therefore be expressed as

$$\mathcal{H}_s = -\hat{\underline{\mu}} \cdot \underline{H}$$

but since the magnetic moment is proportional to the spin quantum number one can write

$$\underline{\mu} = (\text{constant})\ \underline{S}$$

$= \gamma h \underline{S}$ (where γ is the gyromagnetic ratio)

$= g \beta_o \underline{S}$

Therefore

$$\mathcal{H}_s = +g \beta_o \hat{\underline{S}} \cdot \underline{H}$$

where g is the spectroscopic splitting factor, β_o is the Bohr magnetron ($= e\hbar / 2mc$), $\hat{\underline{S}}$ is the spin operator and H is the magnetic field. The eigen values giving the energy levels for this system can be expressed as

$$E = g\beta_o H_z \, m_s$$

where m_s is the electron spin quantum number. The transitions between pairs of these energy levels are allowed only if they obey the selection rule $\Delta m_s = \pm 1$ and the resonance condition which has to be satisfied for these transitions is

$$h\nu = g\beta_o H_z$$

where ν is the Larmor frequency.

It was assumed above for simplicity the g-factor is isotropic but this is not generally the case in solids as we will see later in section B(c).

b) Hyperfine interaction

There can also be further interactions between the electron spin and internal magnetic fields, particularly those due to the magnetism of nuclei in the same molecule. These magnetic interactions between electron spins and nuclear spins are known as hyperfine interactions because they are responsible for the very small splittings known as hyper-

fine structure in atomic spectroscopy. In ESR spectra, these interactions sometimes produce very large splittings but they are still known as hyperfine structure.

The spin angular momentum of a nucleus is described by a quantum number, I, and its magnetic moment, μ_N, is given by the expression $\mu_N = g_N \beta_N \underline{I}$ where g_N is the nuclear g-factor and β_N is the nuclear magneton ($= e\hbar/2mc$) where m is the mass of the proton.

Now if a nucleus with a magnetic moment, μ_N, interacts with an electronic magnetic moment, μ, the interaction energy can be expressed quantitatively as (48)

$$E_N = \alpha \mu \mu_N r^{-3} = A \underline{S} \cdot \underline{I}$$

where α is a constant depending on the ground state wave function, r is the radius of the electron orbit and A is the hyperfine interaction tensor which will be assumed isotropic for simplicity (see section B(c)).

In a magnetic field the spins are uncoupled and hence the nuclear spin angular momentum is quantized separately from the spin angular momentum. The spin hamiltonian is given as

$$\mathcal{H}_s = g\beta_o H S_z + A \underline{S} \cdot \underline{I}$$

The energy levels arising from this hamiltonian canbe expressed as

$$E(m_s\ m_I) = g\beta_o H m_s + A m_s m_I$$

The selection rules governing the allowed electron magnetic dipole transitions are given by $\Delta m_s = \pm 1$ and $\Delta m_I = 0$. These transitions take place

at the following frequencies

$$h\nu = g\beta_o H + A\, m_I$$

where m_I can have the values I, I-1, ... -I. The magnetic field at resonance is

$$H = [h\nu/g\beta_o] - [A/g\beta_o]m_I$$

The hyperfine term causes splitting of each electronic level into 2I+1 components which results in 2I+1 hyperfine lines with the spacing between each line (for constant ν) equal to $A/g\beta_o$ gauss.

Nuclear electric quadrupole interactions can break down the selection rule $\Delta m_I = \pm 0$, leading to the appearance of extra lines in the spectrum, for $\Delta m_I = \pm 1$ or $\Delta m_I = \pm 2$. This effect is a possibility for Cl nuclei, which have a quadrupole moment, and extra lines have been observed in the ESR spectrum of ClO_2 (49); but since such lines would not be resolvable in our spectra, and since they need not be observed for a complete structure determination, I do not discuss quadrupole effects in this thesis.

c) Anisotropy

In the previous two sections dealing with the zeeman splitting and hyperfine splitting, the g-factor and A, the hyperfine coupling constant, were assumed to be isotropic; but this is not generally the case, especially in solids.

A and g are usually to some extent anisotropic and can be represented by symmetric second-rank tensors which can be diagonalized

by a suitable choice of co-ordinate system x, y, z to give three principal components g_x, g_y, g_z and A_x, A_y, A_z. The principal axes of $\underline{g}$ and $\underline{A}$ usually, though not necessarily, coincide. If H has direction cosines ℓ, m, n to the principal axes x, y, z then for this orientation (50)

$$g = (\ell^2 g_x^2 + m^2 g_y^2 + n^2 g_z^2)^{1/2}$$

and

$$A = (\ell^2 A_x^2 + m^2 A_y^2 + n^2 A_z^2)^{1/2}$$

A common case is that of axial symmetry in which if the axis of symmetry is the z axis

$$g_z = g_{||} \qquad g_x = g_y = g_\perp$$

$$A_z = A_{||} \qquad A_x = A_y = A_\perp$$

and if θ is the angle between the axis of symmetry and the magnetic field, H, then the hyperfine coupling constant and the g-factor can be expressed as a function of θ (51).

$$g = [\, g_{||}^2 + (\, g_\perp^2 - g_{||}^2 \,) \sin^2\theta \,]^{1/2}$$

and

$$A = [\, A_{||}^2 + (\, A_\perp^2 - A_{||}^2 \,) \sin^2\theta \,]^{1/2}$$

d) ESR spectum of an unpaired electron interacting with several nuclei in a solid medium

i) Structure of the ESR spectrum

The hyperfine coupling constant and the g-factor are usually to some extent anisotropic as stated in section B(c). The hamiltonian for the zeeman splitting is expressed as (52)

$$\mathcal{H}_z = \beta_o(\underline{S} \cdot \underline{\underline{g}} \cdot \underline{H}) = \beta_o(g_x S_x H_x + g_y S_y H_y + g_z S_z H_z) \quad ..(1)$$

where S_x, S_y, S_z are the spin angular momentum operators along the three axes; H_x, H_y, H_z are the components of the external magnetic field; and g_x, g_y, g_z are the spectroscopic splitting factors along the three axes.

The spin hamiltonian which is used in first order pertubation theory to describe the hyperfine interaction in a system of more than one nuclei can be written as (53)

$$\mathcal{H}_{hyperfine} = g_o\beta_o \sum_i (I_x^i A_x^i S_x + I_y^i A_y^i S_y + I_z^i A_z^i S_z) \quad ..(2)$$

where g_o is the spectroscopic splitting factor of the free electron and g when it is used is that of the species for that particular orientation of the magnetic field, β_o is a Bohr magnetron, S is the spin operator of the electron and I^i that of the nucleus i and A^i's are the hyperfine coupling tensors in gauss.

Combining equation 1 and 2 into a more compact form the total spin hamiltonian of the system can be written:

$$\mathcal{H} = \beta_o \underline{S} \cdot \underline{\underline{g}} \cdot \underline{H} + g_o\beta_o \sum_i \underline{S} \cdot \underline{\underline{A}}^i \cdot \underline{I}^i \quad ..(3)$$

Now if the direction of the magnetic field H is taken to be along the z axis then

$$\mathcal{H} = g\beta_o S_z H_z + g_o\beta_o \sum_i \underline{S}_z \cdot \underline{\underline{A}}^i \cdot \underline{I}^i \quad ..(4)$$

The energy for a given spin state

$$E[m_s m_{I_1} m_{I_2} \cdots] = \langle m_s m_{I_1} m_{I_2} \cdots | \mathcal{H} | m_s m_{I_1} m_{I_2} \cdots \rangle$$

where m_s is the spin quantum number of electrons and m_{I_i} is the nuclear magnetic quantum number $(I_i \ldots\ldots, -I_i)$ of nucleus i, is generally written for a first-order approximation as:

$$E = [\, g\beta_o H_z + g_o\beta_o \sum_i A^i (m_I)_i \,] m_s \qquad ..(5)$$

With the selection rule for transition $\Delta m_s = \pm 1$ and $(\Delta m_I)_i = 0$ the resonance condition is given by

$$h\nu = g\beta_o H_z + g_o\beta_o \sum_i A^i (m_I)_i \qquad ..(6)$$

The field for any particular orientation is given by

$$H_z = (h\nu/g_o\beta_o) - (g_o/g) \sum_i A^i (m_I)_i \qquad ..(7)$$

and the hyperfine splitting by

$$H_z - H_o = -(g_o/g) \sum_i A^i (m_I)_i \qquad ..(8)$$

ii) Relationship of components of g and A tensors to the state of the unpaired electron

In the centers being studied the state of the unpaired electron can be described as a linear combination of hydrogen-like s and p state functions, therefore the following discussion will only include these state functions.

The hyperfine interaction consists of two parts (54) which are: an isotropic part which depends only on the non vanishing component of the wave function at the nucleus; and an anisotropic part which depends only on the non spherically symmetric components distant from the

nucleus. Therefore if the electronic wave functions are expanded in terms of atomic functions only s components contribute to the isotropic interaction and non s components to the anisotropic interaction.

Many different terminologies have been used in relating hyperfine interaction to fractional s and p character. The letters A, B, a and b are used by different authors for different quantities. In this account, I attempt to avoid this confusion by introducing symbols $\mathcal{S}$ and $\mathcal{P}$ as defined below.

The isotropic terms, or the Fermi-contact hyperfine splitting is proportionalto the electron density at the nucleus. The contact of the nucleus and the electron is not directional-dependent and hence this interaction is not a function of the angle between the crystal or molecular axis and the magnetic field (55).

The Fermi-contact term is expressed for an s state as (56)

$$\mathcal{S} = (8\pi/3)(\mu_I/I)\,\psi^2(0) \qquad ..(9)$$

where $\mathcal{S}$ is in gauss, μ and I are the magnetic moment and the spin of the nucleus respectively, and $\psi(0)$ is the amplitude of the s function at the nucleus.

The dipolar or anisotropic hyperfine interaction is the interaction due to the magnetic field at the electron caused by the presence of a nucleus near the electron but not right at the electron. This term averages out to zero in systems which have random tumbling of the species present. This term is very important in solids for it depends on the angles between the principal axes and the magnetic field. The dipolar

hamiltonian is (55)

$$\mathcal{H}_{dipolar} = -[g_o \beta_o g_N \beta_N / r^3](\underline{I} \cdot \underline{S} - 3(\underline{I} \cdot \underline{r})(\underline{S} \cdot \underline{r})/r^2) \quad ..(10)$$

where g_N = nuclear g-factor

g_o = g value of unbound electron

β_N = nuclear magneton

β_o = Bohr magneton

$\underline{r}$ = radius vector from nucleus to the electron

$\underline{I}$ = nuclear spin operator

$\underline{S}$ = electron spin operator

when $\mathcal{H}_{dipolar}$ is expanded out the first term is

$$\mathcal{H}_d \cong [(3\cos^2\theta - 1)/r^3]\, g_o g_N \beta\beta_N (I_z S_z) \quad ..(11)$$

which is generally used to compute the anisotropic (55) hyperfine tensors A_x', A_y', A_z'.

For a p_x state using equation 11

$$A_x' = \mu_I/I \int \psi^2 [(3\cos^2\theta - 1)/r^2]\, r^2 \sin\theta \, dr \, d\theta \, d\phi \quad ..(12)$$

$$= 4/5(\mu_I/I) \langle r^{-3} \rangle \quad ..(13)$$

where $\langle r^{-3} \rangle$ is an average value over the radial part of the p function, also

$$A_y' = A_z' = -2/5(\mu_I/I) \langle r^{-3} \rangle \quad ..(14)$$

Fof convenience I define a quantity

$$P = 2/5(\mu_I/I) \langle r^{-3} \rangle \quad ..(15)$$

Thus for a single p orbital, designated p_x,

$$A_x' = 2\mathcal{P}$$
$$A_y' = A_z' = -\mathcal{P}$$

For an electron whose state can be described as a linear combination of s and p states, two possible cases arise:

(1) axial symmetry, which can be described by a combination of s with a single p orbital (designated p_x). The components of the hyperfine tensor $\underline{A}$ are then $A_{||}$ (i.e. A_x) and $A_\perp$ (i.e. $A_z = A_y$). If α_i^2 is the amount of p character β_i^2 is the amount of s character in the ground state atomic wave functions centered on nuclei i, and if $\sum_i(\alpha_i^2 + \beta_i^2) = 1$ then the components of the hyperfine tensors would be (using equations 9, 13, 14, and 15)

$$A_{||} = \beta^2\mathcal{S} + 2\alpha^2\mathcal{P} \quad ..(16)$$
$$A_\perp = \beta^2\mathcal{S} - \alpha^2\mathcal{P} \quad ..(17)$$

(2) the three principal components all different (i.e. $A_x \neq A_y \neq A_z$). The description of this situation requires that there should be a spin density in an s state and two separate mutually perpendicular p states (eg. p_x and p_z) in the amounts β^2, α_x^2, and α_z^2 where $\beta^2+\alpha_x^2+\alpha_z^2 = 1$. This situation will only arise in a crystal field which lifts the degeneracy of p_x and p_z. (A combined state $c_1p_x + c_2p_z$ represents merely a p state identical to p_x or p_z but with a differently oriented principal axis. This is not the situation discussed here.) The components of the hyperfine tensor then become (using equations 9, 13, 14, and 15)

$$A_x = \beta^2\mathcal{S} + (2\alpha_x^2 - \alpha_z^2)\mathcal{P} \quad ..(18)$$

$$A_y = \beta^2 \mathcal{S} - (\alpha_x^2 + \alpha_z^2)\mathcal{P} \quad ..(19)$$

$$A_z = \beta^2 \mathcal{S} + (2\alpha_z^2 - \alpha_x^2)\mathcal{P} \quad ..(20)$$

Now if the experimental values for the hyperfine tensors are put into equation 16 to 20 they can be solved for the amount of s and p character in the bonds formed, provided that the numerical valus of the ratio $\mathcal{S}/\mathcal{P}$ is known.

(3) The above treatment suggests, as is usually assumed, that an anisotropic hyperfine tensor with $A_x' = -2A_y' = -2A_z'$ indicates spin density in p_x only. It has been pointed out by Tinkham (57) that this is not necessarily the case. Suppose that fractions α_x^2, α_y^2, α_z^2 of the unpaired electron are in p_x, p_y, and p_z. Then:-

$$A_x' = (2\alpha_x^2 - \alpha_y^2 - \alpha_z^2)\mathcal{P} \quad ..(21)$$

$$A_y' = (2\alpha_y^2 - \alpha_x^2 - \alpha_z^2)\mathcal{P} \quad ..(22)$$

$$A_z' = (2\alpha_z^2 - \alpha_x^2 - \alpha_y^2)\mathcal{P} \quad ..(23)$$

If we now represent axial symmetry by writing $\alpha_y^2 = \alpha_z^2$ and introducing the symbol $\delta^2 = \alpha_x^2 - \alpha_z^2$, the components of A' are functions of δ^2 only.

$$A_x' = [2\delta^2]\mathcal{P} \quad ..(24)$$

$$A_y' = [-\delta^2]\mathcal{P} \quad ..(25)$$

$$A_z' = [-\delta^2]\mathcal{P} \quad ..(26)$$

Thus when the anisotropic hyperfine tensor satisfies the condition $A_x' = -2A_y' = -2A_z'$, this means only that $\alpha_y^2 = \alpha_z^2$, not that both quantities are zero. The quantity obtainable from $\underline{A}'$ is not actually α_x^2 but $\delta^2 = \alpha_x^2 - \alpha_z^2$.

This in fact represents the minimum value of α_x^2 consistant with experimental results, since α_z^2 must be positive or zero. Thus the usual analysis given in the preceding section assuming that a hyperfine tensor axially symmetric about the x axis can be interpreted in terms of spin density in p_x only actually gives a minimum value for the p character of the state of the unpaired electron.

Similarly, for the case without axial symmetry, the quantities which can be determined from the components of $\underline{\underline{A}}'$ are the differences in spin density between the least-occupied p state and the other two. Assuming that the p_y is least occupied, we define the two quantities δ_x^2 and δ_z^2 by:-

$$\alpha_x^2 - \alpha_y^2 = \delta_x^2$$
$$\text{and} \qquad \alpha_z^2 - \alpha_y^2 = \delta_z^2 \qquad \ldots(27)$$

Then

$$A_x' = (2\delta_x^2 - \delta_z^2)\mathcal{P} \qquad \ldots(28)$$

$$A_y' = -(\delta_x^2 + \delta_z^2)\mathcal{P} \qquad \ldots(29)$$

$$A_y' = (2\delta_z^2 - \delta_x^2)\mathcal{P} \qquad \ldots(30)$$

The magnetic interactions involving the orbital angular momentum of the unpaired electron are the sole cause for the deviation of the g values from 2.0023 (the free electron value) (55). The part of the magnetic moment arising from the orbital motion of the electrons is modified by the chemical environment in an atom, molecule or crystal, there-

fore the g value likewise depends upon the chemical environment (48). In a solid, since the orbital part of the magnetic moment depends on the crystal field, its magnitude is usually different for different directions of H and shows an angular variation which follows the symmetry of the crystal field. The total g value (spin + orbit) may be anisotropic by an amount which depends on the magnitude of the orbital contribution to the moment and on the asymmetry in the crystal field.

The theory of the g-shifts is described in numerous books such as those written by Slichter (58), Pake (59), and Carrington and McLachlan (60). The following account follows mainly that of Carrington and McLachlan which gives the most precise definitions of the "ficticious spin" and the "anisotropic g-factor".

The g-shift which is observed in solids is related to the spin-orbit coupling which mixes the ground and excited states thereby introducing a small contribution of the otherwise quenched angular momentum to the electronic magnetic moment (58). The g-shift can be exemplified quantitatively by considering the case of an atom with one p electron which is described by the hamiltonian

$$\mathcal{H}_T = \mathcal{H}_1 + V_1 + \lambda \underline{L} \cdot \underline{S} + \beta_o \underline{H} \cdot \underline{\underline{g}} \cdot \hat{\underline{S}} \qquad ..(31)$$

where $\mathcal{H}_1$ contains the principal energy terms (the kinetic energy and free atom potential), V_1 is the potential due to the charge around the atom, $\lambda \underline{L} \cdot \underline{S}$ is the spin-orbit interaction and $\beta_o \underline{H} \cdot \underline{\underline{g}} \cdot \hat{\underline{S}}$ is the electronic zeeman interaction. In this expression, $\underline{\underline{g}}$ represents the experimental observation that the interaction of $\underline{H}$ with the electron spin is often apparently anisotropic. This could not be so if $\hat{\underline{S}}$ represented the

true spin $\underline{S}$ because the interaction of $\underline{S}$ with $\underline{H}$ is necessarily isotropic with the constant of proportionality g_o. The "fictitious spin" $\hat{\underline{S}}$ actually represents the true spin of $\underline{S}$ modified to allow for small residual effects of the orbital angular momentum, and the significance of $\hat{\underline{S}}$ is found by comparing the " effective spin hamiltonian" as written above with the true hamiltonian written in terms of $\underline{L}$, $\underline{S}$, and g_e. In the presence of a magnetic field $\underline{H}$ there will be an interaction between $\underline{H}$ and the orbital angular momentum $\underline{L}$ and therefore the "true hamiltonian" for the magnetic interaction is now written as

$$\mathcal{H} = \beta_o \underline{H} \cdot \underline{L} + g_o \beta_o \underline{H} \cdot \underline{S} \qquad ..(32)$$

where $\underline{S}$ is the true spin.

Let us now consider a potential V_1 of such a nature that it lifts the orbital degeneracy of the once degenerate p states of the atom. For example, a suitable potential would be provided by the following arrangement of charges around the atom X:

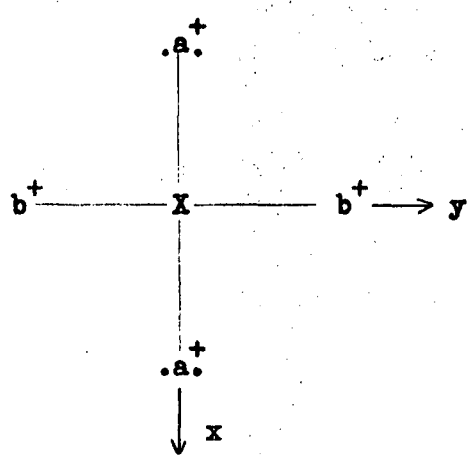

The resultant energy levels shown below are all two fold degenerate be-

cause of the electron spin.

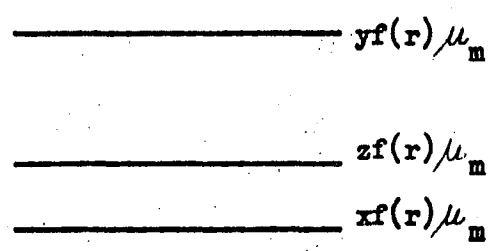

(the spacings are equal if a=b; see reference (58); two orbitals remain degenerate if b=0; the defect in $SrCl_2$ studied in this thesis corresponds to an intermediate case, b≠a). The wave function such as $xf(r)\mu_m$ contain an orbital function xf(r) and a spin function μ_m ($\mu_m = \alpha, \beta$).

Now looking at the effect of $\lambda \underline{L} \cdot \underline{S}$ on the p states it is found that the matrix elements of the form $\langle xf(r)| L_z |xf(r)\rangle$, representing the expectation value of L_z, vanish. This shows that the angular momentum is quenched and has no first order effects on the states. However, it is found in terms of pertubation theory that the spin-orbit coupling ($\lambda \underline{L} \cdot \underline{S}$) mixes very small proportions of various excited states into the ground state. The type of modified wave function ψ'_{xm} calculated by first order pertubation is

$$\psi'_x = xf(r) - \sum_{w=y,z} \left[\langle w | \lambda \underline{L} \cdot \underline{S} | x \rangle / E_w - E_m \right] wf(r) \qquad ..(33)$$

where ψ'_x is spin degenerate. The perturbed states are no longer eigenstates of the true spin $\underline{S}$.

In an external magnetic field $\beta \underline{H} \cdot \underline{g} \cdot \hat{\underline{S}}$ of equation 31 becomes

$$\mathcal{H} = \beta \underline{H} \cdot (g_x \hat{S}_x \underline{i} + g_y \hat{S}_y \underline{j} + g_z \hat{S}_z \underline{k}) \qquad ..(34)$$

For the hamiltonian $\mathcal{H}$ of equations 32 and 34 to mean anything the corresponding matrix elements of $\beta_e H(g_x \hat{S}_x + g_y \hat{S}_y + g_z \hat{S}_z)$ and those of $\beta_e H(L_x + L_y + L_z + g_e S_x + g_e S_y + g_e S_z)$ formed by these hamiltonians acting on the perturbed states must be identical. By equating these matrix elements the principal components of the g-tensor can be expressed in a generalized way using only first order terms in λ as

$$g_p = g_e - 2\lambda \sum_{p \neq q} \langle \psi_o | L_p | \psi_q \rangle \langle \psi_q | L_p | \psi_o \rangle / E_q - E_o \qquad ..(35)$$

The g-shifts obtained for an unpaired electron in a p_x orbital are therefore

$$\begin{aligned} g_x - g_e &\cong 0 \\ g_y - g_e &= -2\lambda/(E_z - E_x) \\ g_z - g_e &= -2\lambda/(E_y - E_x) \end{aligned} \qquad ..(36)$$

In these expressions only first-order energy terms have been considered. Others such as Inui, Harasawa, and Obata (62) have taken into account the change of the wave function due to spin-orbit interaction which results in the addition of (negative) $1/\text{energy}^2$ terms in the above expressions for the g-shifts.

C. Previous Structural Determinations of Defects in Alkali Halides by ESR

The use of electron spin resonance has made it possible to determine the structures of a variety of defects in alkali halides (mainly X-irradiated single crystals at low temperatures). Models for the electron deficient or trapped hole type defects have been proposed by Seitz (26), Varley (63), Nagameya (64) and others but the structures of these defects first observed using U.V. and Visible spectroscopy were

uncertain and many of them still remain so. The structures of the defects now known include; the V_K center (36), or X_2^- ion(Xis a halogen atom); the H center (35), an X_2^- "crowdion" on a single site, so that it could be designated X_4^{3-}; the V_t center (45), an F_3^{2-} ion distorted from linearity by a neighbouring group of vacancies (see figure 1); a mixed halogen structure FCl^- in KCl : KF mixed crystal (37); and the superoxide ion O_2^- as an impurity in KCl (65,66).

a) The F-center

The F-center was the first colour center to have its structure determined unequivocally. The structure, determined by electron spin resonance, was found to agree with the model proposed by deBoer (67) which depicts an F-center as an electron trapped at a halide ion vacancy. The paramagnetic resonance of the F-center (68) in KCl was found to consist of a single line of nearly gaussian shape with a width of 56 gauss and a g value of 1.995 . Kahn and Kittel (69) said that the g-shift showed that the electron spends a large portion of its time near the ions surrounding the trapping site. Kip, Kittel, Levy andPortis (70) theoretically determined the line shape and width of the resonance line in KCl using deBoer's model and found that they were in good agreement with experimental values. Also using $K^{39}Cl$ and $K^{41}Cl$, they showed that the hyperfine interaction of the F-center electron with the nuclear spins of its six neighbouring cations was mainly responsible for the broadening of the resonance peak. The line width change due to the different isotopes of potassium was not exactly in the ratio of magnetic moments. This was attributed to a weaker interaction of the F-center with the twelve next

nearest neighbour halide ions. Linewidths in NaCl and KBr calculated from KCl results using the ratio of hyperfine coupling constants also gave remarkable agreement with experimental line widths. Feher (71) using electron spin double resonance technique, which gave better resolution, experimentally determined the hyperfine interaction of the F-center electron in KCl with its neighbours (K^+) and its next nearest neighbours (Cl^-). Also the hyperfine interactions in LiF and NaF were observed directly (72,73).

With the structural determination of the F-center showing that it consists of an electron trapped at a halide vacancy, the search for an equally fundamental imperfection consisting of a hole (electron deficiency) trapped at an alkali vacancy, which Seitz (22) called the "antimorph of the F-center" (26), was initiated. Seitz speculated that the antimorph of the F-center might be the center responsible for the V_1 absorption band (74) but this has never been proved. Indeed no ESR signal has yet been found which can be correlated with the V_1, V_2, V_3, or V_4 absorption bands; but the search for such signals has brought about the structural determinations of the following trapped hole center.

b) The V_K-center

The first analysis of the electron spin resonance of a V center was reported by Känzig (75) who obtained an ESR spectrum from single crystals of KCl, NaCl, KBr and LiF irradiated at -180°C. The center observed was thought to be associated with the optical V_1 band since it bleached at about the same temperature. Later Delbecq, Smaller and Yuster (76) and Lambe and West (77), working independently, showed that the

halogen$_2^-$ center which Känzig had discovered was a new center (now usually called the V_K center).

The ESR spectrum obtained for the V_K center in alkali chlorides (KCl) is composed of sets of seven almost equally spaced lines which have an intensity ratio of 1:2:3:4:3:2:1 . These were recognized as arising from the interaction of an electron or hole equally with two equivalent chlorine nuclei of spin 3/2. In the case of an equal interaction with two nuclei (subscripts 1 and 2), equation 8 of section B(d) becomes

$$H_z - H_o = -(g_o/g)\, A\, [(m_I)_1 + (m_I)_2] \qquad ..(1)$$

and for two nuclei of spin 3/2 for which each m_I can assume the values -3/2, -1/2, +1/2, +3/2, equation 1 indicates seven equally-spaced lines. The relative intensities of these are given by the number of different combinations of $(m_I)_1$ and $(m_I)_2$ giving rise to the same line and this gives intensities in the ratio 1:2:3:4:3:2:1 .

Chlorine, however, has two isotopes: Cl^{35}, which is 75% abundant and Cl^{37}, 25% abundant. Therefore three types of molecule-ions are possible: Cl^{35}-Cl^{35}, Cl^{35}-Cl^{37}, and Cl^{37}-Cl^{37} which are 9/16, 6/16, and 1/16 abundant respectively and allcan give rise to an electron spin resonance spectrum.

Cl^{35} and Cl^{37} have slightly different magnetic moments ($[\mu_{37}/\mu_{35}] = .83$) and since the hyperfine coupling is proportional to the nuclear magnetic moments, μ, the following relation holds.

$$[A^{35}/A^{37}] = [\mu_{35}/\mu_{37}]$$

where A^{35} and A^{37} are the hyperfine splittings of Cl^{35} and Cl^{37} respectively.

The molecule-ions Cl^{35}-Cl^{35} and Cl^{37}-Cl^{37} both give rise to seven-line spectra with line intensity in the ratio 1:2:3:4:3:2:1 but the intensity of the Cl^{37}-Cl^{37} spectrum will be 1/16 that of the Cl^{35}-Cl^{35} spectrum. The hyperfine splitting for the Cl^{37}-Cl^{37} molecule-ion will be less than that of the Cl^{35}-Cl^{35} molecule-ion as shown by

$$A^{37} = .83\ A^{35}$$

The spectrum of the Cl^{37}-Cl^{35} molecule-ion will be different from the other two spectra since there are now two non-equivalent nuclei and hence the degeneracies of the lines in the previous seven line spectra are removed. The configuration (3/2,1/2) and (1/2,3/2) no longer appear at the same field and therfore theline for like nuclei of degeneracy two will split into two lines of equal intensity and so on. The intensity of each Cl^{37}-Cl^{35} line is 6/9 that of the outermost line of the Cl^{35}-Cl^{35} spectrum. The position of the lines in the Cl^{37}-Cl^{35} spectrum are displaced from the Cl^{35}-Cl^{35} lines; this displacement can be expressed as equal to

$$0.17\ A^{35}\ m_I^{37}$$

where m_I^{37} is the nuclear magnetic quantum number of the Cl^{35} nucleus A^{35} is the hyperfine splitting of the Cl^{35}-Cl^{35} spectrum, and 0.17 is the value of $(A^{35}-A^{37})/A^{35}$ (see figure 3).

Kanzig (36) found that there was more than one set of lines for a particular orientation of the crystal. This was explained by the

Figure 3 - Isotope effects in KCl of a V_K-center (schematic)

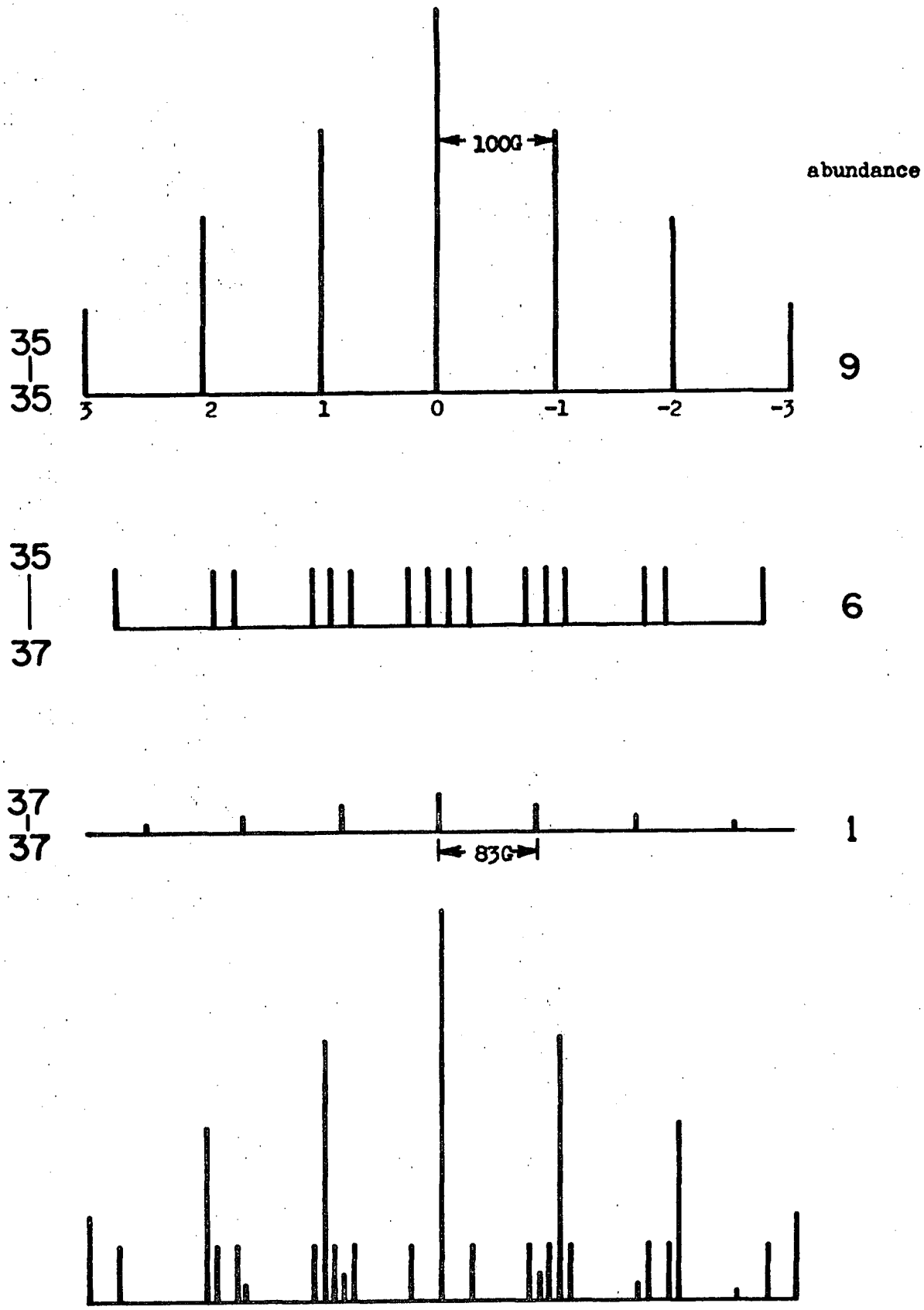

existence of more than one orientation of the centers within the crystal, together with the anisotropy of the hyperfine splitting and the g-factor, which causes the seven line spectrum to have a different spacing and a different center at each orientation. The spectra were consistent with random orientation of centers along directions of the type (100), with approximate axial symmetry about the molecular axis, the hyperfine tensor having its largest principal component A_z along the molecular axis, and smaller components in the perpendicular directions, with $A_x = A_y$ although the x and y directions are not crystallographically equivalent.

The unpaired electron giving rise to the spin is a p electron in a σ^*3p antibonding orbital (with some s-admixture). Therefore the molecular orbital of the molecule ion is made up essentially of a combination of 3p functions, one centered on each halogen nuclei which have their rotational symmetry along the line joining the nuclei, which is a (110) direction. The principal axes of the g-tensor (x, y, z) with respect to the molecule are shown in the following diagram in which the y axis points out of the page.

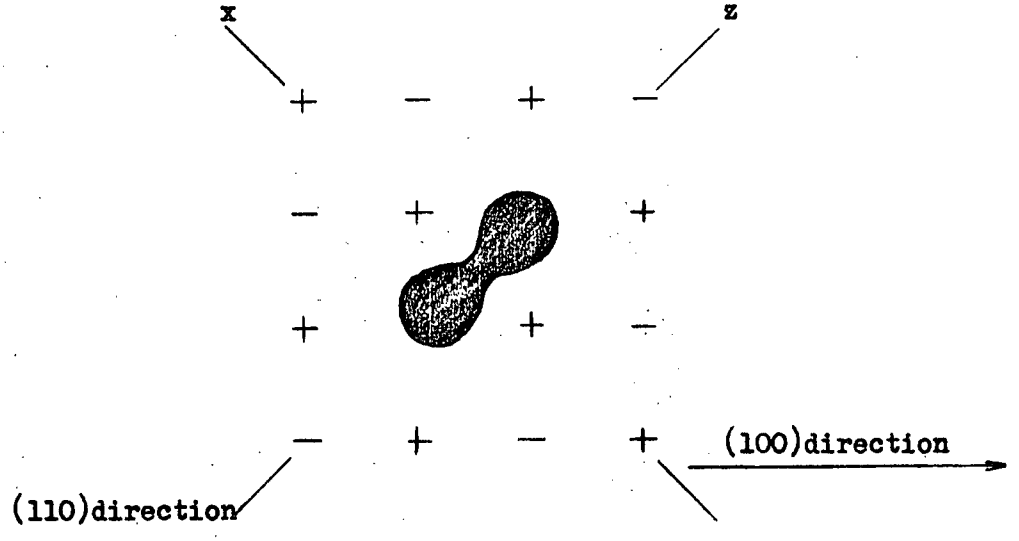

Now if the angle θ between the molecular axis and the d.c. magnetic field is changed there will be two effects:

(1) there will be a g-shift displacing the center of the hyperfine patterns,

and(2) there will be a change in the magnitude of the hyperfine splitting.

For any orientation of the crystal in the magnetic field at least two spectra will be observed simultaneously. When the magnetic field is parallel to the (100) axis of the crystal the spectrum obtained (see figure 4) is a combination of the 90° spectrum (1/3 of the molecule-ions) and the 45° spectrum (the remaining 2/3).

Table II below indicates the spectra expected for certain special directions of the magnetic field. One can readily see from figure

Table II

Direction of field	Angle θ	Abundance
(1 0 0)	45°	4
	90°	2
(1 1 0)	0°	1
	60°	4
	90°	1
(1 1 1)	35.26°	3
	90°	3

4 that the hyperfine splitting decreases as the angle θ, between the bond axis and the magnetic field,increases.

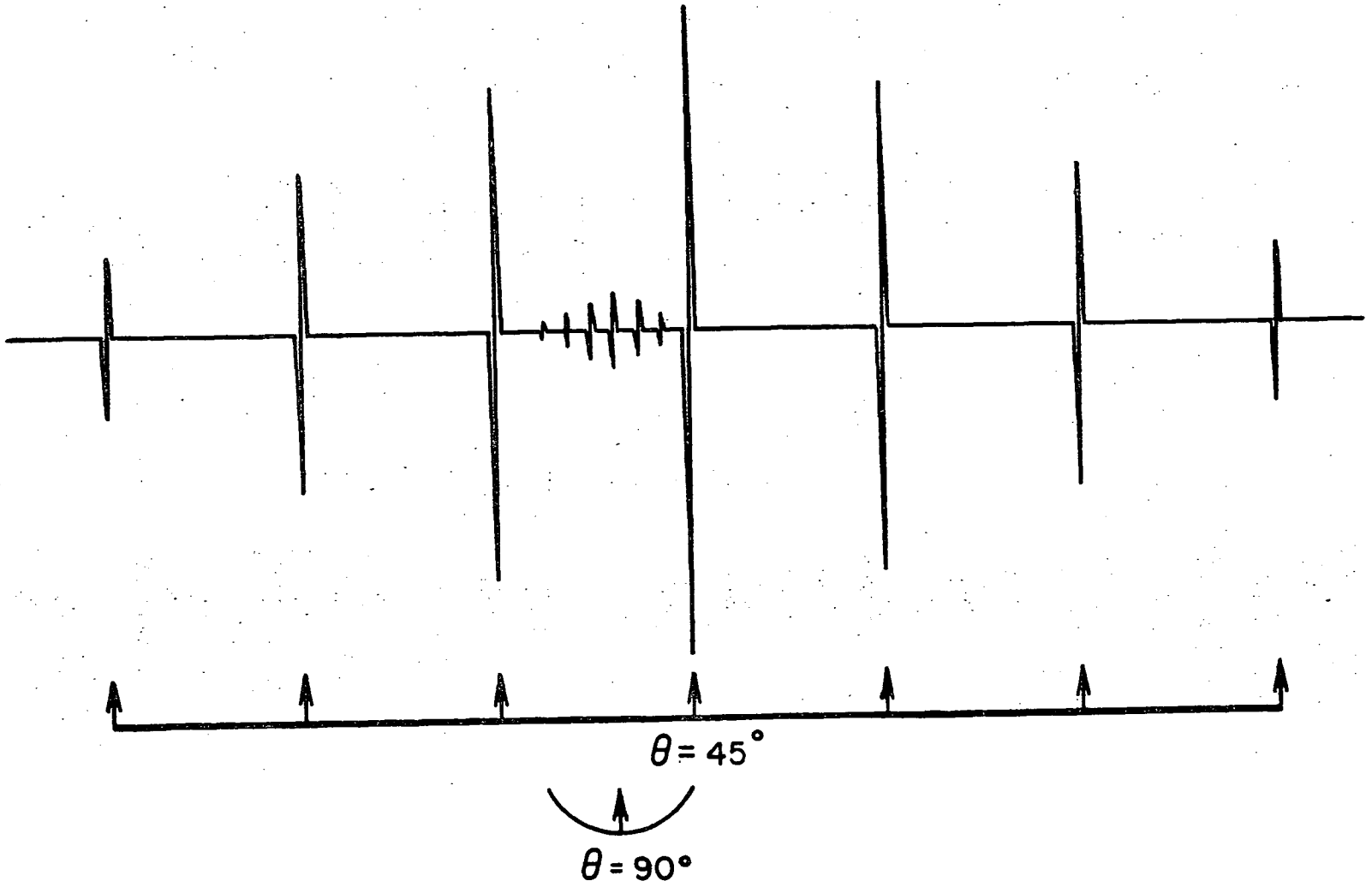

Figure 4 - Spectrum of a Cl^{35}-Cl^{35} molecule ion with H // [100],** (V_K-center, in KCl)

Numerical data on the g tensor and hyperfine tensors are given later in this thesis in table IV, page 69.

The V_K center in alkali fluorides was first discovered by Känzig (34) in LiF and later studied by Bailey (77) in LiF, NaF, KF, RbF, and CsF. Bailey found that the V_K center was stable in all the alkali fluorides at liquid nitrogen temperature but unstable at room temperature. The results for LiF agreed with Känzig's results (36). He also found in studying the series of fluorides that the line width of the V_K spectrum depends rather heavily on the magnetic moment of the nearest neighbour atoms (the alkalies).

c) The H-center

After Compton and Klick (78) showed that the H center must be different from any of the models previously suggested by Seitz (26) and Varley (63), Känzig and Woodruff studied the paramagnetic resonance of the H center in KCl (35) and then in KBr and LiF (39) and derived a detailed model of the H center. The H centers were produced by irradiating single crystals at 20°K and were studied at low temperatures. In determining the structure of the H center Känzig used similar arguments to those he used in determining the structure of the V_K center (see previous section). In order to study the H center, the derivative of the dispersion signal was used since if the spectrometer was tuned to measure pure absorption, the H center resonance, the V_K center resonance and the F center resonance, which appear together in these spectra, were completely saturated at 20°K by a very low microwave power.

The H center spectrum taken at the same orientation as the

V_K center spectrum is very similar to the V_K resonance. In the H center spectrum, however, there is a group of lines (with the main seven lines of the V_K center split in a ratio of 1:2:3:4:3:2:1) corresponding to each line in the V_K spectrum. The primary splitting (between the center lines of adjacent groups) for the H center was about 10% larger than the splitting in the V_K center and showed the same orientation dependence. The complete analogy of the orientation effects for the H center spectra to those of the V_K center spectra indicated that the axis of the major hyperfine interaction was the same for both types of centers namely the (110) axes of the crystal.

The secondary splitting (between adjacent lines within a group) in the H center spectrum causes each line of the basic halogen$_2^-$ spectrum to be split into a miniature spectrum of the same kind (see figure 5 for the primary and secondary hyperfine splitting of the Cl^{35}-Cl^{35} molecule-ion in the H center).

The complex spectrum can be interpreted as arising from identical strong interactions of the unpaired spin with two equivalent chlorine nuclei (1 and 2) as in the V_K spectrum and identical weak interactions of the unpaired spin with two other equivalent chlorine nuclei (3 and 4). For this case, equation 8 of section B(d) becomes

$$H_z - H_o = -(g_o/g)[A^{12}((m_I)_1 + (m_I)_2) + A^{34}((m_I)_3 + (m_I)_4)] \quad ..(2)$$

The first term in equation 2 as in equation 1 of section C(c) gives rise to seven equally spaced lines of intensity 1:2:3:4:3:2:1 . The second term gives rise to seven equally spaced lines for each of the first part

which have an intensity ratio of 1:2:3:4:3:2:1 (see figure 5).

The unpaired electron was found to spend 4-10% of its time on ions 3 and 4. The four halide ions involved in the H center were found to be in a straight line along the (100) direction in the crystal (see figure 1).

A similar type of center was found in KBr but it was hard to determine the secondary splitting because of the existence of two equally abundant isotopes of bromine (Br^{78} and Br^{81}) and also additional splitting due to second order hyperfine and quadrupole effects which arise because of the high magnetic moment of bromine.

In LiF a center with the same structure as an H center was found and since there is only one isotope of fluorine (F^{19}) with a nuclear spin of 1/2 the hyperfine spectrum of the H center is rather simple. The strong interaction of the unpaired electron with two equivalent fluorine nuclei (like the V_K center F_2^- (34)) gives rise to three lines with an intensity ratio of 1:2:1. The weak interaction with the next two fluorine nuclei, which are also equivalent, splits the first lines into a miniature (secondary) pattern of three lines with the intensity ratio 1:2:1. This experiment was done using the derivative of absorption so that the F center resonance was completely saturated. The H center and V_K center spectrum, however, appeared together.

The g-shift found for the H center, previously discussed, was about half the g-shift found for the V_K center. This difference can be explained using the general discussion in the last part of section B(d) for the specific case of a Cl_2^- molecule ion. Figure 6 below repre-

Figure 5 - H-center (hyperfine interactions) in KCl

primary (2 Cl, I= 3)

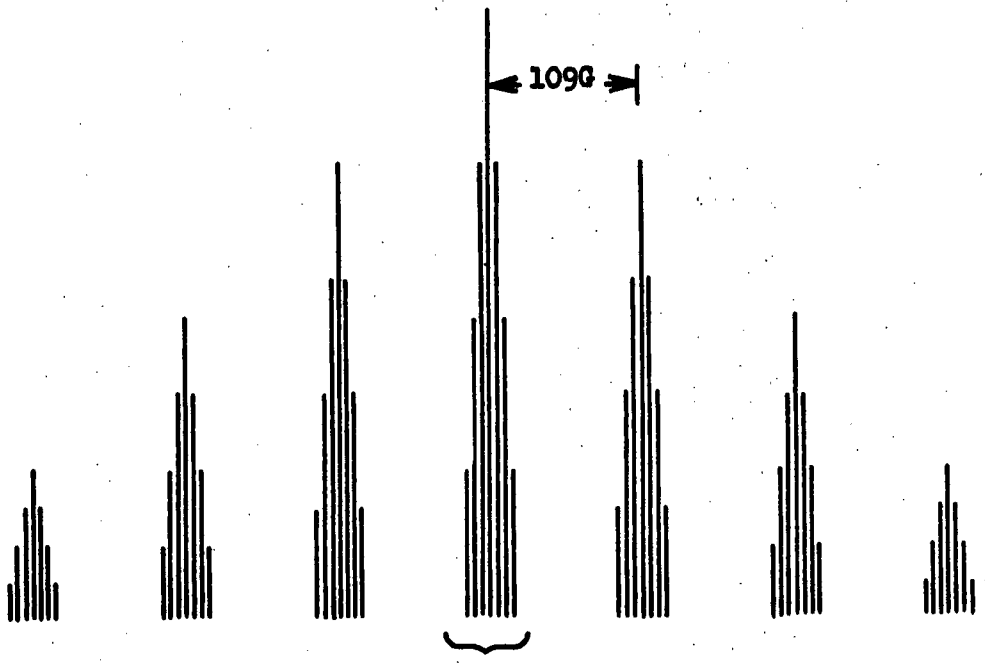

secondary splitting (2 Cl, I= 3)

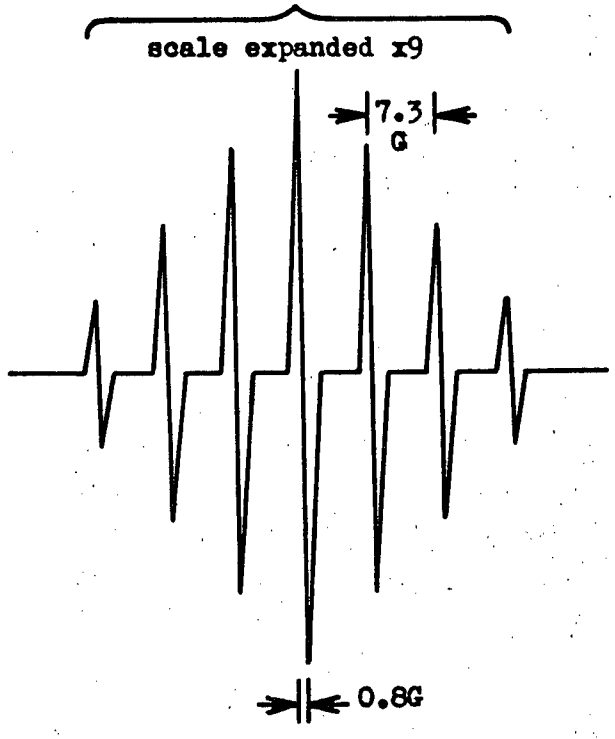

sents the orbital energy levels (79) of the X_2^- molecule-ion for both the V_K and the H center (36,38) as a function of internuclear distance

Figure 6

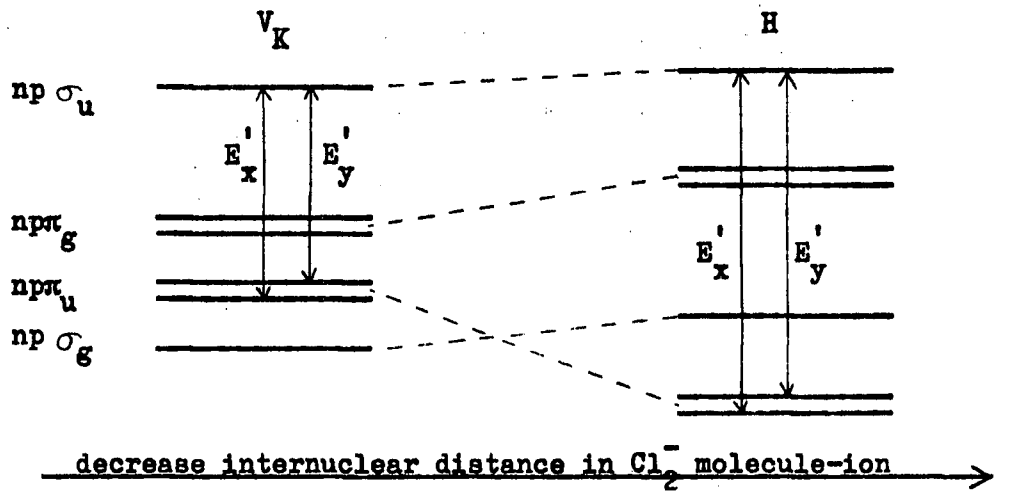

in the Cl_2^- molecule-ion. The g-shifts are produced by the optically forbidden transitions E_y' and E_x' shown in figure 6 which arise from the admixture of orbitally excited states with the groundstate of the molecule-ion (36).

The g-shifts using a modified form of equations 36 of section B(d) are (62,80):

$$g_x - g_o = 2\lambda\alpha^2/E_y'$$
$$g_y - g_o = 2\lambda\alpha^2/E_x' \qquad ..(3)$$
$$g_z - g_o \cong 0$$

where α^2 is the fraction of p character in the bond joining the two chlorines in the Cl_2^- molecule-ion.

For axial symmetry, the degeneracy of the π levels is not

lifted by the crystalline field (the difference between E_x' and E_y' vanishes) and therefore $E_x' = E_y'$ which can now be called E_g. Equations 3 show that the g-shift is inversely proportional to the forbidden transition energy E_g and since E_g for the H center is about twice as large as E_g for the V_K center, the g-shift for the H center is about half that of the V_K center. The difference in g-shifts between the two centers also indicates that the internuclear distance of the two nuclei in the halogen$_2^-$ molecule-ion is less in the H center than in the V_K center (see figure 6). This led Känzig to a model for the H center which is shown in figure 1 along with the model of the V_K center. The H center can be described (39) as a halogen$_2^-$-molecule ion located in a halide vacancy. The resulting crowding accounts not only for the reduced internuclear distance as compared to the V_K center, but also for the additional interactionsof the unpaired electron with two more halide ions. This configuration may be characterized as a "crowdion" (81) stabilized by a hole. (The term "crowdion" was coined by Paneth as a descriptive designation for a short linear region of compression.)

The paramagnetic center previously discussed was called the H center since it had the production and bleaching characteristics of the optical H band (39). The antimorph of this center, an interstitial Li, has been found in irradiated LiF (82).

d) Other electron-deficient centers

Although most attention has been focussed on the V_K and H centers, other electron deficient centers have since been discovered and their structures have been determined by electron spin resonance. Most

of these centers have been found in irradiated LiF at low temperatures. Two of these are the V_t (F_3^{2-}) and the V_F (bent F_2^-) centers. The other centers found in LiF (excluding the V_K and H centers) were of such weak intensity that they could not be identified. Also in a mixed crystal of KCl-KF, an FCl^- center has been identified. More research is being done using fluorides than other halides since the spectra obtained are simple and are interpretable even for rather complex centers. This is because fluorine has only one isotope, F^{19}, with a nuclear spin of 1/2 and a large nuclear magnetic moment which gives large hyperfine splittings.

The V_F center found by Känzig (83) in irradiated LiF at 77°K was found to be the closest approach yet known to the antimorph of the F center although the similarities with Seitz's " V_1" model are limited. The V_F center is a hole trapped at an Li vacancy but the hole is localized on two fluoride ions so that an F_2^- molecule-ion results, with a bent bond(see figure 1). The hyperfine spectrum of the V_F center is closely related to that of the self-trapped hole or V_K center in LiF (84). The spread and anisotropy of the hyperfine spectrum are about the same as that of the V_K center indicating that the electron is localized almost full time on the fluoride ions. The basic spectra, however, consist of four lines of roughly equal intensity which shows that the two fluoride ions are non-equivalent with respect to the magnetic field. There are special orientations of the molecule where there is still the familiar three-line pattern of intensity 1:2:1 which shows that the two fluoride ions are equivalent in these instances. The main difference between the V_F and the V_K center in LiF is that in the latter case the two fluorine

nuclei are equivalent for every direction of the magnetic field so that the 1:2:1 pattern always results (see reference 36). This center has not yet been observed in KCl, KBr, or NaCl.

The V_t center (F_3^{2-}) which is also produced by irradiating LiF at 20°K was found by Cohen, Känzig and Woodruff (33,45). This center resembles Seitz's model of the V_4 center but optical studies have not yet been carried out on the V_t center so that a definite assignment of the V_t center to the V_4 band is not warranted. The model proposed for the V_t center (supported by ESR studies (33)) consists of an electron deficiency localized on three fluoride ions which form an isosceles triangle (see figure 1). ESR studies showed (33) that the lines in the V_t center split in a way similar in detail to the V_F center except, that since there are three nuclei of spin 1/2 in the V_t center, there are twice as many lines. The basic spectra mainly consist of eight lines of equal intensity which are accounted for by three non-equivalent fluoride ions. There are also cases where the magnetic field is in such a position that the two outer fluorine ions become equivalent thus producing basic spectra of six lines with the intensity sequence 1:2:1:1:2:1 where two lines are degenerate. This center has not yet been identified in other alkali halides.

Since mixed halogen molecules such as FCl, BrCl and ICl are well known and since stable F_2^-, Cl_2^- and Br_2^- species have been observed in crystals, it seemed reasonable to Wilkins (37) that stable FCl^-, $BrCl^-$ and ICl^- ions might be produced in mixed alkali halide crystals. Wilkins and Gabriel (37) produced an FCl^- ion in a mixed KCl-KF crystal at liquid nitrogen temperature by irradiation. The FCl^- ion produced was

found to be oriented along the (111) direction unlike the V_K (Cl_2^- and F_2^-) centers which are oriented along the (110) direction. The FCl^- ion can be described as an interstitial fluorine atom or an (FCl^-) ion trapped at an anion vacancy. The main feature of the spectra is the double set of four equally spaced lines of equal intensity. These lines are produced by the unpaired electron interacting more or less equally with an F^- ion of spin 1/2 and a Cl^- ion of spin 3/2. The resonance absorption line is split by the F^- into two lines which in turn are both split by Cl^- into four lines of equal intensity. The more intense lines in the spectra were found to be due to the $(F^{19}\text{-}Cl^{35})^-$ ion and intensity measurements enabled the lines due to the $(F^{19}\text{-}Cl^{37})^-$ ion also to be identified. The ratio of the two sets of lines was in accordance with their relative isotropic abundance. The separation of the two sets of lines was found to be consistent with the relative magnetic moments of the chlorine isotopes.

From the viewpoint of studying chemical reactivity, it is a little unfortunate that the most extensive information on electron deficient defects is for the fluorides, which are the most resistant to loss of electrons by chemical attack. If fluorine is being used as an oxidizing agent, however, it is important to know the ESR spectroscopic characteristics of fluorine-containing centers, since these are very likely to appear as intermediates.

APPARATUS AND PROCEDURE

A. Electron Spin Resonance Spectrometers

Two X-band spectrometers were used in the course of the work. One was equipped with a varian 6 inch magnet while the other instrument, a varian E3 bench model, had a 4 inch magnet.

The spectrometer with the 6 inch magnet, which is similiar to the varian V-4500 ESR spectrometer, was built in the Chemistry Department with modifications to give more sensitivity and stability. A block diagram of this spectrometer is shown in figure 7. The microwave power is provided by a water cooled klystron oscillator which delivers about 300 milliwatts over its tuning range, 8.6 to 10 Gc./sec. The klystron frequency is stabilized by an automatic frequency control (AFC) system which locks the klystron on the resonant frequency of the cavity. The klystron is coupled to a wave guide which transfers the microwave output via a magic - T bridge and accessory equipment to a rectangular reflector type cavity that resonates in the TE 102 Mode. The microwave cavity is situated in the 2.5 inch gap between the poles of a 6 inch water cooled electromagnet that supplies the variable field. A 100 Kc./sec. modulating magnetic field is superimposed on the changing magnetic field by a pair of auxiliary coils mounted one on each side of the cavity. The resonance absorption signal is detected by a microwave crystal detector using a silicon diode which is situated in one of the arms of the magic - T bridge. The signal is passed through an amplifying system to a phase sensitive detector and thence to a recorder which graphically records the first derivative absorption signal. The sensitivity of the spectrometer is approximately $3 \times 10^{-13} \Delta H$ moles of electron spins where ΔH is the peak width in gauss at half height. The magnetic field was measured using a

Figure 7 - Block diagram of a 100 Kc. (6 inch) ESR spectrometer

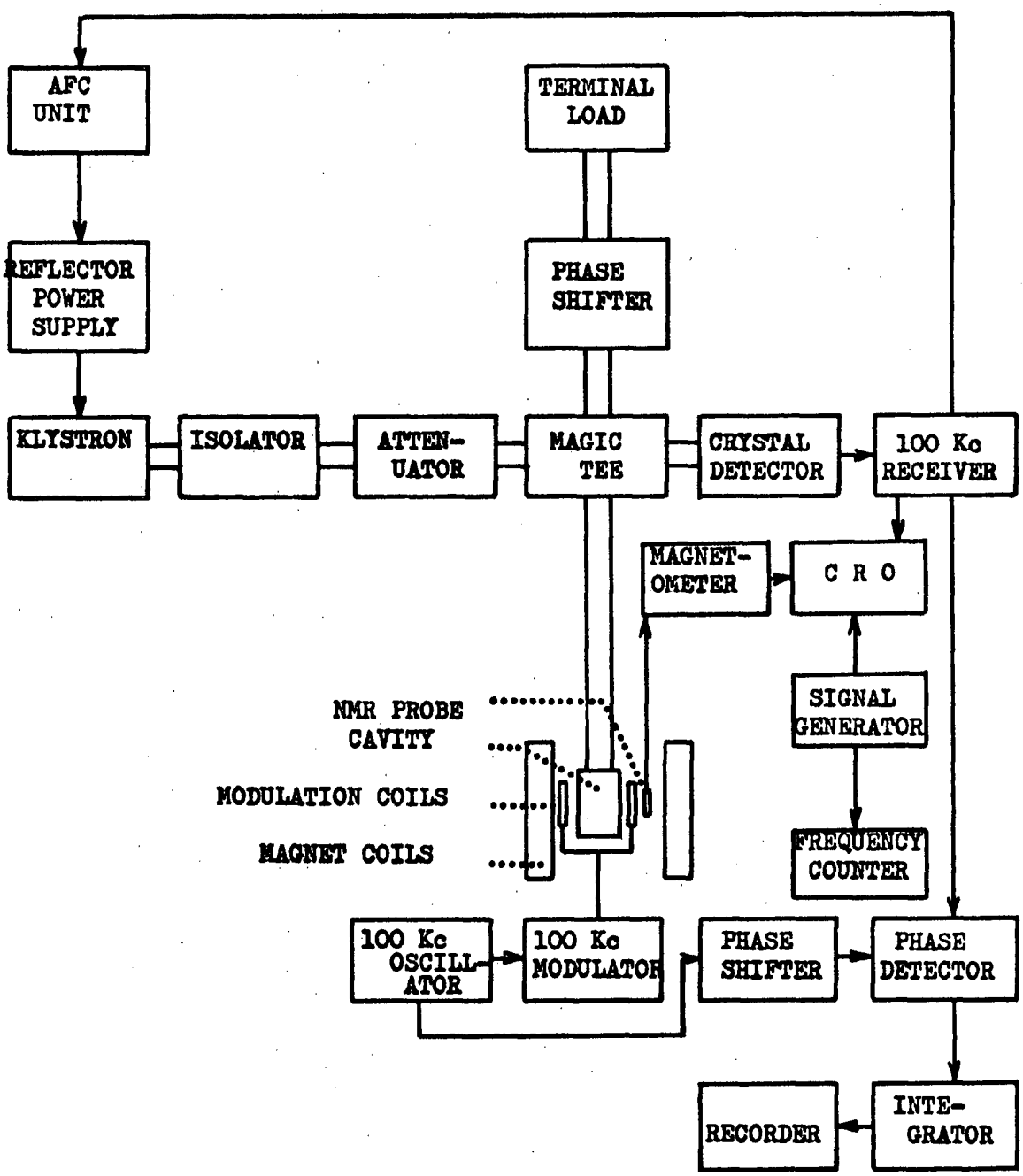

proton resonance magnetometer. The magnetometer consists of a probe coil containing glycerol which is inserted in the magnet gap beside the cavity. The coil is connected to a marginal oscillator which is frequency modulated at 20 c./sec. The proton resonance signal is displayed on an oscilloscope and a signal generator is tuned to zero beat. The frequency of the signal generator is measured by an electronic counter.

The varian E3 bench model is nearly completely a solid state unit. The block diagram is shown in figure 8. The spectrometer consists of three main parts: (i) a console system which contains the console power supply, the 100 Kc./sec. modulation unit, the magnetic field regulator, and a recorder; (ii) a 9.5 Gc./sec. microwave bridge which consists of a microwave system for excitation and observation of the ESR signal, an AFC which stabilizes the klystron, a klystron d.c. power supply and a preamplifier for signal amplification; (iii) a 4 inch water cooled magnet system which has an accessible air gap of 1.2 inches in which the cavity sits. The spectrometer has a sensitivity of 10^{11} ΔH spins.

The advantages of this spectrometer are: frequency can be read off the frequency dial on the microwave bridge; the magnetic field can be read off the console panel; and the recording system (fixed chart and moving pen with adjustable zero for the vertical axis) is more convenient than a continuous strip chart when comparison of successive scans is needed to confirm faint details, to follow kinetic effects, or to observe changes in spectrum with orientation of a crystal.

B. Vacuum Sublimation of Ionic Solids

Solid samples of various types were used, including analytical reagent grade powders without further treatment, and single crystals from

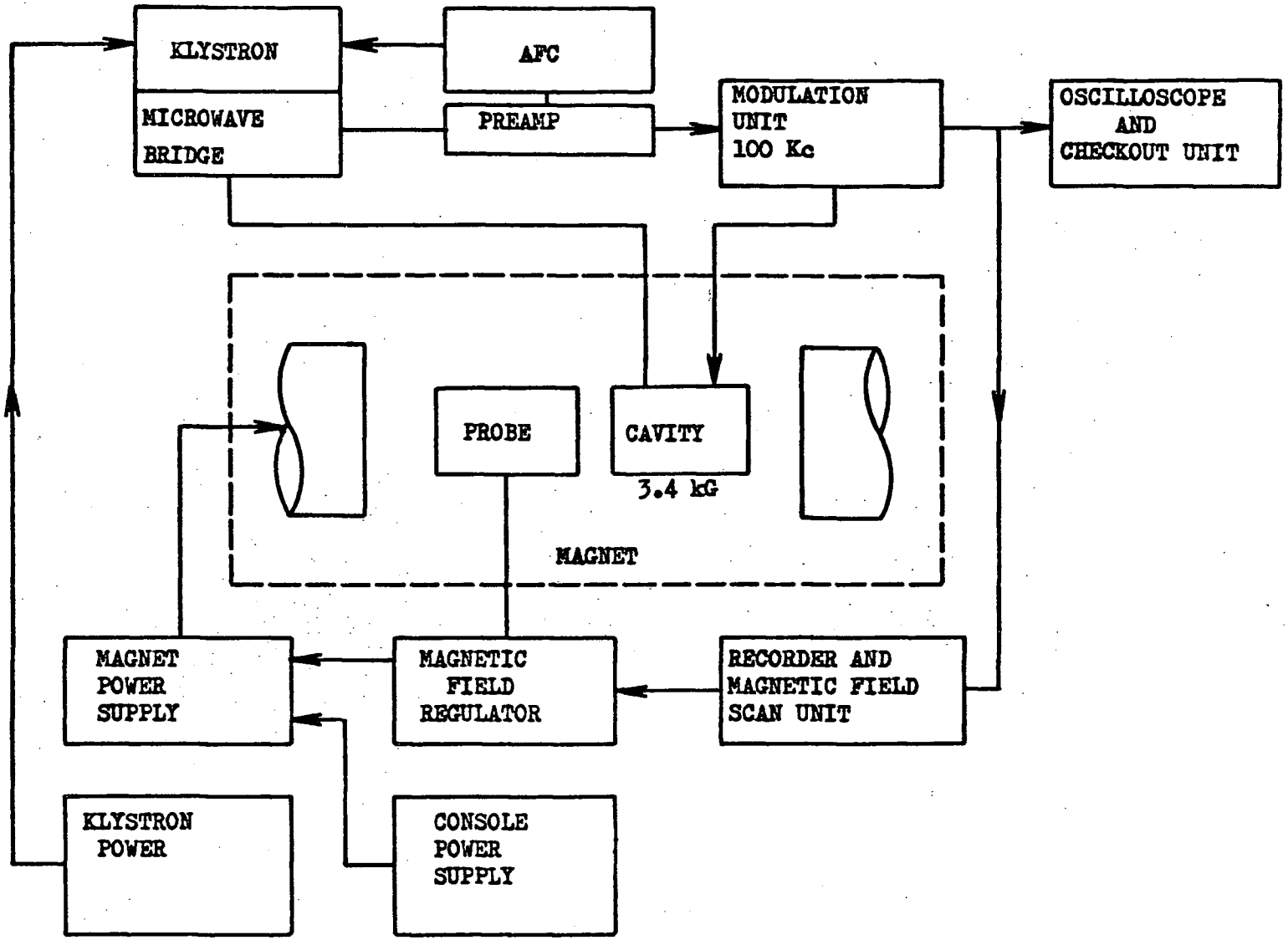

Figure 8 - Block diagram of an E-3 ESR spectrometer

various sources. Each type of sample is described in detail later. Only the preparation of vacuum-sublimed material is given here, because it requires an extensive description of apparatus and procedure.

The vacuum-sublimed particles were made in an apparatus designed by Adams (85) which is shown in figure 9.

The apparatus consists of the main vessel B, side arm A, water cooled condenser C and the scraper G. A,B, and C are made of quartz. The scraper G consists of a tungsten rod H sealed into a pyrex B-10 cone at J and K; the scraper blade is made of platinum and is spot welded to H at I. The side arm A is heated by three heaters L, M, N which are made of chromel-A and are encased in Alumina and glass wool. The rheostat was set to allow a current of about 4 amps to flow into the heater system L, M, and N. This setting was used for KI, KBr, KCl, and NaCl which have melting points around 800°C and sublime rapidly close to their melting points.

The sample to be evaporated (KCl, NaCl, KBr, or KI) is placed in side arm A. The apparatus is connected at O to the collector (usually an ESR sample tube - figure 12) and to a vacuum system, and is evacuated by a mercury-diffusion pump to 10^{-5} mm Hg. The sample is outgassed by heating it to a temperature below the evaporation temperature (current of about 2.5 amps) while the sample is connected to the pumps. Outgassing is discontinued when the pressure measured by a Veeco ionization gauge remains constant after disconnecting the system from the pumps. Cooling water and heaters (current of 4 amps) are turned on after completion of outgassing. The sample evaporates and condenses out on the water cooled quartz surface of C. When a thin layer of film has been formed the heaters and water are turned off. The film is scraped off and allowed to fall down

Figure 9 - Evaporated film apparatus

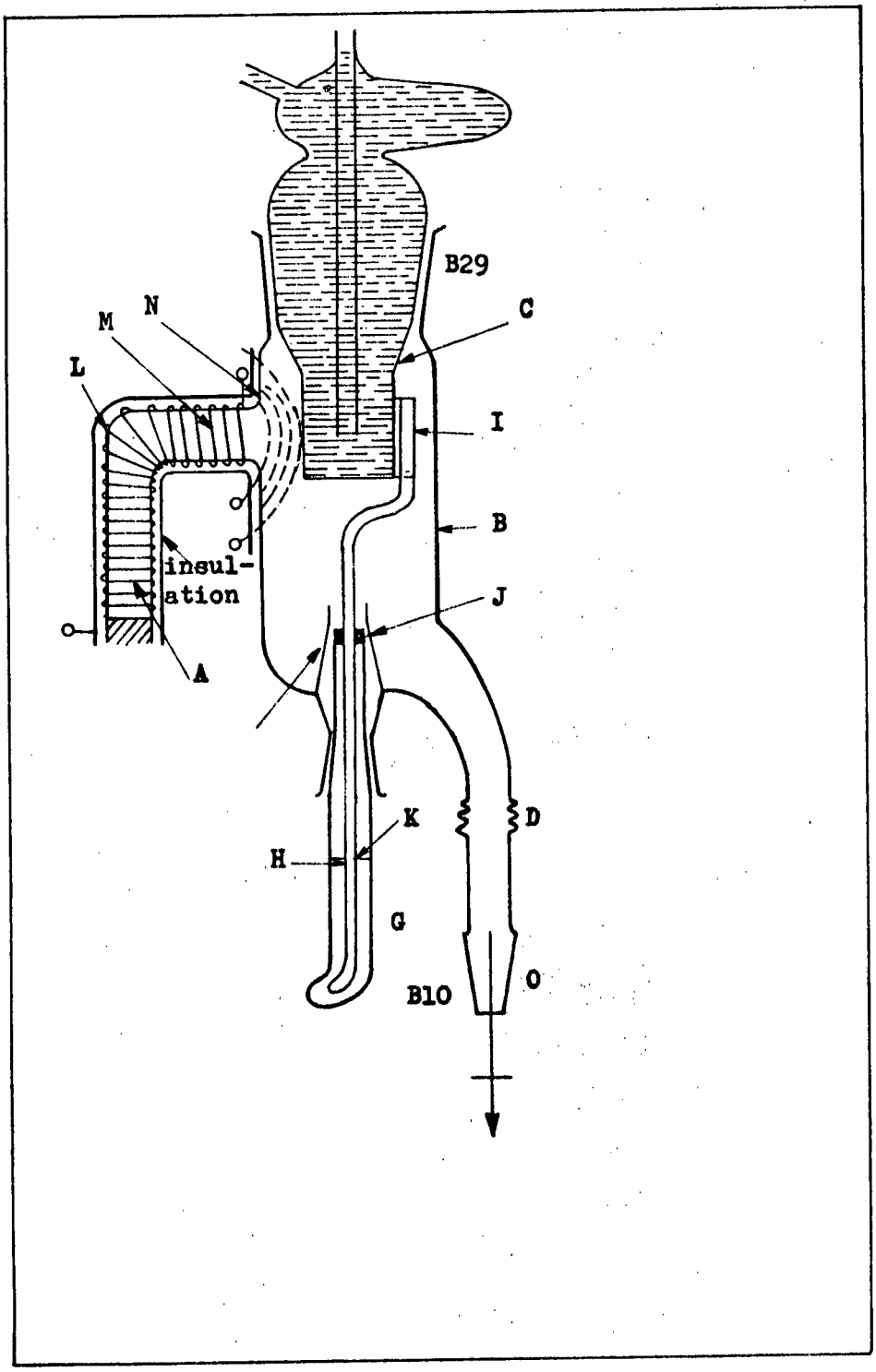

past D into the collector. The procedure is repeated until there is about .5 mm of sample in the sample tube. The sample is then sealed off under vacuum at C in the reaction apparatus (figure 12).

The B.29 and B.10 joints at the top and bottom of vessel B are lubricated with high temperature grease, apiezon T, and are cooled by a stream of air while the heaters are operating.

C. Handling of Halogens

The transfer of chlorine and fluorine from high-pressure cylinders to pyrex storage bulbs, together with drying in the case of chlorine and removal of HF from fluorine, has been confined to a single extensive vacuum system which is shared by everyone in the laboratory. Since halogens are used in this system, mercury-diffusion pumps are not suitable. A three stage Balzer diffusion pump containing silicone oil is used. The advantage of silicone oil over mercury is that if by accident halogens are passed through the pump only volatile products are formed which do not clog the pump.

The stopcocks are lubricated with Kel-F grease with which the halogens do not react. Since this grease is more likely to streak than hydro-carbon types all taps are of the right-angled pattern which is less likely to develop leaks from streaking. For pressure measurements of Cl_2 sulfuric acid manometers are employed which operate non-linearly with some air in the closed limb (see figure 10). The vapor pressure of the sulfuric acid is about 7×10^{-4} mm Hg.

A chlorine and fluorine disposal line is connected to all parts of the system. It is separated from the main vacuum line, but served by the same pump. Chlorine is trapped out by liquid nitrogen in removable

traps and disposed of in aqueous sodium hydroxide. Fluorine is directly absorbed into soda lime.

The pressure in the vacuum system is determined using a Veeco-R.G. 75P ionization gauge with a 'non-burn-out' iridium filament. Care must be taken when using this gauge, for the filament is damaged by contact with any halogen (even I_2). The pressure obtained using liquid nitrogen traps in front of the gauges is about 1×10^{-6} mm Hg.

a) Chlorine drying system

The chlorine obtained from Matheson Company was quoted as 99.5% pure. Uncondensable gases and water vapor were removed in the purification system shown in figure 10. The procedure is as follows.

Chlorine from the stock cylinder is admitted to the 2 liter bulb A with stopcocks 2, 4, and 5 closed. The chlorine is allowed to flow into the system until a pressure of one atmosphere is reached as shown on the sulfuric acid manometer F. The non-condensable gases are removed by opening tap 4 and allowing the chlorine to condense into two liquid nitrogen cooled traps (not shown) while the non-condensable gases are pumped away. The chlorine is transferred back into bulb A by condensing it in K. Tap 4 is then closed.

Water vapor is removed from the chlorine by the sulfuric acid bulbs D and E. These, as well as the storage bulb B, are evacuated along with connecting systems back to stopcock 5. Then stopcocks 6, 7, 8, 9, and 12 are closed and 10, 11, 13, and 14 are left open. Stopcock 5 is opened slowly, allowing the chlorine to bubble through the drying traps D and E via C to the storage bulb B. When half the chlorine has bubbled through, the remainder is pulled through by putting a liquid nitrogen dewar at

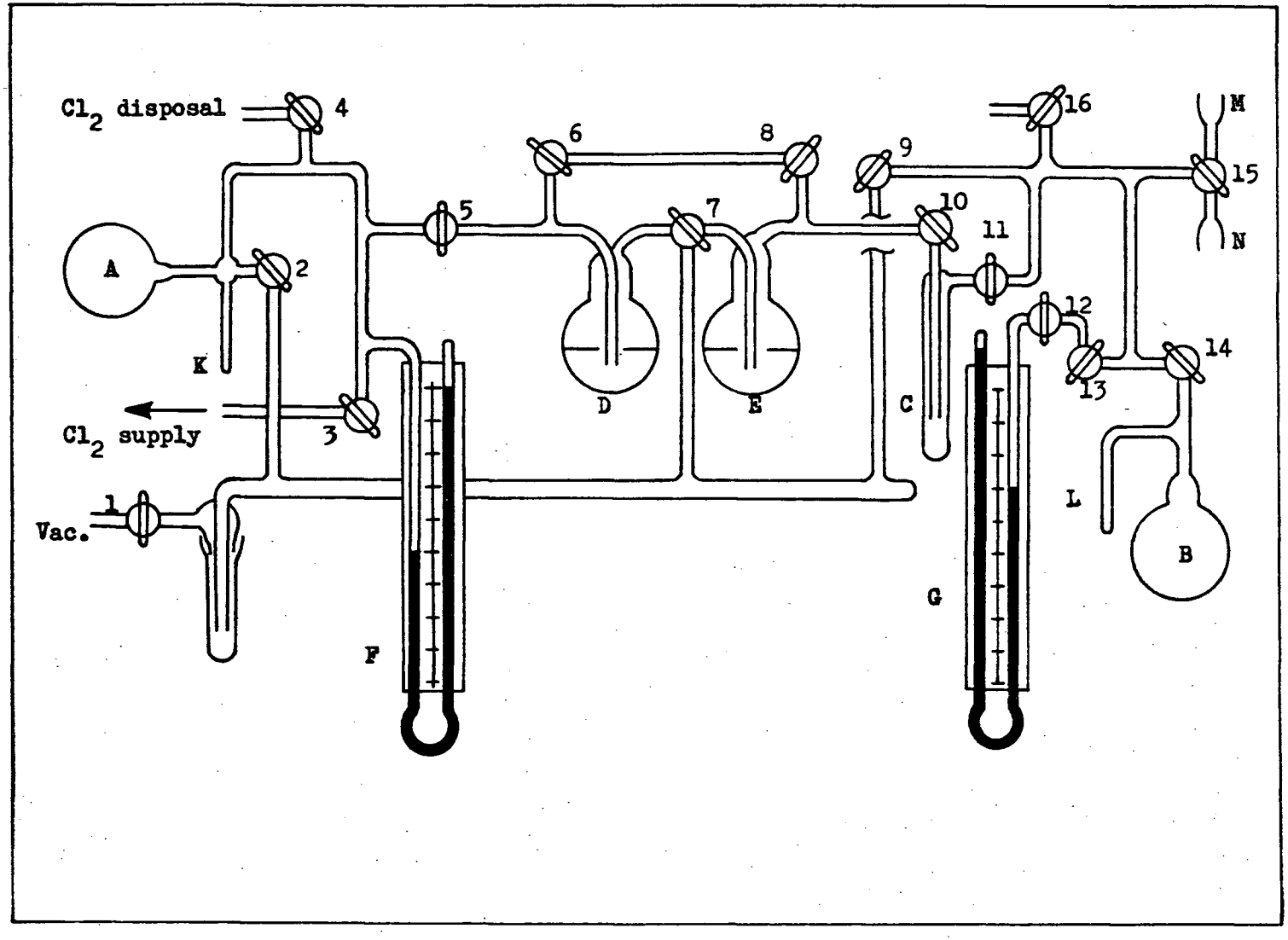

Figure 10 - Chlorine purification system

finger L. Stopcock 14 is closed and the dewar is removed. The chlorine is taken from storage bulb B, as required for use in different systems, via M or N. The pressure of the gas can be measured by the sulfuric acid manometer G.

b) Fluorine handling system

Fluorine was handled in pyrex and quartz systems which were not affected by the fluorine so long as it was dry.

Matheson Company fluorine which was quoted as 98% pure was used. The main impurity is hydrogen fluoride which is removed by passing the fluorine through a sodium fluoride trap (see C, figure 11).

The fluorine (cylinder pressure 300 p.s.i.) is admitted to the system via a series of expansion volumes between monel needle valves (86) connected to the pyrex system by copper tubing and a kovar seal at D. The system is initially evacuated to 10^{-3} mm Hg by a rotary pump, flushed with fluorine and then re-evacuated through the disposal line. Fluorine is then allowed to enter the system (see figure 11) (taps 2, 4, and 5 closed and 1, 3, and 6 open) and its pressure is measured by a spiral gauge A. This consists of a mirror on a hollow pyrex spring which is free to rotate when there are pressure differences between outside and inside surfaces of the spiral. The gauge is used as a null meter. A known pressure of carbon dioxide is admitted (tap 7) and fluorine is admitted through tap 6 to bring the scale indicator back to its initial position. The valves at the fluorine cylinder and tap 3 are closed. Tap 5 is opened and the system is evacuated except for the fluorine in the storage bulb B. The B.10 socket at tap 2 is the point of attachment for reaction systems to be charged with fluorine. The pressure of fluorine usually used is approximately 29 cm of

Figure 11- Fluorine handling system

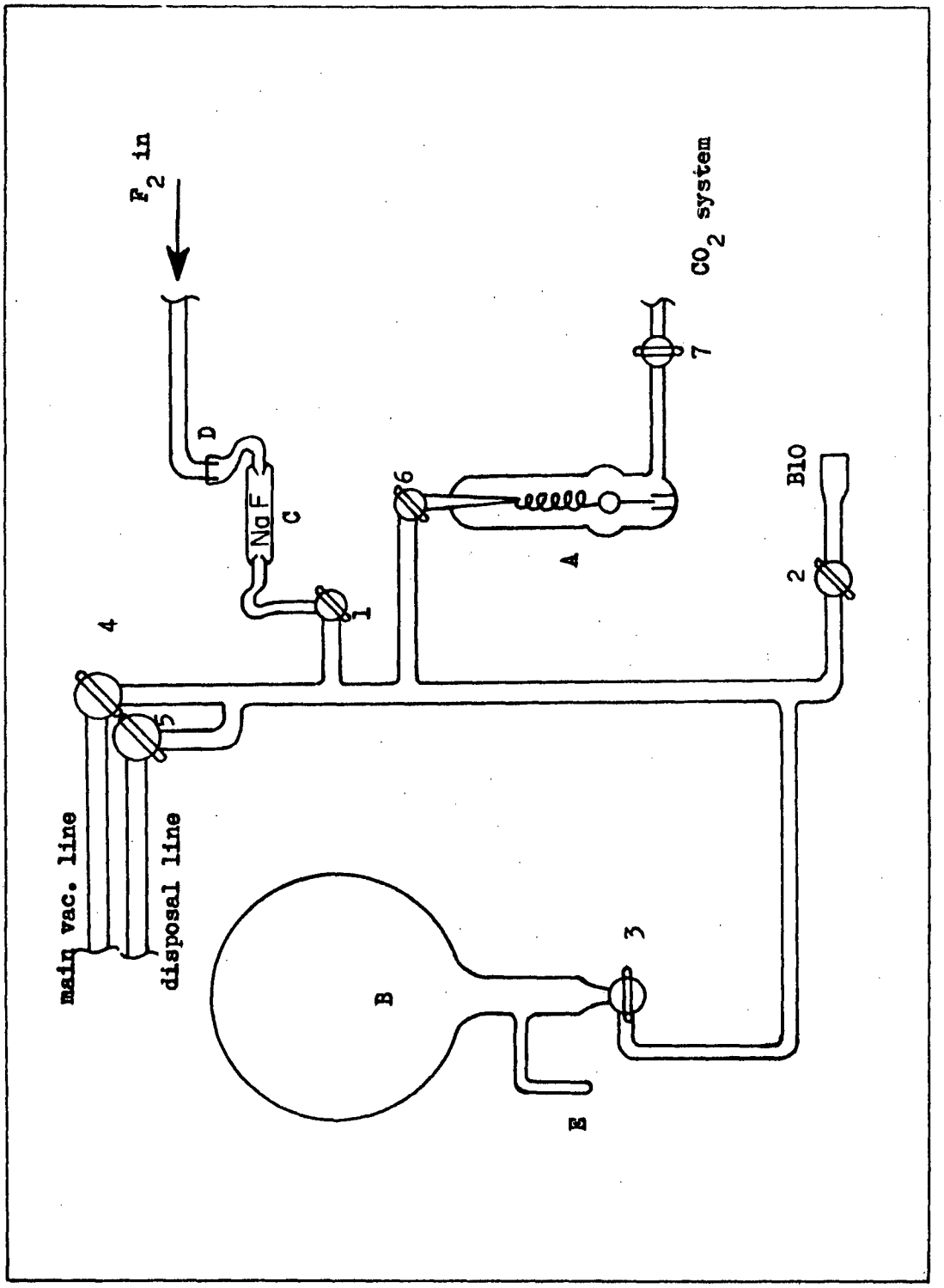

Hg which is obtained by putting liquid nitrogen at finger E.

D. Reaction Apparatus

The reaction apparatus shown in figure 12 and figure 13 are both constructed with quartz and pyrex in a design which enables the 6 mm quartz tube to be inserted into an ESR spectrometer.

Apparatus 1 in figure 12 has a circulation system which enables the chlorine and fluorine to be circulated over the solid by convection. Apparatus 1 has a glass bead at B which breaks up the sample to allow it to pass down the 3 mm inner tube of the circulation system; a constriction at C to permit flame sealing under vacuum; two quartz-pyrex graded seals F and G; and a Kel-F greased right-angled tap at D which allows the attaching of the reaction apparatus at E to other systems (usually a portable vacuum system) without breaking vacuum.

Apparatus 2 in figure 13 is a self sufficient reaction vessel for it has its own storage bulb B for fluorine or chlorine. Kel-F grease is used on all joints and the quartz-pyrex junction is the B.10 joint below stopcock 1.

E. Reaction Procedure

The reaction apparatus was evacuated to a pressure of 10^{-5} mm Hg as measured by a Veeco-R.G. 75P ionization gauge. The samples were transferred into the apparatus by several methods. Single crystals and powders direct from the storage bottle were transferred in a dry box and the sample tube was afterwards evacuated. Vacuum-sublimed particles were transferred under vacuum.

The apparatus was mounted securely in the cavity of the ESR spectrometer. The procedure was then usually as follows: a blank run was

Figure 12 - Reaction apparatus 1

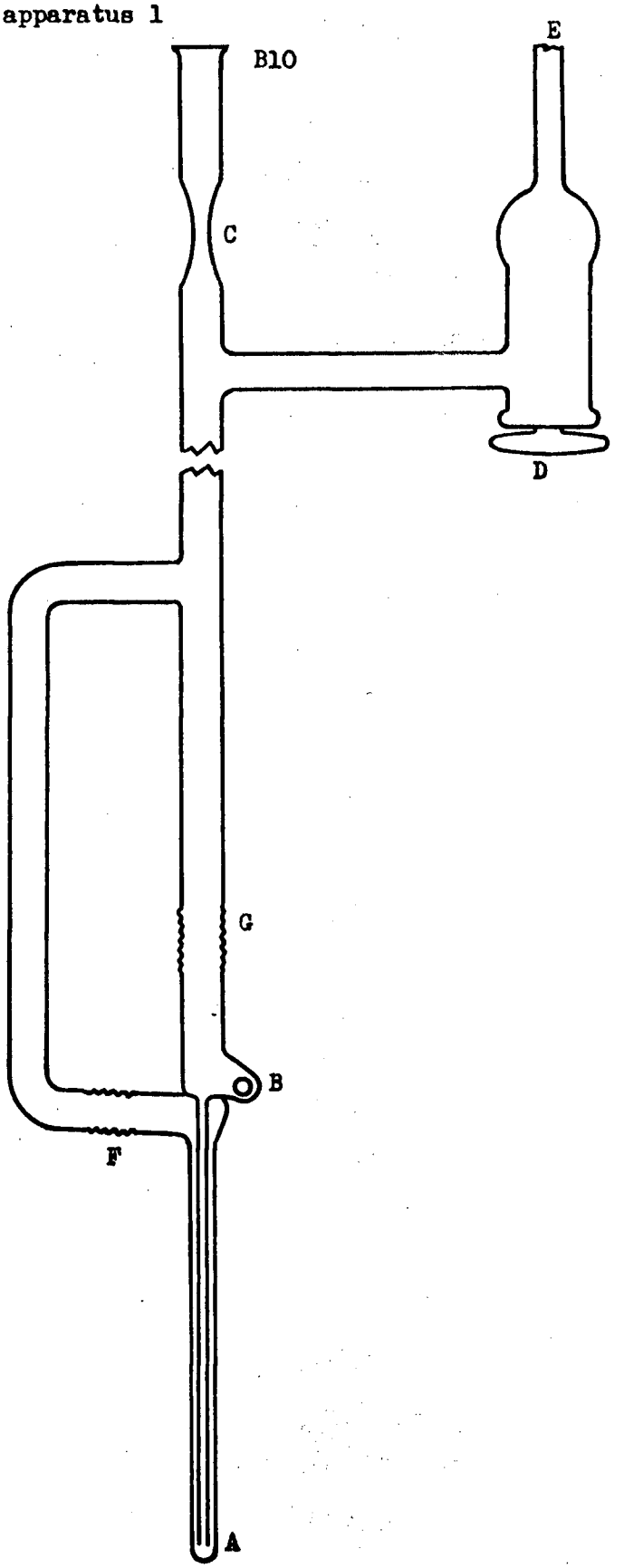

Figure 13 - Reaction apparatus 2

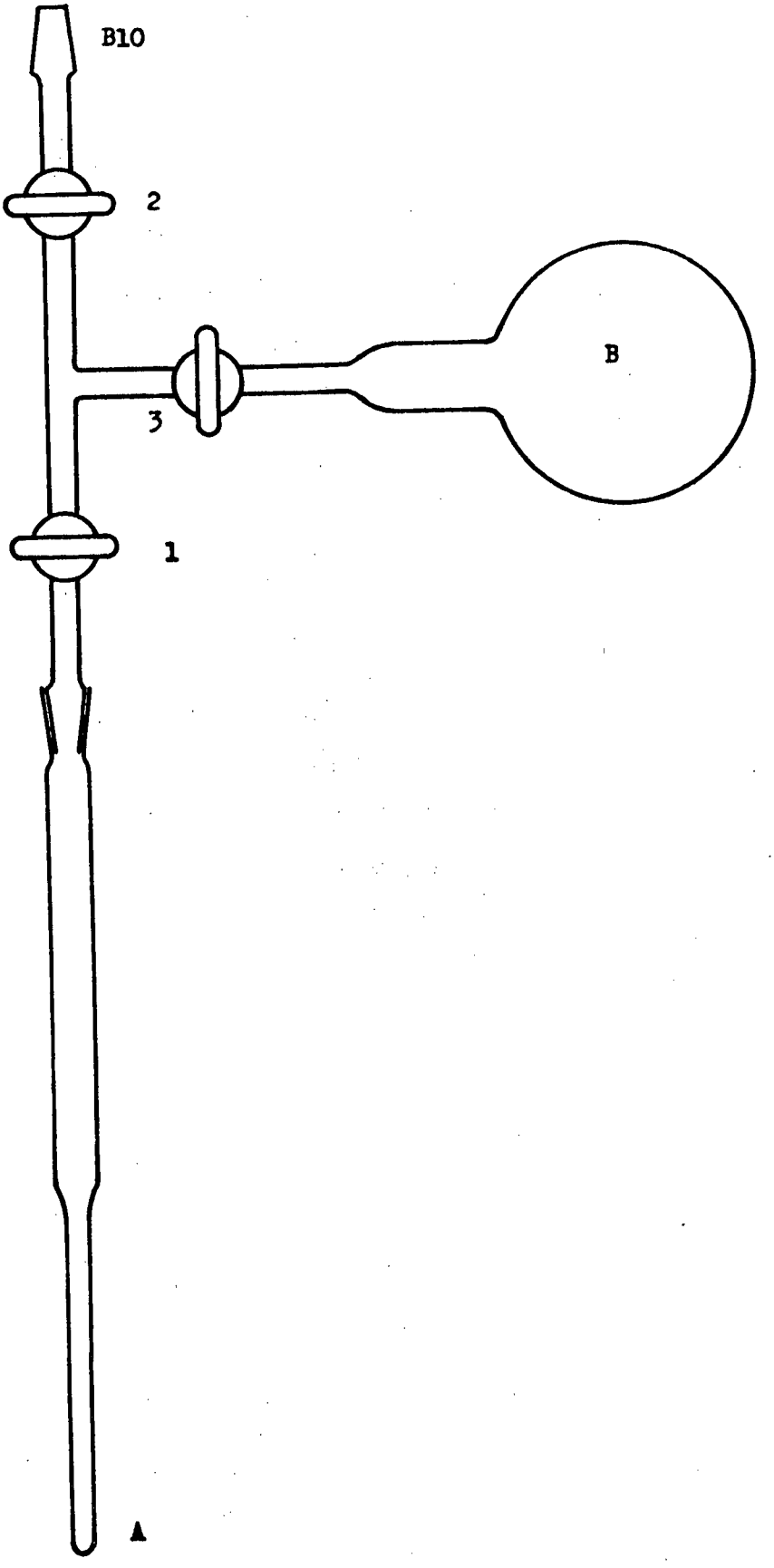

taken of the sample (after the spectrometer was tuned) to check if any signals were initially present. Fluorine was then added. The time was noted. If a signal appeared its growth was followed by scanning through it at known times. If no peak appeared within 5-30 minutes the fluorine was removed and any peak which appeared thereafter was studied both in its growth and its decay. When a peak appeared after the removal of the fluorine, chlorine was sometimes added to determine its effect on the growth and decay of the ESR signal. In order to confirm faint details of the spectra obtained, many successive scans were done.

The procedure described above was used for both powders and crystals. The crystals which produced stable paramagnetic species were carefully removed from the reaction apparatus and mounted with plibond glue in a crystal holder. The exposure of these crystals to air did not affect the paramagnetic species - even the partly reacted $SrCl_2$ was no longer deliquescent. The holder consisted of three sides p, q, r which are mutually perpendicular to each other (i.e. one-half of a cubical box). A polystyrene rod was in turn attached perpendicularly to each of the sides and the crystal was rotated about the vertical axis which was perpendicular to the magnetic field. Spectra were obtained at 5 to 15 degree intervals with an accuracy of $\pm 2^{\circ}$.

GROUP I - HALIDES

A. Summary of Systems Investigated for ESR Signals

Table III

Solid	Type of solid sample	Treatment	ESR signals
NaCl & KCl	vacuum-sublimed powder	F_2	signal associated with Cl atoms and assigned as an H-center
	reagent grade powder; untreated	F_2	no signal
	single crystal (Harshaw)	F_2 & irradiation (room temp.)	no signal
KBr	vacuum-sublimed powder	Cl_2 & F_2	signal unidentifiable for lack of observable hyperfine structure
	single crystal (Harshaw)	Cl_2 & irradiation (room temp.)	no signal
KI	vacuum-sublimed powder	Cl_2	no signal

B. Reactions of NaCl and KCl with F_2

The vacuum sublimed particles of KCl and NaCl were prepared by the procedure described in section B of the Apparatus and Procedure section of this thesis. The surface area of these particles as measured (86) by the B.E.T. method using krypton adsorption at 77°K was found to be in the range of 20 to 36 m^2/g. Morrison and Harrison (87) using an electron microscope found that the particles appear as well formed cubes with sides of about 0.1 micron.

a) Analysis of the spectra

Figure 14 shows a number of spectra obtained in NaCl and KCl by treatment with fluorine and development in vacuo as described in detail in the kinetics section (c). Of the NaCl samples (a) and (b) contained the greatest amounts of coherent material and (d) appeared to be entirely randomly orientated. The KCl films broke up readily to give fairly well powdered samples. The five spectra in figure 14 are all adjusted to a standard microwave frequency ν = 9.4679 Gc/sec. and the scales at the bottom of the diagram indicate the position at various orientations of the center line and the line at nuclear magnetic number m_{12} = +1, for the H- center model.

The most conspicuous part of all the spectra is ABCD, which is qualitatively of the form to be expected (88) for a single line, the position of which is fixed by an anisotropic but axially symmetric g-factor. The known centres in single crystals with which will be compared with the present results are all close to axial symmetry; the conventional terminology, θ for the angle between the magnetic field and the molecular axis of the defect with subscripts $\perp$ and $\parallel$ to signify $\theta = 0^\circ$ and $\theta = 90^\circ$ respectively will be used. On this basis,

Figure 14 - ESR spectra obtained in F_2 treated NaCl and KCl

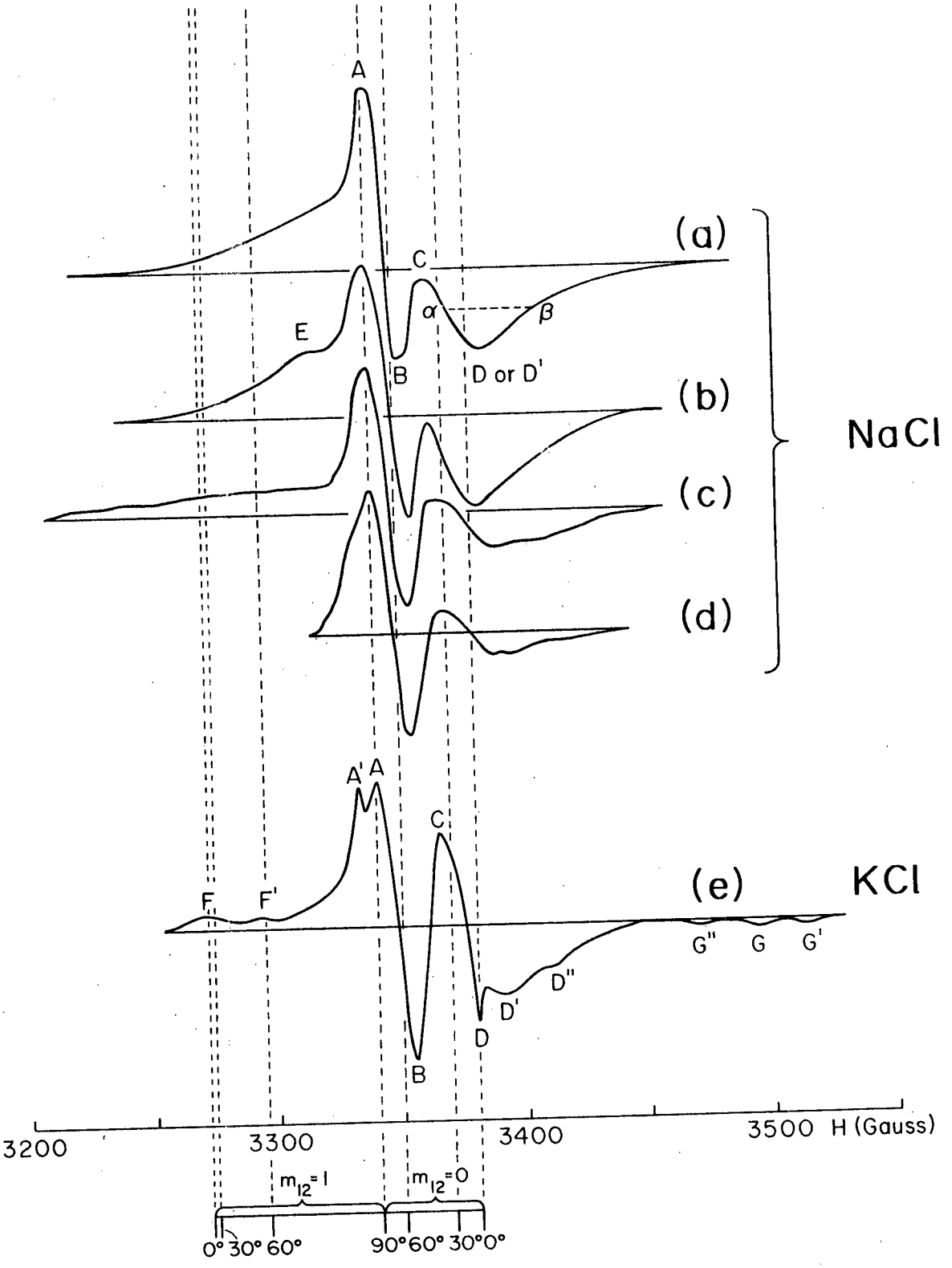

$g_\perp$ should be very close to A and $g_{||}$ fairly close to D; the latter position is somewhat uncertain, especially for NaCl, in which the region around D shows no resolved structure and it is not clear whether the peak corresponds to D or D' in the KCl spectrum. The g-values calculated from A and D (table IV) are consistent with the interpretation that ABCD is generated by a line without hyperfine interactions. Such structures as FCl^-, F_2^-, Cl_2^- (V_K) and Cl_4^{3-} (H) all have such a line, with g-values comparable to those calculated from the present spectra, except in the case of O_2^-. (In table IV the features indicated are peaks and troughs (single letter in first column) and spacings between them (two letters in the first column), the latter being expressed in gauss. Comparison with computed spectra (see section b) indicates that the values marked with * should be amended to : $g_\perp = 2.0231$, $g_{||} = 1.9995$, and $A_\perp^{34} = 4$.)

Further elucidation of the structure of the defect depends on the information which the spectra will yield on hyperfine interactions. The existence of these is most clearly seen in the KCl spectrum, Fig. 14e. I distinguish a "primary splitting", giving rise to the features marked F and G. This I call A^{12}, anticipating that I attribute the splitting to interaction with two Cl nuclei designated 1 and 2. All the features marked by letters with prime or double prime superscripts I consider to arise from "secondary splitting", which I attribute to interaction with two more distant nuclei 3 and 4, hence designate A^{34}.

The primary splitting at $\theta = 0^\circ$, A^{12}, calculated as FD, DG or $\frac{1}{2}$FG, is of the same order as $A_{||}^{12}$ in the V_K and H-centres in alkali chlorides, especially that for the H-centre in KCl. This value is on

$g_\perp$ should be very close to A and $g_{||}$ fairly close to D; the latter position is somewhat uncertain, especially for NaCl, in which the region around D shows no resolved structure and it is not clear whether the peak corresponds to D or D' in the KCl spectrum. The g-values calculated from A and D (table IV) are consistent with the interpretation that ABCD is generated by a line without hyperfine interactions. Such structures as FCl^-, F_2^-, Cl_2^- (V_K) and Cl_4^{3-} (H) all have such a line, with g-values comparable to those calculated from the present spectra, except in the case of O_2^-. (In table IV the features indicated are peaks and troughs (single letter in first column) and spacings between them (two letters in the first column), the latter being expressed in gauss. Comparison with computed spectra (see section b) indicates that the values marked with * should be amended to : $g_\perp = 2.0231$, $g_{||} = 1.9995$, and $A_\perp^{34} = 4$.)

Further elucidation of the structure of the defect depends on the information which the spectra will yield on hyperfine interactions. The existence of these is most clearly seen in the KCl spectrum, Fig. 14e. I distinguish a "primary splitting", giving rise to the features marked F and G. This I call A^{12}, anticipating that I attribute the splitting to interaction with two Cl nuclei designated 1 and 2. All the features marked by letters with prime or double prime superscripts I consider to arise from "secondary splitting", which I attribute to interaction with two more distant nuclei 3 and 4, hence designate A^{34}.

The primary splitting at $\theta = 0^o$, A^{12}, calculated as FD, DG or $\frac{1}{2}$FG, is of the same order as $A_{||}^{12}$ in the V_K and H-centres in alkali chlorides, especially that for the H-centre in KCl. This value is on

the one hand much too large to represent the interaction of an O_2^- ion with neighbouring ions of the host lattice, and on the other hand much too small to represent hyperfine interaction with a fluorine nucleus (table IV). The evidence is thus strong that the signal here described arises from a defect structure of chlorine atoms and is therefore relevant to our predictions from kinetics of chlorine exchange, (In a number of runs on both NaCl and KCl, a signal which is probably caused by an oxygen-containing impurity was obtained. This is a single narrow line, about 5 gauss wide, at g = 2.007. It appeared to be unaffected by fluorine and had no influence on the signal under discussion other than to abscure part of the spectrum around the point C.)

The secondary splitting is indicated as about 20 gauss at $\theta = 0^\circ$ by the distances from the points D, F and G to their "satellites" with prime superscripts. There is a possibility of confusion between splittings arising from more distant ions, as in the H-centre, and those arising from isotope effects within the Cl_2^- ion, particularly the species $(Cl^{35}Cl^{37})^-$. Since the nuclear spin of Cl^{37} is 17% less than that of Cl^{35} the degeneracics of the nuclear spin levels are lifted in the mixed-isotopic ion to give a splitting 17% of A^{12}, which at 0° is very close to the 20 gauss here observed. However, the lines for the mixed isotopic species are displaced from the corresponding $(Cl_2^{35})^-$ line by half-integral, not integral, multiples of the isotopic splitting (36). This is not what is here observed. These lines probably represent a secondary splitting like that of the H-centre rather than an isotope effect both for this reason and because, as discussed in detail below under "Computations", the intensity ratio of peaks F and A is wrong for the V_K centre and

Table IV

Important Features of Spectra and proposed assignments for H-center model.

Feature	Assignment			Tensor	Data for KCl	Known values in single crystals			
						H-center	V_k-center	$F_2^-(V_k)$	O_2^-
	m_{12}	m_{34}	θ	Component	(NaCl in brackets)	(KCl, 20°K)	(KCl)	(LiF)	(KCl)
A	0	0	90°	$g_\perp$	2.0251* (2.0256)	2.0223	2.0438	2.013	1.953
D	0	0	0°	$g_\parallel$	2.0015* (>1.9962)	2.0023	2.0010	2.003	2.436
F D	1, 0	0	0°	$A_\parallel^{12}$	107.5	109	101	887	-
D G	0,-1	0	0°	$A_\parallel^{12}$	112.5				
A'A	0	1, 0	90°	$A_\perp^{34}$	8.0*	2.9	-	-	-
A B	0	-	90°	$A_\perp^{34}$ and σ (not resolved)	13.3 (15.0)	-	-	-	-
D D'	0	0,-1	0°	$A_\parallel^{34}$	14.5	7.3	-	-	-
D D''	0	-1,-2	0°	$A_\parallel^{34}$	18.0 (1/2 $\alpha\beta$ = 18.5)				
F F'	1	0,-1	0°	$A_\parallel^{34}$	22.5				
G''G	-1	1, 0	0°	$A_\parallel^{34}$	20.0				
G G'	-1	0,-1	0°	$A_\parallel^{34}$	20.0				

requires a strongly anisotropic secondary splitting to account for it.

The proposed value $A_{||}^{34} = 20$ gauss is to be compared with the known value for the H-centre in KCl at very low temperatures, 7.3 gauss. The features representing secondary splittings and linewidths which remain to be discussed in the NaCl and KCl spectra likewise show marked broadening relative to low-temperature values. The region AB of the spectra, together with the partly-resolved peak A' in KCl, represents essentially the 90° spectrum, and the overall extent of this region is too large to be accounted for by the combined effect of primary splitting, secondary splitting and linewidth, if the 20°K H-centre values are used, i.e. $A_{\perp}^{12} \sim 0$ (degree of approximation not, however, specified), $A_{\perp}^{34} = 2.9$ gauss, linewidth = 0.8 gauss in KCl. The H-centre spectrum has not been studied in NaCl single crystals, presumably because the linewidth would be close to the V_K centre value of 4.5 gauss and hence the secondary splitting would not be resolved. In the spectra, if the region $\alpha\beta$ in NaCl and the region DD'D in KCl is to be interpreted as arising from a secondary splitting of about 20 gauss abscured by the linewidth, a linewidth of about 10 gauss in KCl or 20 gauss in NaCl seems to be indicated.

Although one cannot unequivocally assign the defect under study as an H-centre (the close similarity of V_K and H spectra, which arise from rather different variants of Cl_2^-, is enough to invite caution), the above comparisons of parameters at 20°K and room temperature agree very well with that assignment. The g-values and the primary splitting are essentially molecular properties of Cl_2^-, and hence likely to remain unchanged from 20°K to room temperature; but secondary splitting and linewidth involve coupling with nuclei outside the molecule-ion,

and are hence likely to be broadened by increasing thermal motion of the lattice. The broadening should be less for the secondary splitting than for the linewidth, since atoms 3 and 4 are weakly bonded to the Cl_2^- ion.

b) Computations

Most of the above argument does not depend on the results of a precise computation of the powder spectrum from the proposed parameters; but there are several considerations which make it desirable to attempt such computations. The degree of accuracy to which the g-values are given by points A and D should be determained. The extent to which the region A'AB can be analyzed into $A_\perp^{12}$, $A_\perp^{34}$ and linewidth should be established. The possibility of accounting for the part of the NaCl spectrum downfield of A in terms of partly-oriented material should be studied. Finally, the intensity rations of the various features of the spectrum are of some interest. For example, the type of spectrum shown in Fig. 14a or b, in which the negative peaks at B and D are of comparable size, is not uncommon; the spectrum of adsorbed O_2^- is another example (89). Yet the shape generated by a line narrow in comparison to the gap AD should have the peak at D markedly smaller than that at A; a large D peak is really an anomaly.

In a situation with as many variables as the present one, the establishment of the dependence of the powder spectrum on each requires many computations with trial values. For this purpose it was found necessary to use programmes severely restricted in their scope (i.e. written for the V_K and H situations only) but using very little computer time, rather than to rely on comprehensive but time-consuming programmes, one of which (90) was available and was used in one or two computations.

No programme was devised which was both sufficiently rapid and adequate in integrating over θ smoothly, but a programme which required about two minutes in an IBM 7040 computer was found useful especially for the KCl spectrum. The features essential to the characterization of the defect are given here.

Computations have been made for the $(Cl_2^{35})^-$ or $(Cl_4^{35})^{3-}$ ion only; and in the expression for the magnetnetic field at resonance H_{res} only terms linear in the magnetic quantum numbers m_{12} (sum of magnetic quantum numbers for nuclei 1 and 2) and m_{34} (the same, for nuclei 3 and 4) are retained:

$$H_{res} = (h\nu/g\beta_o) - (g_o/g)A^{12}m_{12} - (g_o/g)A^{34}m_{34} \qquad (1)$$

where $$g^2 = g_{||}^2 + (g_{\perp}^2 - g_{||}^2)\sin^2\theta \qquad (2)$$

and $$(A^{12})^2 = (A_{\perp}^{12})^2 + \left((A_{||}^{12})^2 - (A_{\perp}^{12})^2 \right)\cos^2\theta \qquad (3)$$

and a similiar expression gives the angular dependence of A^{34}. In table IV, and throughout the preceding section, I have written A^{12} or A^{34} for quantities which should strictly have the factor (g_o/g) attached to them; but for the present work it is permissible to ignore this factor, since the error thus introduced is never greater than about one gauss, and is comparable to other approximations in the treatment such as the neglect of terms in m^2 and the lifting of degeneracies in m_{12} by second-order effects which become noticeable (36) in single-crystal spectra close to 90°.

At any fixed orientation θ, the spectrum of a V_K center consists of seven lines, with the spacing A^{12} and intensities in the ratio 1:2:3:4:3:2:1, corresponding to values of m_{12} from +3 to -3; i.e. the

degeneracy associated with m_{12} is $(4 - m_{12})$. In the H-center, each line is split into a similar group of seven described by the quantum number m_{34}; and the lines having Gaussian shape (36), with half-width σ at the point of maximum slope, the intensity of micromave absorption at magnetic field H is given by

$$I(\theta) = \sum_{m_{12}=3}^{-3} \sum_{m_{34}=3}^{-3} (4 - m_{12})(4 - m_{34}) \exp\left(-(H-H_{res}(m_{12},m_{34}))^2/2\sigma^2\right) \qquad (4)$$

If in a powdered sample of n particles, a number dn have orientations between θ and $\theta+d\theta$, the probability $P(\theta)$ is defined by $dn = nP(\theta)d\theta$. In a random powder, $P(\theta) = \sin\theta$. The problem of computing a powder spectrum is then the evaluation of the intergral

$$I = \int_0^{\pi/2} I(\theta)P(\theta)d\theta \qquad (5)$$

and the observed derivative-of-absorption spectrum is dI/dH as a function of H. In the programmes which have been used most extensively, $I(\theta)$ is calculated according to equations (1) to (4) for a number of values of θ spaced at equal intervals, usually 1°, and the results are summed in a histogram of I against H.

The effects of preferential orientation on the powder spectrum may be computed by including in $P(\theta)$ a suitable function to describe the preference. Thus, for example, I have considered the possibility that the defects in each crystal are oriented at random in all possible directions of the type (110), like the V_K and H centers, but that the coherent material in the solid samples might have a tendency for (110) to be alligned

parallel to the field H. In this circumstance, a function showing a preference for the angles 0°, 60°, and 90°, in the ratios of 1:4:1 is needed. Accordingly I have written

$$P(\theta) = \sin\theta + f(10^2 x^4 + 0.4(2^{-1/2} - x^{1/4})) \qquad (6)$$

where $x = \cos\theta\,(1 - \cos\theta)$. The parameter f increases with the fraction of oriented material in the sample. the function multiplied by f has fairly sharp maxims at 0°, 60°, and 90°, the last-mentioned being somewhat underweighted. A similar function could be devised to represent any desired orientation.

In considering in qualitative terms the features of a powder spectrum, it is perhaps best to think in the first instance of one line (with small linewidth) and the intensity I_m contributed to the spectrum by this line at any value H of the magnetic field. I_m is proportional to $P(\theta)d\theta/dH_{res}$, i.e. a line gives the largest contribution where it is moving most slowly as θ changes. Thus, for example, every line in the spectrum, with or without hyperfine interaction, produces a noticeable feature in its 0° position, because although $P(\theta)$ is zero at 0° in a random sample, $dH_{res}/d\theta$ is also zero; but at 90°, the center line of the spectrum is stationary and gives a prominent peak, while the hyperfine lines are moving rapidly and contribute very little. In my example, computations showed that the shape of the region A'AB of the spectrum is very insensitive to $A_\perp^{12}$, which consequently cannot be found with any accuracy from my results and was taken as zero (H-center value at 20°K). The splitting A^{34}, on the other hand, changes sufficiently slowly with θ to produce marked effects in this region of the spectrum.

Conclusions from computed spectra are as follows:-

(a) A V_K center should give a powder spectrum with two prominent lines each like AB, of roughly equal intensity. The reason for this is that the line at $m_{12}= 1$ is subject to two motions as θ changes, the downfield motion of the center of the spectrum opposed by the diminuation of A^{12}, and in consequence is almost stationary over a wide range of θ. Thus it becomes as prominent in the powder spectrum as the center-line $m_{12}= 0$.
(b) The H-center model, with strongly anisotropic secondary splitting, gives a spectrum similar to that observed in KCl (figure 14e), in which the region A'AB is the most prominent feature of the spectrum, and the features F, F', A', A B, D, D', D'', G'', G, and G' are all present in the computed spectrum although the relative intensities of the experimental spectrum are not precisely reproduced, and the integration over θ is not smooth enough for the identification of the smallest features, G'', G, G', to be absolutely certain. The features which are most important in establishing the values of the components of the g and A tensors, A, D, F, G, F', G', and G'' are uniformly about 3.5 gauss downfield of the expected position, so that in the experimental spectrum $g_\perp$, for example, is to be located 3.5 gauss upfield of A. This means that the g-values in table I should all be corrected downwards by 0.0020, but the splittings are estimated correctly. There is one exception: computation shows that the gap A'A is not, as anticipated, equal to $A_\perp^{34}$, but has about twice that value, so that the value given for $A_\perp^{34}$ in table I must be halved. The final values for the parameters of the defect in KCl are:-

$$g_\perp = 2.0231 \pm 0.001$$

$$g_\parallel = 1.9995 \pm 0.001$$

$$A_\perp^{12} \quad \text{uncertain}$$

$A_{||}^{12} = 110 \pm 3$

$A_{||}^{34} = 20 \pm 3$

$A_{\perp}^{34} = 4 \pm 1$

$2\sigma \sim 10$

(c) Apart from the prominent feature D, which is fortunately the important feature in the determination of $g_{||}$, the shape of the spectrum in that region is very sensitive to the precise values of the parameters, and $g_{||}$ cannot be determined very precisely from the spectra like those obtained for NaCl, in which this region is completely unresolved.

(d) The intensity ratios, especially of A, B, and D, are roughly correct for completely random orientation in spectra (c) and (d) for NaCl. Even in the KCl spectrum, D is proportionately somewhat too large, and in the NaCl spectra (a) and (b) it is very much too large. The dependence of the shape of the spectrum on orientation distribution is not simple. Thus it might be thought that the most probable angle could be deduced from the positions of C (generated principally by the lines $m_{12} = 0$) and E (figure 14b from $m_{12} = 1$); but the scales at the bottom of figure 14 indicate that these two positions do not give a consistent result for the most probable angle, which is indicated by C as less than 45° and by E as about 75°. However, computations using the function of equation (6), with 60° as the most probable angle, reproduced the section BCD of spectra (a) and (b) very well. The part of the spectrum downfield of A is very sensitive to the values taken for secondary splitting and linewidth, and many reasonable values give a pronounced dip, instead of a rise, in the region of E. To reproduce the observed spectra, it is necessary that the lines $m_{12} = 1$, $m_{34} = -1$, -2 should lie in the region of E and that the linewidth should be sufficient to destroy the resolution of the hyperfine

splitting even at $\theta = 0^{\circ}$. For a full study of this point it is necessary to carry out an extensive set of computations with a wide range of values of $A_{\perp}^{12}$, $A_{||}^{34}$, $A_{\perp}^{34}$, and σ, which would be a project in itself.

c) Kinetics

Contrary to expectation, the ESR signal did not appear during the exposure of the alkali chloride to F_2, but shortly after the fluorine was pumped out. The growth of the signal sometimes started immediately after removal of fluorine and sometimes after an induction period of a few minutes. Figure 15a shows two separate runs, one (A) in which a small signal appeared during contact with fluorine and started to grow immediately upon evacuation, and one (B) with an induction period. Run A is from the work of Adams referred to in the introduction to this thesis (section A(c)) and run B is from my work. The two growth curves are superimposable from the start of the rise up to the point of inflection. Figure 15b shows plots of log(peak height) against time for one of these curves (B) and another similar reaction (C), suggesting that the peak height varies as exp(+kt), which would indicate that the defect is formed auto-catalytically. Since the growth period is short, quantitative results to establish the rate law unequivocally are difficult to obtain. The reaction does not appear to be markedly affected by F_2 pressure (between 14 and 40 cm Hg) or time of contact (from 3 to 30 minutes). The entire experimental procedure could be repeated several times with similar results, except that the rate of growth of the peak and its maximum size were not reproducible. The best spectra for study of both spectroscopic details and kinetics were obtained sometimes on the first fluorination, sometimes on the second or third. The reaction of the solid with fluorine

Figure 15 - Growth and decay of the ESR signal after F_2 treatment

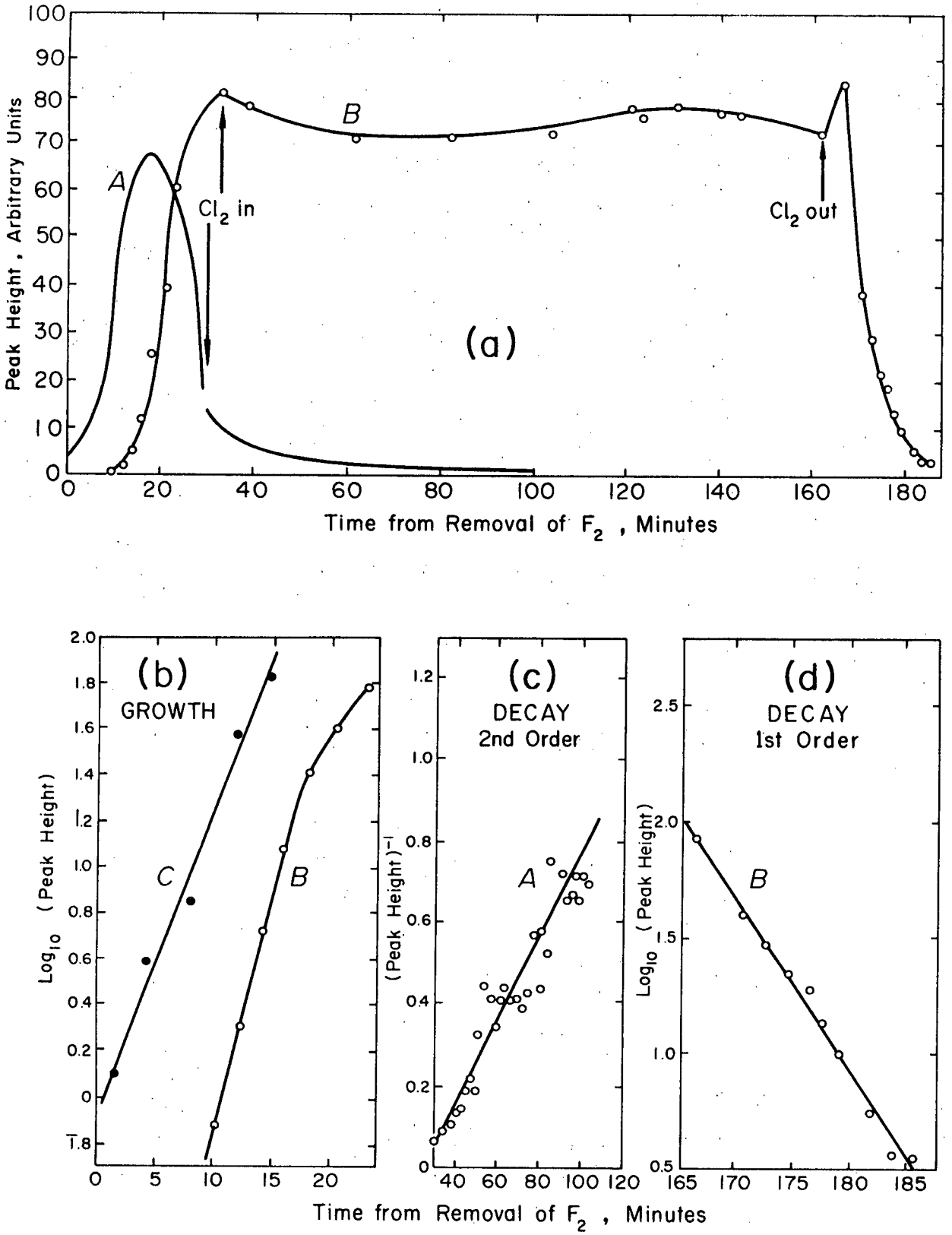

was remarkably slow. In the preliminary work of Adams, two samples were analyzed gravimetrically for fluoride after the experiment. One, after a single fluorination, was found unreacted within the limits of error (about 2%) and another, after several fluorinations of several minutes each at 40 cm Hg, was 25% converted to NaF. (As was previously (16) reported, remarkably low reactivity with F_2 was noted for samples of powdered NaCl of a different type).

The growth of the signal was usually followed by the predicted decay, which was usually very rapid and, as predicted, was slowed down or even arrested altogether by the presence of Cl_2 gas. This is to be interpreted in terms of blocking by Cl_2 of sites at which two defects could combine to desorb a Cl_2 molecule. In the previous detailed analysis of exchange kinetics (17) these sites were considered to be anion vacancies forming part of the structure of the defect with the unpaired spin. This was postulated as analogous to the F_3^{2-} ion (V_t center) known (38) in LiF. Since the present study seems to rule out this structure for the defect, indicating instead an H-center structure, which should not be associated with anion vacancies, the previous kinetic schemes may require some ammendment, with less emphasis placed on vacancies as a means of migration at room temperature. It has been suggested speculatively (39) that positively charged halogen atoms may be mobile even at extremely low temperatures in the KCl lattice, and that these may be responsible for the formation of H-centers.

Whatever amendments to the mechanistic schemes in the bulk of the solid may be necessary, it is still reasonable that desorption of Cl_2 from pairs of defects combining at the surface may be prevented by preadsorption of Cl_2 in surface vacancies; and the prediction that the

decay of the defect should exhibit second-order kinetics is still valid. The experimental results, however, show that, as exemplified by figure 15d, the decay is first-order when it occurs in the absence of chlorine. Decay in the presence of chlorine was more difficult to study, since it required the introduction of chlorine at precisely the right stage in the decay for the subsequent decay to proceed at a convenient rate. Figure 15c shows that the decay represented in curve A of figure 15a follows a second-order law.

The growth and decay processes, and the blocking of the former in the presence of F_2 and the latter in the presence of Cl_2, are both explicable in terms of mechanisms involving surface defects. For the autocatalytic growth, it is suggested that fluorine enters into some state of combination with surface Cl^-, but that the oxidation of Cl^- with release of the Cl atom (probably positively charged) into the bulk cannot be completed until a surface vacancy is available to receive F^-. During contact with the gas, these vacancies may be blocked by molecularly-adsorbed F_2. On pumping out, they are made available, and the reaction of chlorine-fluorine complexes commences, producing surface F^-, positive holes in the bulk, possibly gaseous molecules, and further anion vacancies in the surface, leading to the autocatalytic effect.

For the decay processes, the first-order law suggests that the arrival of a single defect at the surface is the rate-determining step. This may indicate rapid surface migration by way of surface vacancies. When many of these are blocked by the presence of chlorine, the decay requires the simultaneous presence of two electronic defects at an immobile surface site, giving rise to the second-order law.

By contrast, my results suggest an almost complete absence of vacancies in the bulk of the vacuum-sublimed crystals, if the assignment of the electronic defect under study as an H-center be accepted. (There is actually no known ESR signal in an alkali halide single crystal associated with the anions of the pure crystal and representing a defect with high-temperature stability). There is no obvious reason why this center should be intrinsically unstable at high temperatures in the perfect lattice; and the mechanism proposed (7) for its destruction on warming above 20°K involves transfer of an electron to another defect, an F-center. My material does not contain F-centers, because the electronic damage was carried out oxidatively, and not by X-irradiation. This in itself might be sufficient to explain the possibility of observing the H-center in this material; but I have not been able to obtain any corresponding signal from single crystals or ordinary coarsely-powdered NaCl, which suggests that I am concerned with a special property of the vacuum-sublimed material. This property may be a very low vacancy concentration, caused by efficient equilibration of the crystals at room temperature as they grow on the water-cooled quartz condenser. A conspicuous feature of the earlier kinetic work[10,17] was that particles of similar size (about 1000 Å) prepared by sublimation into a stream of nitrogen were active for chlorine exchange at room temperature only on the surface, not in the bulk. Since the nitrogen gas was probably at a fairly high temperature in the region of condensation, these particles might readily be formed with higher defect concentrations.

The mechanistic schemes proposed previously also indicated

the removal of vacancies from the bulk by adsorption of Cl_2 at the surface. For Cl_2, this would be reversible on pumping out; but for F_2 gas, the sequence of steps suggested above locks the vacancies in the surface as they become occupied by F^- on pumping out. It is possible that this process will effectively dispose of a low vacancy concentration in the bulk, but will not remove the vacancies completely if the initial frozen equilibrium state is much above room temperature.

These considerations indicate that the relationship between vacancies, electronic defects and chemical reactivity may not be a simple one. I suggest that electronic defects with unpaired spins are readily formed in vacuum-sublimed material because it consists of essentially perfect crystals devoid of trapping sites; and that the formation of electronic defects leads to a high reactivity for chlorine exchange. Yet it is unusual to conclude that the more perfect the crystal, the higher its reactivity; and for the chemical reaction with F_2, this material was noticeably unreactive.

GROUP II - HALIDES

A. Summary of Systems Investigated for ESR Signals

Table V

Solid	Type of solid sample	Treatment	ESR signals
$SrCl_2$	reagent grade powder; single crystal	F_2	signal associated with Cl atoms and assigned as an interstitial Cl atom.
	single crystal	irradiation (low temp.)	F-center-like spectrum observed, but signal not yet identified.
		irradiation (room temp.)	no signal.
$MgCl_2$	reagent grade powder	F_2	no signal.
	reagent grade powder	thermal decomp.	signal, basically of six lines, believed to arise from an impurity such as Manganese.
$BaCl_2$	reagent grade powder	thermal decomp.	six line spectrum attributed to Manganese impurity.

B. Reaction of $SrCl_2$ with F_2.

Both powders and single crystals of $SrCl_2$ were used in the reactions with fluorine. The powder samples were made by heating the hydrated $SrCl_2$ (Mallinckrodt analytical reagent grade $SrCl_2 \cdot 6H_2O$) at about 120°C in a quartz tube while pumping the water off with a rotary vacuum pump. The samples were heated for about 16 to 20 hours and then sealed off in storage bottles until used.

The single crystals were made by two methods:

(1) by heating the sample under vacuum at a temperature (120°C) which is sufficient to remove the waters of hydration. The sample was then melted and cooled very slowly over a period of about two days. The crystal formed by cooling the melt slowly was cleaved along rather ill-defined cleavage planes.

(2) by the Bridgman-Stockbarger technique (91). The crystals grown by this method were generously donated by Dr. J. A. Morrison of the National Research Council. The starting material was $SrCl_2 \cdot 6H_2O$ which was melted with $PbCl_2$ in a graphite crucible. The $PbCl_2$ was used to react with the water and prevent the formation of Sr oxide and hydroxide. The excess $PbCl_2$ and the Pb oxide and hydroxide formed are more volatile the $SrCl_2$ and therefore evaporated off. The melt in the graphite crucible was thenlowered through a sharp temperature gradient. A crystal nucleus formed first at the tip (bottom of the crucible) and continued to grow as the crucible was lowered until the entire melt solidified.

The main precaution in handling the $SrCl_2$ samples was to

keep them out of contact with moist air for $SrCl_2$ is deliquescent. Therefore, the transferring of the samples was carried out in a dry box or in vacuo.

a) Results

Figure 17 shows the ESR spectra obtained in $SrCl_2$ by treatment with F_2. The spectra are adjusted to a common microwave frequency ν = 9.2442 Gc./sec.

The room temperature reaction of $SrCl_2$ with fluorine produces a paramagnetic species in powder samples as well as single crystals. The signal due to this center was found to grow in the presence of fluorine; and when the fluorine was removed the growth of the signal stopped. In reactions with powdered samples as wellas single crystals there was an initial rapid growth of the signal (in some cases after an induction period varying from 5 to 15 minutes) followed by a slow growth which continued for as long as four hours (reaction was not followed for a longer time). The fluorine pressure usually used was 29 cm of Hg since it was found that when higher pressures were used the reaction proceeded to such an extent that the single crystal spectra looked exactly like the powder spectra (Fig. 17a).

The reaction of F_2 with the single crystals of $SrCl_2$ initially starts with the appearance of nuclei (presumably of SrF_2) on the surface of the crystal which spread out quickly covering the whole surface of the crystal. After the reaction had been stopped by removal of F_2, there was usually a sharply defined interface between the reacted region (which is pale yellow, probably on account of the presence of Cl_2 or ClF) and the remaining unreacted crystal. The center

giving rise to the ESR spectrum was found by sectioning the solid to be present in the reaction interface and not in the deeper layers of the unreacted crystal. A weak signal was also found in the outer reacted layers, but it did not appear to have strongly-developed orientation-dependent structure. The species formed was found to be very stable even when the crystal was exposed to air for periods up to even a month. Evidently the reacted layer of SrF_2 protects the inner material from moist air.

The spectra in figure 17 can be interpreted in terms of a model in which the resolved hyperfine interaction of the unpaired electron is with a Cl atom with a nuclear spin of 3/2 (a more detailed explanation of the model is given in the discussion section (b)). The spectra are based on sets of four almost equally spaced lines of equal intensity; but such a set of lines is not seen undisturbed in any spectrum which seems to indicate that the centers exist in a range of situations in the crystal lattice (as discussed below, the variable displacement seems to be translational rather than orientational). The nearest approach to a simple four line spectrum is seen in the lines EFGH in figure 17b, in which H is parallel to a four-fold axis of the crystal.

A rough computation showed (see figure 16) that the main features of the powder spectrum of figure 17a can be accounted for by a hyperfine tensor and a g-tensor which are both axially symmetric about the x-axis. This sort of model reproduced the seemingly extra peak E as well as the peaks ABC and D. The splitting of the four lines ABCD in the powder were found to be about 80 gauss.

The single crystal spectra showed, however, that the defect was not axially symmetric about any axis of rotation of the single crystal. This indicates that the hyperfine tensor has different components (A_x, A_y, A_z) in three mutually perpendicular principal directions, whichare identified by the changes in the spectrum on rotation of the crystal as a four-fold axis (z) and two two-fold axes (x and y) of the crystal.

The directions and values of A_x and A_z were found by rotating the crystal to locate special orientations in which maximum and minimum splittings were observed (refer to Fig. 17b and c). When H was parallel to a four-fold axis (Fig. 17b) A_z was found (spectrum EFGH) to be 16 gauss and with H parallel to a two-fold axis A_x was found (Fig. 17c, ABCD) to be 92 gauss (which is the largest component of the hyperfine tensor). This spectrum also should show A_y directly but due to the complexity of the spectrum the value of A_y had to be confirmed by a more detailed analysis of the spectra of Figs. 17b and 17c . If one assumes that the defects in a single crystal are randomly orientated in the sense that the x-axis can be any two-fold axis, any one orientation of the crystal presents the defect to the magnetic field in two or three distinct orientations, so that the overall spectrum is composed of two or three groups of four lines. Table VI shows for the special orientations of Fig. 17b and 17c , the hyperfine splitting which should be observed and the relative abundance of the defects oriented to give each splitting. The table also gives the direction cosines (ℓ,m,n) of the magnetic field with respect to the x, y, z axes of the defect.

Figure 16 - Computed spectrum of the defect in $SrCl_2$
(10 gauss linewidth)

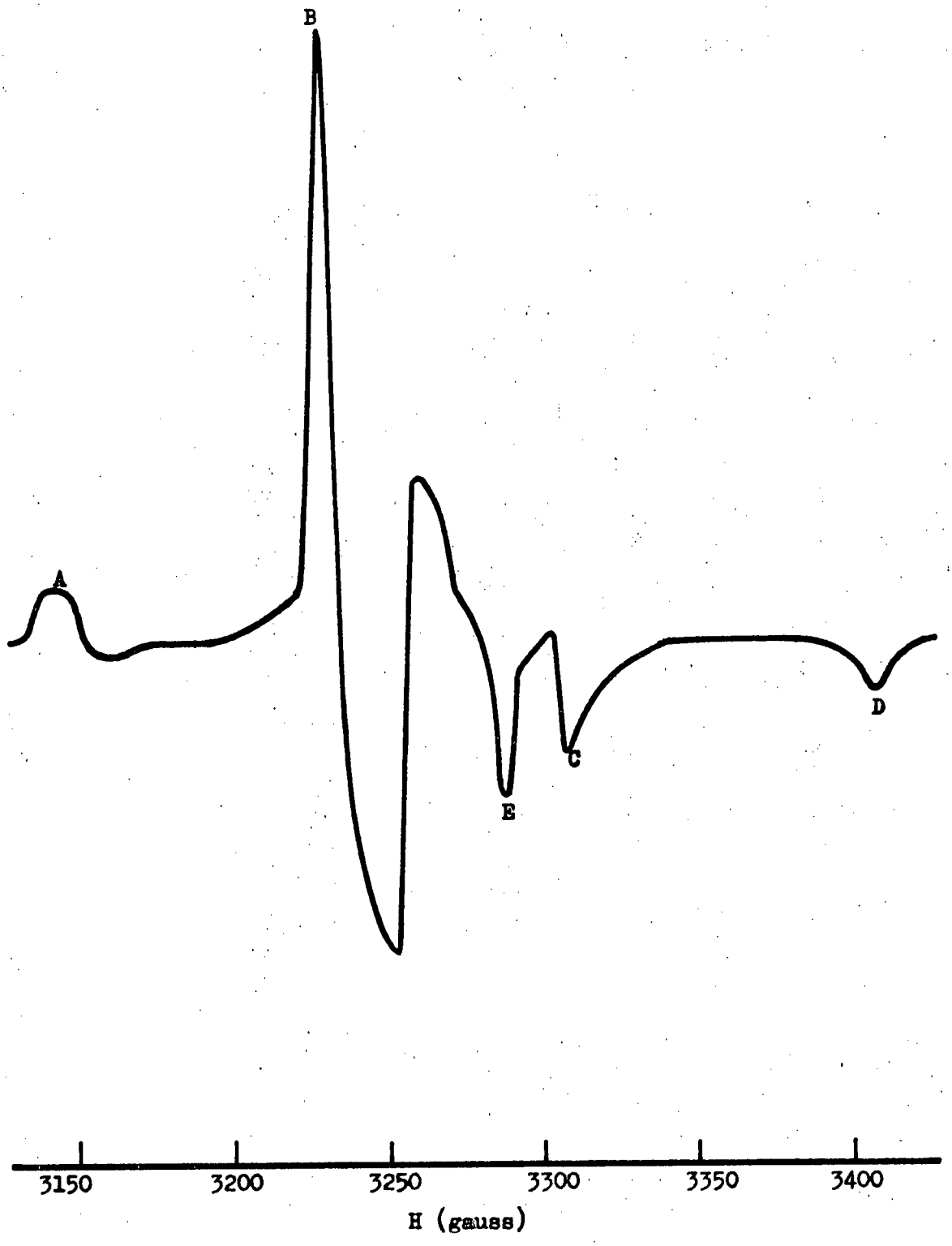

Table VI

Direction of magnetic field	Direction cosines (ℓ, m, n)	Hyperfine splitting $A=(\ell^2A_x^2+m^2A_y^2+n^2A_z^2)^{1/2}$	Peaks	Abundance
H parallel to C_4 (figure 17b)	(0 , 0 , 1)	A_z	EFGH	1
	$(1/\sqrt{2}, 1/\sqrt{2}, 0)$	$(1/2A_x^2+1/2A_y^2)^{1/2}$	ABCD	2
H parallel to C_2 (figure 17c)	(1 , 0 , 0)	A_x	ABCD	1
	(0 , 1 , 0)	A_y	EFGH	1
	$(1/2, 1/2, 1/\sqrt{2})$	$(1/4A_x^2+1/4A_y^2+1/2A_z^2)^{1/2}$	IJKL	4

It is now possible to evaluate the component A_y from three separate four-line spectra. The agreement between these three spectra of the A_y value makes it possible to determine that the spectrum in figure 17c which displays A_y directly is EFGH . The value of A_y = 40gauss was given by all three sets of lines.

Since the g-factor tensor ($\underline{g}$) and the chlorine hyperfine splitting tensor ($\underline{\underline{A}}$) are assumed to have the same principal axes, the principal components of the g-tensor can be obtained from finding the mid-points of the four-line spectra corresponding to A_x, A_y, and A_z . The g values and A values obtained for the defect are tabulated below in table VII with the limits of their accuracy.

Gardner (92) studying Cl atoms produced by irradiating Cl_2 adsorbed on silica gel obtained values for the components of the g-tensor, $g_x = 2.003 \pm 0.001$ and $g_y \sim g_z \sim 2.012$ are similar to my values

Table VII

Parameters of the defect	
g_x	$= 2.0028 \pm 0.0010$
g_y	$= 2.0194 \pm 0.0020$
g_z	$= 2.0162 \pm 0.0010$
A_x	$= 92 \pm 1$ gauss
A_y	$= 40 \pm 2$ gauss
A_z	$= 16 \pm 1$ gauss

for a Cl atom in a $SrCl_2$ lattice. My single crystal results permit a more precise analysis of the defect and its effect on the chlorine 3s and 3p orbitals than was possible in Gardner's work on randomly-oriented Cl atoms . (A closer analysis of the g values and A values will be given in the next section (b) under Discussion; and comparative values of parameters for Cl atoms in three different situations are given in table X).

As previously mentioned the lines obtained even in the single crystal have powder like shape. This is illustrated in figure 17b and 17c by the spectra having apparently the positive half of the normal derivative peak at low field and the negative half of the peak at high field. A complete analysis of the linewidth is not possible both because of this "powder" character and because of incomplete resolution of some of the lines in the spectra (Fig. 17c). The linewidth, however, is clearly anisotropic and there is a strong indication that the minimum linewidth

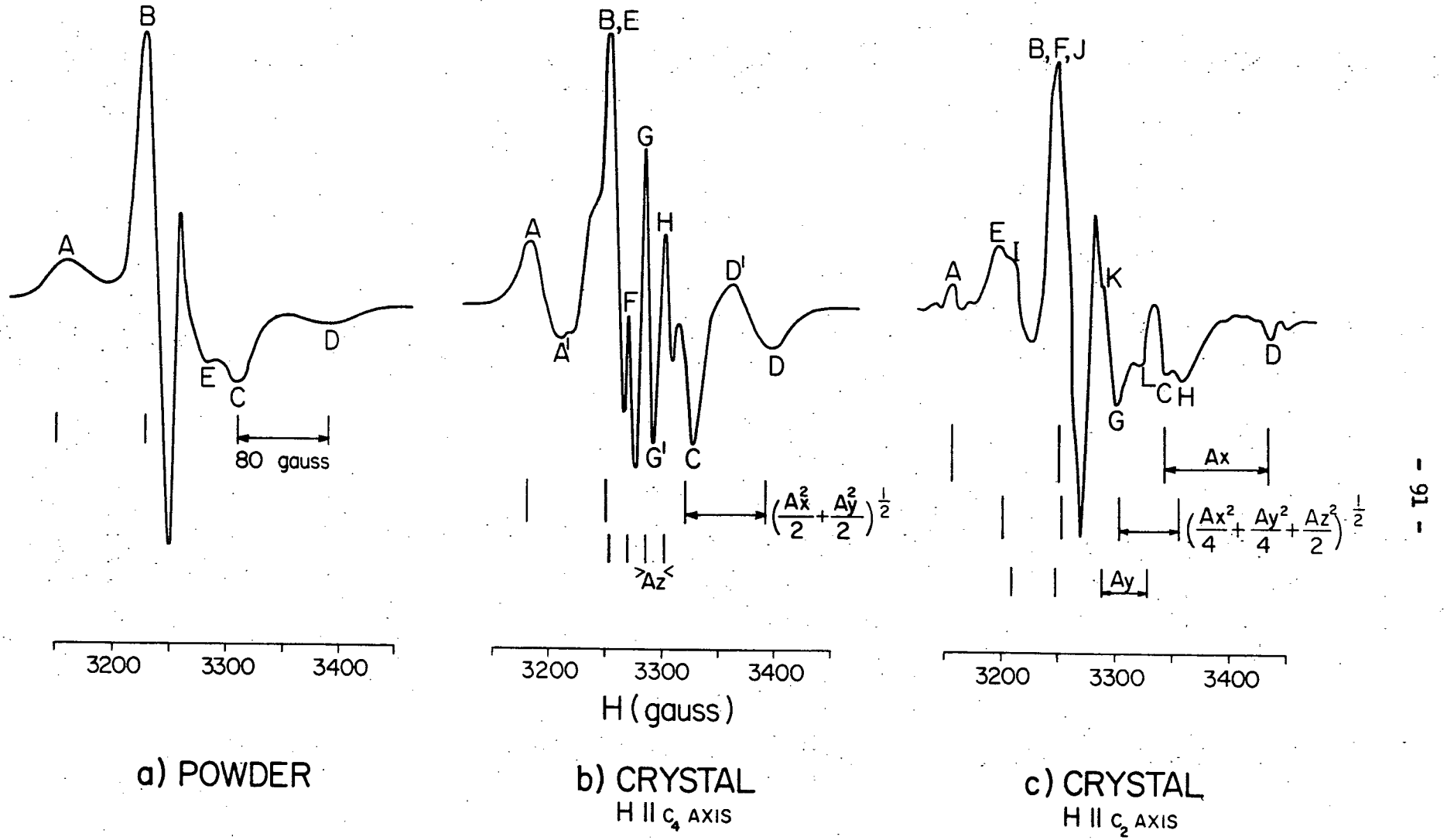

Figure 17 - ESR spectra obtained in F_2 treated $SrCl_2$

is seen along the z axis (figure 17b, spectrum EFGH) while the maximum linewidth is seen along the four-fold axes $\perp$ to z which will be called xy. The linewidth $2\sigma_z = 7 \pm 2$ gauss is estimated as, for example, the interval GG' and the linewidth $2\sigma_{xy}$ as AA' or DD' (all on figure 17b).

Since the lines are not normal derivative peaks the values obtained for the hyperfine components will depend on where measurements are taken on the "powder-like" peaks. In measuring the hyperfine component A_x using the (powder type) peaks ABCD in figure 17c one gets a maximum value of 92 gauss when measuring from the tops of the low field peaks to the bottom of the high field peaks. In figure 17b the peaks appear to be an intermediate between "powder peaks" and "single crystal peaks" in character. The value of A_y, however, shows that the peaks are close to "powder" peaks since a reasonable value of A_y was obtained by taking the hyperfine lines as the tops of A and B and the bottoms of C and D but not by taking those lines to be at the points where the spectrum returns to the baseline (or half-way between, e.g. A and A'). The component of the g-tensor g_y does not change, within experimental error, using any of the above methods for determining A_y.

The relative intensities of the lines also indicate powder character. The intensities of the lines in a single crystal should be equal but this is not the case. The inner lines in each of the four-line groups are generally more intense than the outer ones. The intensity ratio of the different groups of lines was found to be roughly consistent with the expected abundances shown in table VI. For example, in figure 17b peak D should be twice as intense as peak H, the ratio calculated from (peak height times linewidth) is 2.3 to 1; and in figure 17c the prominence of the peaks IJKL is roughly consistent with the abundance of four times

greater than that of ABCD or EFGH.

b) Discussion

It is necessary to know the crystal structure of the lattice one is dealing with when attempting to construct a model of the defect under study. Strontium chloride has a fluorite lattice, with a lattice constant of 6.977 Å at 26°C. Each anion is surrounded tetrahedrally by four cations at a distance of 3.021 Å and octehedrally by six anions at a distance only 16% greater, 3.488 Å. The anisotropy as shown by the spectra in figure 17 show clearly that the chlorine atom responsible for the ESR signal cannot be in the highly symmetrical environment of a normal anion site i.e. a tetrahedral hole of the cation sub-lattice. Neither can it be in an octahedral hole, which would otherwise be an obvious place for an interstitial atom. Both of these positions would give isotropic interaction with the neighbouring anions and cations. Any displacement whatever of the Cl atom from an anion site must bring it within a distance less than 3.488 Å of at least one Cl^- ion. It is thus surprising that the ESR spectra show no evidence of a strong covalent interaction with one or more neighbouring anions leading to the formation of such structures as Cl_2^- which are well-known in alkali chlorides (36,39) i.e. there is no indication that the spectra might be basically 7-line like the V_K-center. Estimates of the probable bond length in a free Cl_2^- ion range (93,94,95) from 2.16 to 2.70 Å and the molecule-ion forms readily in KCl in which the separation of anion sites is 4.450 Å.

One is therefore led to propose the presence of an anion vacancy adjacent to the neutral Cl atom. This would permit the atom to

move from an anion site in a direction which increases its distance from all other anions i.e. towards the vacancy along a four-fold axis. This direction is identified as the z axis, along which both the hyperfine interaction and the linewidth have their minimum values.

The linewidth in colour centers has been attributed mainly to unresolved hyperfine interaction between the center and its nearest neighbours (36,39,70). In the $SrCl_2$ defect the nearest neighbours to the Cl atom are two Sr atoms which have no nuclear spin (there is a 7% abundance of Sr^{87} with I= 5/2 but it is of such low concentration that its effect may not be seen). The next nearest neighbours, the Cl^- ions, must therefore by their interaction with the Cl atom cause the observable linewidths. It is known that the closer the ions are to the defect the stronger is the interaction and therefore the larger the linewidth; on this basis it is possible to correlate the linewidth with the distance between the defect and the surrounding neighbouring anions. The closest anions to the defect lie, relative to the anion site from which the Cl atom is displaced, along the four-fold axes perpendicular to z which may be designated $(x \pm y)$ since they bisect the angles between the two-fold axes x and y. The maximum linewidth , as seen in figure 17b designated ABCD, was observed with the magnetic field oriented along the direction $(x \pm y)$. The minimum linewidth observed with H parallel to the z axis is of course consistent with the absence of an anion neighbour in that direction. On this basis the linewidth of ABCD in figure 17c which is due to the anions should be equal to some value between $2\sigma_{xy}$ and $2\sigma_z$ since the anions are closer than for the interaction causing $2\sigma_z$ but farther away from the Cl atom than the interacting Cl^- ions causing the linewidth $2\sigma_{xy}$.

i) Model of the defect

We must now consider two possibilities, both illustrated in figure 18. (In the figure the solid circles represent species lying in that plane. For each dotted circle there are two ions, in planes lying $\pm a_o/2\sqrt{2}$ above and below the plane of the diagram. X marks vacant anion sites.) The Cl atom may lie exactly half-way between two anion sites and hence at the mid-point of the line between two neighbouring cations (figure 18b), or it may lie in an intermediate position as shown in figure 18a. In either case, the 3p orbital of the Cl atom oriented along the cation-cation line should be strongly stabilized electrostatically and hence doubly occupied in the ground state. Thus the two-fold axes x and y are not equivalent in respect of the environment of the displaced atom. Since the high value of A_x and the close correspondence of g_x to the free-electron value (g=2.0023) indicate that the half-filled state is p_x, the line of the two nearest-neighbour cations is identified as the y axis.

The relative stabilization of p-states in the other two principal directions is most easily visualized first in the situation of figure 18b. P_z is oriented towards two tetrahedral holes of the cation sublattice, marked X in the diagram, which are the normal anion sites of the $SrCl_2$ lattice. P_x is oriented towards the normally unoccupied octahedral holes, and should be somewhat less stabilized than p_z in conformity with the experimental indication that p_x is the half-filled state. The crystal field splitting of the p-orbitals is presented below. Figure 19 gives an energy level diagram for the $3p^5$ case (it also includes the 3s orbital the position of which is uncertain).

Figure 18 - Models of the defect in $SrCl_2$

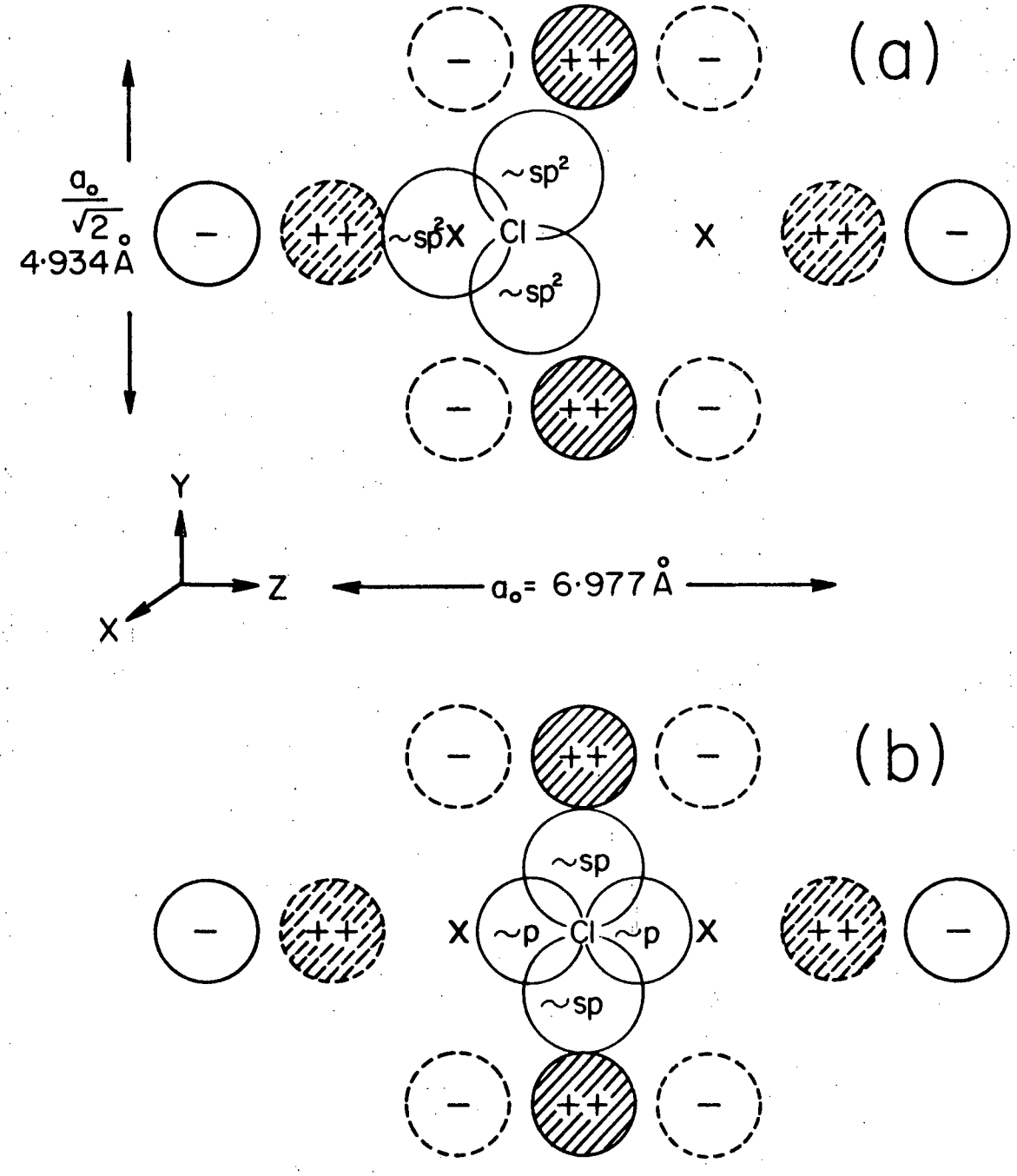

Figure 19

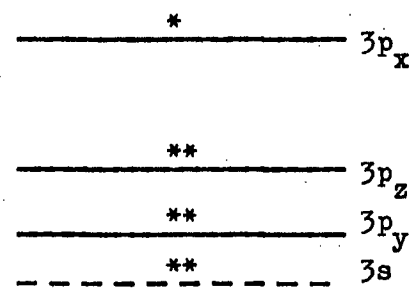

It is useful to think of the defect as a molecule composed of the Cl atom and two neighbouring cations, with its symmetry modified by the remainder of the environment, particularly the cations which determine the positions of the octahedral and tetrahedral holes referred to above. (Evidence on the involvement of orbitals on the nearest cations is assessed in detail below.) On this basis, the arrangement of figure 18a may be thought of as a C_{2v} molecule, and it is useful to compare my results with, for example, the study by Cole (96) of ClO_2 molecule produced as a defect in $KClO_4$. The coordinate system I use corresponds to that used by Morton (97) and later by Carrington andMcLachlan (60) in discussing ESR spectra of C_{2v} molecules; Morton changed the assignment of coordinates used by Cole for ClO_2 on the basis that the unpaired electron was probably in an orbital of b_1 symmetry rather than a_1 as assumed by Cole. My assignment of the unpaired electron to the p_x orbital, perpendicular to the plane of figure 18a, likewise represents b_1 symmetry.

If the geometry of the defect is as shown in figure 18b, its symmetry is nominally higher: $D_{\infty h}$ if one thinks of three atoms only, modified to D_{2h} by the rest of the environment. This symmetry has three twofold axes, while C_{2v} has only one; but the properties of a D_{2h} molecule

may be very different in these three directions, while for C_{2v} the orbital electronic properties often approximate to axial symmetry about the x axis, as implied by the suggestion of sp^2 hybridization in the yz plane in figure 18a.

My results thus seem most consistent with the model of fig-18b, with the degeneracy of the 3p orbitals completely lifted (energy increasing in the order p_y, p_z, p_x as shown in figure 19), the 3s and $3p_y$ doubly occupied, and the spin density mostly in p_x but partly in p_z. This model is developed quantitatively below in terms of the components of the g and A tensors.

ii) g -shifts

The observed spectroscopic splitting factors were found to deviate from the free electron value. Table VII gives the measured components of the g-tensor referred to the x, y, z axes of the defect , see figure 18a and 18b. The g_x component is very close to the free electron value $g_e = 2.0023$. The components g_y and g_z show a rather large positive deviation from g_e, indicating that the resonance arises from an electron deficiency in the halide ion noble gas configuration.

The calculation by first-order perturbation of the g-shifts brought about by spin-orbit coupling between p-orbitals whose degeneracy has been lifted by a crystal field is well known (58,60,92) and is discussed briefly in section B(d)(ii) of the introduction of this thesis. Using the model of the defect previously discussed, the p orbitals split by the crystal field for the $3p^5$ configuration of the Cl atom are shown in figure 19. The $3p^5$ configuration can also be expressed as a hole in the $3p^6$ complete shell and hence it can be treated as a positively charged electron

in a $3p^1$ configuration. Using this terminology the energy level diagram of figure 19 would have to be inverted, as shown in figure 20 below.

Figure 20

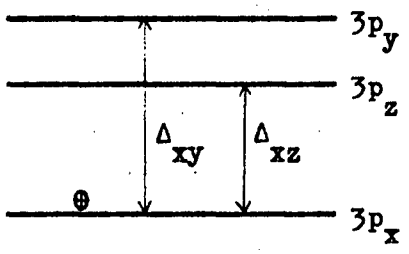

The relative energies indicated for the p_x, p_y and p_z orbitals correspond to the experimentally determined g-shifts, as discussed below. The transitions shown in figure 20 are responsible for the g-shifts since the ground state p_x is mixed with the upper states p_z and p_y by the L_y operator and the L_z operator respectively. If the energy differences between the states connected by the spin-orbit interaction are Δ_{xy} and Δ_{xz} as shown in figure 20 and the spin-orbit coupling constant is λ, the resulting shifts from the free electron g value g_o are (from equations 36 of the introduction):

$$\Delta g_x \cong 0$$
$$\Delta g_y = -2\lambda\alpha_x^2/\Delta_{xz}$$
$$\Delta g_z = -2\lambda\alpha_x^2/\Delta_{xy}$$

where α_x^2 is the amount of p_x-character of the unpaired electron. The values of the g-shifts were found experimentally to be 0.0, 0.0171 and 0.0139 for Δg_x, Δg_y and Δg_z respectively. The g-shifts are inversely proportional to the energy of the transition from the ground state to the higher energy states. The values of the g-shifts thus indicate that the p orbitals are in the order shown in figure 20. Using the experi-

mental values for the g-shifts, with $\lambda = -586\ cm^{-1}$ (which is 2/3 of the doublet separation of the $(ns)^2(np)^5$ state and has a negative sign for the positive hole situation), and using $\alpha^2 = 1.0$, the maximum upper limit of the transition energies is calculated. The calculations show that $\Delta_{xy} = 10.5$ eV, and that p_z lies 2 eV below p_y, i.e. $\Delta_{xz} = 8.5$ eV. The following section on the interpretation of the hyperfine tensor shows that the state of the unpaired electron (or hole) has nearly completely p-character of which at least 80% is due to the p_x orbital. Therefore the value of α_x^2 has a minimum value of 0.8 which gives a minimum value for Δ_{xy} and Δ_{xz} of 8.4 eV and 6.8 eV respectively. The true energy values of the transitions are somewhere between these values for $\alpha_x^2 = 1$. These figures may be compared with a crystal field splitting of about 15 eV found in Gardner's work,(92). Although the splitting is somewhat smaller ($\sim$10 eV) in the $SrCl_2$ defect it is still larger than the familiar range of d-orbital splittings.

iii) Interpretation of the hyperfine tensor

The terminology used below to relate the hyperfine interaction to the fractional s and p character has been explained in section B(d)(ii) of the introduction of this thesis. A_x, A_y, and A_z are used for the principal components of the hyperfine tensor; and A_{iso} and A'_x, etc. for the same data analyzed into isotropic and anisotropic contributions. The symbols $\mathcal{S}$ and $\mathcal{P}$ were introduced in equations 9 and 15 of the introduction of this thesis to relate these to properties of atomic orbitals and are defined as

$$\mathcal{S} = (\mu_I/I)(8\pi/3)\psi^2(0)_{3s \text{ or } 4s}$$

$$\mathcal{P} = (\mu_I/I)(2/5)\langle r_{3p}^{-3} \rangle$$

in which for a Cl^{35} nucleus $(\mu_I/I) = 2.76 \times 10^{-24}$ gauss cm^3.

The s character of the state of the unpaired electron is probably chiefly 3s, and for this Whiffen's value (98) of $\psi^2(0)$ for Cl^{35} which is 10.64 a.u. or $71.8 \times 10^{24} cm^{-3}$ is used. This is slightly higher than the value of $69 \times 10^{24} cm^{-3}$ used by Känzig and Woodruff (39), and gives a maximum valve for $\mathcal{S}$. To determine the greatest possible effect of any 4s admixture, I have also made some calculations using a minimum value of $\mathcal{S}$ calculated from Känzig and Woodruff's value $\psi^2(0)_{4s} = 5.72 \times 10^{24} cm^{-3}$. For $\langle r_{3p}^{-3} \rangle$ I followed Känzig et al. (36,39,) and Gardner (92) in using Sternheimer's value (99) of $55.6 \times 10^{24} cm^{-3}$. Whiffen (98) and Morton (97) (who I will call W and M) give a somewhat smaller value of 6.71 a.u. which is $45.3 \times 10^{24} cm^{-3}$. Adoption of this value would not signifigantly alter any conclusions which were drawn from the calculations. However both values were used for comparison in table VIII(a) and (b).

With the above selection of numerical values one has:

$\mathcal{S}_{max}$ = 1662 gauss (3s, Whiffen)

$\mathcal{S}_{min}$ = 132 gauss (4s, Känzig)

$\mathcal{P}_{max}$ = 61.5 gauss (Sternheimer)

$\mathcal{P}_{min}$ = 50.0 gauss (W and M)

Using the results of the discussion on the occupancy of the p orbitals in section B(d)(ii) of the introduction, I assume that the state of the unpaired electron can be represented by contributions from an s-orbital, p_x, p_y, and p_z, the fraction of the spin density in the four states being β^2 in s, α_x^2 in p_x, α_y^2 in p_y, and α_z^2 in p_z. However,

Table VIII

Character of the state of the unpaired electron.

a) Using s, $3p_x$, and $3p_z$ orbitals

		3s orbital				4s orbital			
A_z		positive		negative		positive		negative	
β^2	(%)	1.3	1.1	.8	.7	14.4	12.0	9.7	8.0
δ_x^2	(%)	69.3	69.4	83.9	84.0	60.1	61.8	76.4	77.8
δ_z^2	(%)	29.4	29.5	15.3	15.3	25.5	26.2	13.9	14.2
ρ/δ	assumed	.037	.030	.037	.030	.464	.378	.464	.378
ρ	from expt'l results	63.5	63.4	52.4	52.4	73.2	71.2	57.6	56.5

b) Using s, $3p_x$, and $3p_y$ orbitals

		3s orbital				4s orbital			
A_z		positive		negative		positive		negative	
β^2	(%)	5.1	4.2	2.5	2.1	40.8	35.5	24.8	21.1
δ_x^2	(%)	72.1	72.8	64.2	64.5	45.0	49.0	49.5	52.0
δ_y^2	(%)	22.8	23.0	33.3	33.4	14.2	15.5	25.7	26.9
ρ/δ	assumed	.037	.030	.037	.030	.464	.378	.464	.378
ρ	from expt'l results	35.1	34.8	56.1	55.8	56.2	51.7	72.7	69.3

as pointed out in the introduction one can only determine experimentally the difference of the occupation of two of the p-orbitals from that of the third orthogonal one. Therefore assuming that p_y is least occupied and using equations 27, 28, 29 and 30 of section B(d) of the introduction the expressions for the components of the hyperfine tensor are:

$$A_x = \beta^2 \mathcal{S} + (2\delta_x^2 - \delta_z^2)\,\mathcal{P}$$
$$A_y = \beta^2 \mathcal{S} + (-\delta_x^2 - \delta_z^2)\,\mathcal{P}$$
$$A_z = \beta^2 \mathcal{S} + (2\delta_z^2 - \delta_x^2)\,\mathcal{P}$$

from which the quantities relating to orbital occupancy are calculated as

$$\beta^2 \mathcal{S} = (1/3)(A_x + A_y + A_z)$$
$$\delta_x^2 \mathcal{P} = (1/3)(A_x - A_y)$$
$$\delta_z^2 \mathcal{P} = (1/3)(A_z - A_y)$$

The above expressions may be converted to the corresponding expressions for p_z (if p_z is the least occupied state) by interchanging subscripts y and z on both the A's and the δ's.

Since each of the above expressions reppresents a positive quantity using the experimentally determined values of A_x, A_y, and A_z from table VII of the results section, one can readily see that A_x must be positive, A_y must be negative and A_z is indeterminate. I full generality, A_y is also indeterminate because if the expressions are set up with p_z as the least occupied state instead of p_y then A_y must be positive.

Table VIII (a) and (b) give calculated values of β^2, δ_x^2, and

$\delta^2_{z \text{ or } y}$ for the 3s and 4s cases. The evaluation of these parameters requires a value for $\mathcal{P}/\mathcal{S}$. The value of $\mathcal{P}/\mathcal{S}$ varies with the s orbital; for a 3s orbital it is $\mathcal{P}_{max}/\mathcal{S}_{max} = 0.037$ and $\mathcal{P}_{min}/\mathcal{S}_{max} = 0.030$ and for a 4s orbital $\mathcal{P}_{max}/\mathcal{S}_{min} = 0.464$ and $\mathcal{P}_{min}/\mathcal{S}_{min} = 0.378$.

Table VIII(a) shows the calculated results assuming that p_y is the least occupied p orbital and using A_x positive, A_y negative, and A_z both as positive and negative (which I will call case 1).

Table VIII(b) has p_z as the least occupied orbital and A_x positive, A_y positive, and A_z positive and negative (case 2). Both tables show that s character is much increased if it is assumed to be 4s, especially in case 2. The two possible values for the s character as seen from table VIII(b) are then 24.8% and 40.8%. I consider these to be the least likely of all possible values and therefore indicate with some reservations that the 3s orbitals are mainly involved. Table IX summarizes the results obtained by using the 3s and 3p orbitals and indicates that the unpaired electron is of almost pure p character. The value of δ^2_x and δ^2_y or δ^2_z are the minimum value of the amount of p-character since (using equations 27 of section B(d)(ii) of the introduction) for case 1:

$$\delta^2_x = \alpha^2_x - \alpha^2_y$$

and

$$\delta^2_z = \alpha^2_z - \alpha^2_y$$

Since α^2_y is either positive or zero δ^2_x and δ^2_z are a minimum value of the p-character. It is difficult to choose between the values obtained using 3s orbitals with A_z either positive or negative just from the numerical data. I chose, as the most likely set, the values given in the right hand column of table IX, which support the model of figure 18b and the indica-

tions from the g-shifts that p_y lies lowest of the p-orbitals in a position closest to the 3s orbital (as shown in figure 19). It is reasonable that the p_y orbital is least occupied by the unpaired electron and it is possible that the 3s and the $3p_y$ form a pair of sp hybrid orbitals.

It should be noted, however, that the calculation using 4s give a very much lower value of δ_z^2/β^2, the two possible values being 1.78 and 1.43. Thus the possibility that the orbitals in the yz plane are sp^2 hybrids, in conformity with figure 18a, cannot be entirely ruled out, although a large contribution from the 4s orbital seems unlikely.

It is not possible to determine unequivocally from the available data whether there is substantial delocalization on the two nearest cations. The values of $\wp$ from the experimental results (bottom of table IX) are for most calculations within the range of theoretical estimates (61.5 to 50.00 gauss) suggesting localization of the electron; but table X shows that our values for the components of the A tensor resemble those found in ClO_2 more closely than those found by Gardner for a Cl atom adsorbed on SiO_2. Those latter values seem a little high, both relative to theoretical values and relative to the double values of the hyperfine constants found in the work of Känzig et al on Cl_2^- ions (39), which as Gardner points out, should be comparable. Evidently the range of uncertainty in these comparisons is such that no definite conclusion can be drawn on this point. In general, however, the similarity between the values of g and A components for the defect studied here and for ClO_2 is striking.

In table X the subscripts a, b, c and d are defined as follows:

Table IX

Character of the state of the unpaired electron

from hyperfine splitting and known constants of 3s and 3p orbitals

	Range in the calculations	Values considered most likely (p_z, with A_z negative)
s-character, $10^2\beta^2$	0.8% to 5.1%	0.8%
p-character, $10^2(\delta_x^2 + \delta_{y \text{ or } z}^2)$	94.9% to 99.2%	99.2%
$10^2\delta_x^2$	69.3% to 83.9%	83.9%
$10^2\delta_y^2$ or $10^2\delta_z^2$	15.3% to 33.3%	15.3%
$(\delta_y^2$ or $\delta_z^2)/\beta^2$	4.5 to 22.6	19.1
$P=(\mu_I/I)(2/5)\langle r_{3p}^{-3}\rangle$	35.1 to 63.5 G	52.4 G

Table X

g and A tensor components for Cl atoms in various environments

Component	Cl defect in $SrCl_2$ (this work)	ClO_2 in $KClO_4$ (Cole[96], Morton[97])	Cl adsorbed on SiO_2 (Gardner[92])
g_x	2.0028	2.0036	2.003 [c]
g_y	2.0194	2.0183	2.012 ± 0.004
g_z	2.0162	2.0088	
$A_{iso} = \beta^2\delta$ (G)	12 [a]	15	11
$A'_x = A_x - A_{iso}$ (G)	80 [a]	58 [b]	184 [c,d]
$A'_y = A_y - A_{iso}$ (G)	-52 [a]	-31 [b]	-92 [c,d]
$A'_z = A_z - A_{iso}$ (G)	-28 [a]	-27 [b]	-92 [c,d]

[a] Negative sign assumed for A_y and A_z.

[b] Assignment of co-ordinate system is that of Morton, not that first suggested by Cole.

[c] I have changed the designation of the axis of symmetry from z in Gardner's paper to x here, to facilitate comparison with the other data.

[d] Calculated from Gardner's $B = 2.58 \times 10^{-2} cm^{-1} = 276$ gauss, assuming axial symmetry.

iv) Reaction mechanism

It should be recalled that the defects giving rise to the ESR signal are known to lie close to the reaction interface; though evidently not near enough to allow any interaction with the large magnetic moments of the fluorine nuclei. One may envisage the reaction as involving the successive removal of cations (to the growing SrF_2 crystals) and discharged anions (to the gas phase as Cl_2 or ClF). The removal of each anion provides the necessary situation for displacement of an anion in the immediately subjacent layer.

While the position indicated in figure 18b has been identified as the most probable one to which my quantitative data refers, it should be recalled those data refer to the maximum value of the hyperfine interaction, and that the "powder" character of the lines in the single crystal spectra suggested the existence of a continuous range of values below this maximum. The reaction mentioned above must occur by the following reaction mechanism to assure the production of the defect; the oxidized anions are removed to the gas phase somewhat ahead of the migration of the cations to the growing SrF_2 crystals. Thus anion vacancies

are created near to the reaction interface which enables the defect to be formed. The displacement of the underlying anions towards the vacancy is aided by the discharge of the anion which provides the unpaired electron. In turn, the neutralization of the anions loosens the attachment of surrounding cations so that they can start to move towards their ultimate positions in the SrF_2 lattice.

The Cl atom approaches the reaction interface (i.e. the anion vacancy) along the z axis, which may thus be thought of as a "reaction coordinate" and may pass through a range of positions of the type illustrated in figure 18a, exhibiting its maximum hyperfine splitting when it passes between two cations in the special position of figure 18b. It is possible that in this condition the Cl atom is at the top of an energy barrier for migration; and in that case the defect I have studied in this work may be called a transition complex.

The spectra are thus consistent with the reaction scheme:

$$1/2F_2(g) + Cl^-(\text{subsurface}) \longrightarrow F^-(SrF_2) + Cl(\text{subsurface})$$

$$Cl(\text{subsurface}) \longrightarrow Cl(\text{interstitial}) \text{ (defect under study)}$$

$$Sr^{2+}(\text{surface}) \longrightarrow Sr^{2+}(SrF_2) \text{ (disorientation of 2-fold axes)}$$

$$Cl(\text{interstitial}) \longrightarrow 1/2Cl_2(g) \text{ (determines 4-fold axis for next layer of defects)}$$

A. Computations

a) Fortran 4 computer programme

```
C       THE DEFECT IN F2 TREATED KCl AND NaCl
        DIMENSION ANS(5000),Y(100)
        DIMENSION HS(20), DER(1000),ZN(1000)
        LOGICAL ITR,JTR
        EQUIVALENCE(NII,NI)
        CALL PLOTS
C                F O R M A T S
1       FORMAT (8F10.0)
2       FORMAT(1X,3HI=I3,6HIHI=I4,6HH(I)=F10.3,12HARRAY(IHI)=F6.2)
3       FORMAT(1X, 13F10.2)
4       FORMAT(1X,2I10)
5       FORMAT(I6,F10.3         )
6       FORMAT(16I5)
C               I N P U T   S T A T E M E N T S
```

IMAX: THE OVERALL HISTOGRAM SUBDIVISION

NI : NUMBER OF ANGLE CALCULATIONS

NP : DIVISIONS OF $\frac{1}{2}$ NORMAL CURVE

A : g_o

B : $(A_{\perp}^{12})^2$

C : $(A_{||}^{12})^2 - (A_{\perp}^{12})^2$

D : $g_{||}^2$

E : $g_{\perp}^2 - g_{||}^2$

F : $(A_{\perp}^{34})^2$

G : $(A_{||}^{34})^2 - (A_{\perp}^{34})^2$

CAY(K): $h\nu/\beta$

SIG : σ ON NORMAL CURVE

DXX : DIVISION OF NORMAL CURVE AS A FRACTION OF σ

```
2095    WRITE(6,2096)
2096    FORMAT(1H1)
        READ(5,6)IMAX,NI,NP
        IF(IMAX.EQ.0) GO TO 2005
        WRITE(6,7)IMAX,NI,NP
7       FORMAT(35H NUMBER OF HISTOGRAM SUBDIVISIONS =,I5,5X,31H NUMBER OF
       1ANGLE CALCULATIONS =,I5,5X,/41H NUMBER OF SUBDIVISIONS OF NORMAL
       1CURVE = ,I5)
```

APPENDIX

```
      READ(5,1)A,B,C,D,E,F,G,CAY
      WRITE(6,8)A,B,C,D,E,F,G,CAY
8     FORMAT(3H A=,F12.5,5X,3H B=,F12.5,5X,3H C=,F12.5,5X,3H D=,F12.5,/
     15X,3H E=,F12.5,5X,3H F=,F12.5,5X,3H G=,F12.5,5X,3H K=,F12.5)
      READ(5,1)SIG, DXX
      WRITE(6,9)SIG,DXX
9     FORMAT(8H SIGMA=,F12.5,5X,5H DX=,F12.5)
      PI1=3.14159265/(2.0*FLOAT(NI))
C               I N I T I A L I Z E   A R R A Y
      DO 11 I=1,5000
11     ANS(I)=0.
      THE =0.
      DX=0.5*DXX**2
       Y(1)=1.
      DO 210 I=1,NP
210   Y(I+1)=EXP(-DX*FLOAT(I*I))
       WRITE(6,3)(Y(I),I=1,NP)
      WRITE(6,3)
      HCC=CAY/SQRT(D)
      Z2=3.0*(A*SQRT((B+C)/D)+SQRT(F+G)+1.5*SIG)
      Z=2.0*Z2
      FACT=FLOAT(IMAX)/Z
      HM=HCC-Z2
      HMAX=HCC+Z2
      DS=DXX*SIG*FACT
      WRITE(6,12) HM,HCC,HMAX
12    FORMAT(13H H MINIMUM=,F12.5,5X,12H  H CENTER=,F12.5,5X,12H  H
     1MAXIMUM=,F12.5/)
      WRITE(6,13)
13    FORMAT(68H CENTER(H)  DPRIM(H)  DSECND(H)  CENTR(M)  DPRIM(MOD)
     1DSN(MOD)  DX(MOD))
      DO 1000 IT=1,NII
      THE= THE + PI1
       SN=SIN(THE)
      SINTHE=SN**2
      COSTHE= 1. - SINTHE
      UU=SQRT(F+G*COSTHE)
      TX=1./SQRT(D+E*SINTHE)
      TT=A*SQRT(B+C*COSTHE)*TX
      HH=CAY*TX
      HV=HH - HM
      T=TT*FACT
      U=UU*FACT
      HC=HV*FACT
      WRITE(6,3) HH,TT,UU,HC,T,U,DS
      ITR=.TRUE.
      DO 20 I=0,3
      AA=I
      HT1=(4.0 - AA)*(SN)
      DHP=AA*T
      HP1=HC+DHP
      HP2=HC-DHP
```

```
      JTR=.TRUE.
      DO 30 J=0,3
      JMAX=4
      JD=1
      BB=J
      HT2=HT1*(4.-BB)
      DHS=BB*U
      HS(1)=HP1+DHS
      HS(2)=HP2+DHS
      HS(3)=HP1-DHS
      IF (ITR) GO TO 38
      IF (JTR) GO TO 39
      HS(4)=HP2-DHS
37    TDS=0.
      DO 40 K=0,NP
      DO 50 JJ=1,JMAX, JD
      L=(HS(JJ)+TDS)
      HH=HT2*Y(K+1)
      IF(L.LE.IMAX) GO TO 400
      WRITE(6,4) L
      L=IMAX
400   CONTINUE
      ANS(L)=ANS(L)+HH
      IF(K) 44,50,44
44    CONTINUE
      L=(HS(JJ)-TDS)
      IF(L.GT.0) GO TO 403
      WRITE(6,4)L
      L=1
403   CONTINUE
      ANS(L)=ANS(L)+HH
50    CONTINUE
49    TDS=TDS+DS
40    CONTINUE
      JTR=.FALSE.
30    CONTINUE
      ITR=.FALSE.
20    CONTINUE
1000  CONTINUE
      FACT1=1./FACT
      DO 203 I=1,IMAX
      ZN(I)=(FLOAT(I)+0.5)*FACT1+HM
203   CONTINUE
      IM1 = IMAX - 2
      DO 206 I = 2,IM1
      DER(I) = 6.0*ANS(I+1) - ANS(I+2) - 2.0*ANS(I-1) - 3.0*ANS(I)
206   CONTINUE
      WRITE(6,130) (I,ZN(I),ANS(I),DER(I),I=1,IMAX)
130   FORMAT(3(5X,I5,3F10.2))
      CALL ALPLOT(ZN,ANS,IMAX,7H Y AXIS, 7 ,  8.0,7H X AXIS, 7 , 10.0)
      CALL PLOT(12.,0.,-3)
      CALL ALPLOT(ZN,DER,IMAX,7H Y AXIS, 7 , 8.0,7H X AXIS, 7 , 10.0)
```

```
      CALL PLOT(12.,0.,-3)
      GO TO 2095
39    JMAX=2
      GO TO 37
38    JMAX=1
      IF(JTR) GO TO 37
      JD=2
      JMAX=3
      GO TO 37
2005   CALL PLOTND
      END
```

b) Computed spectrum obtained for defect in KCl

The spectrum obtained, using the Fortran 4 computer programme found in (a) of this Appendix, for the defect in KCl is shown in figure 21.

Figure 21 - Computed spectrum obtained for defect in KCl

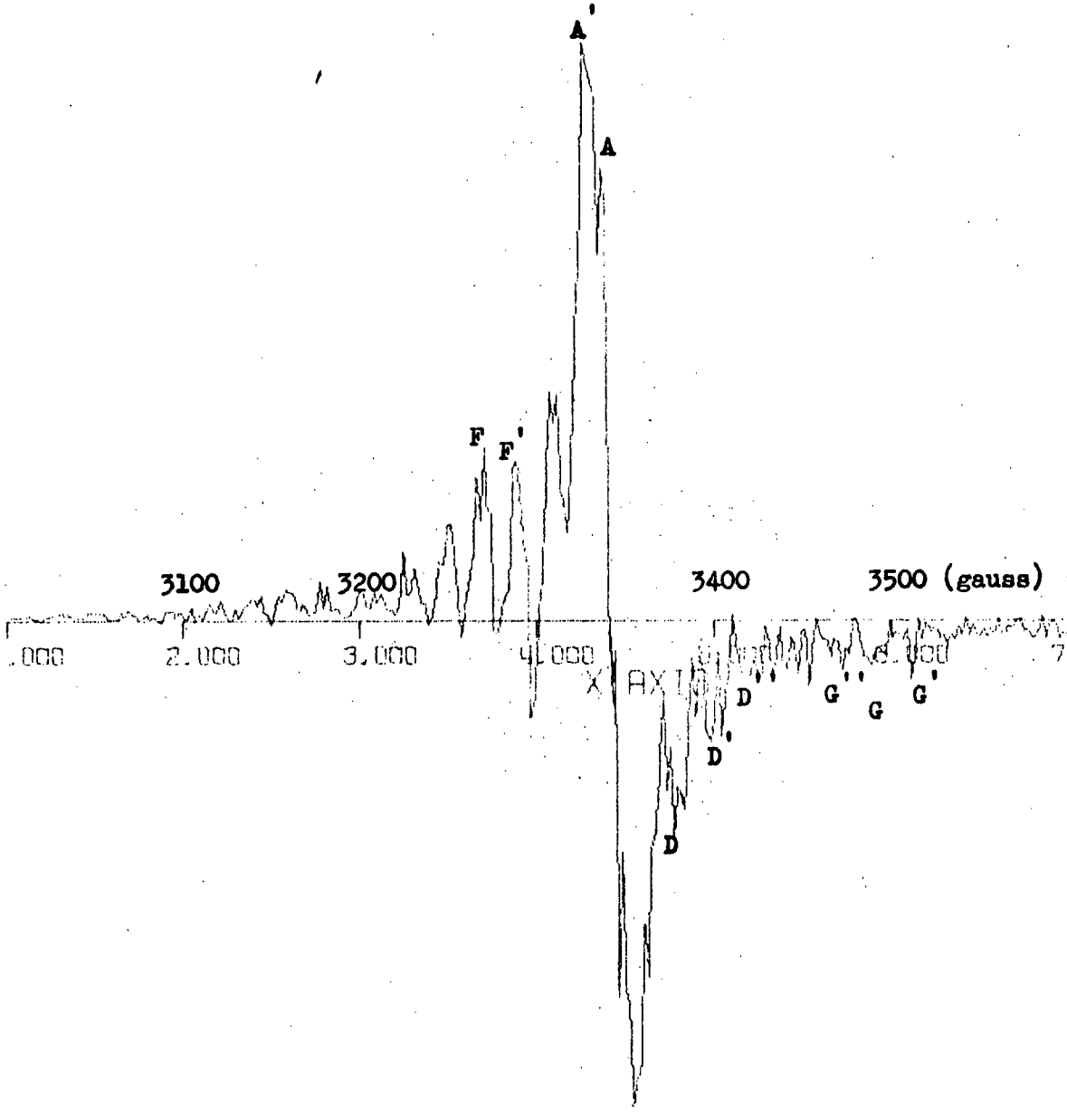

BIBLIOGRAPHY

BIBLIOGRAPHY

(1) S. K. Deb and A. D. Yoffe, Trans. Faraday Soc. 55, 106 (1959).

(2) A. K. Galwey and P. W. M. Jacobs, Proc. Roy. Soc. (London) A254, 455 (1960); F. Solymosi and K. Dobo, Proc. Intern. Symp. Reactivity Solids 5th Munich, 1964, 467 (1965).

(3) H. C. Clark, A. Horsfield, and M. C. R. Symons, J. Chem. Soc. (London) 1961, 7; M. M. Pavlyuchenko, M. P. Gilewich, and A. K. Potapovich, Proc. Intern. Symp. Reactivity Solids 5th Munich, 1964, 488 (1965).

(4) P. W. M. Jacobs, J. G. Sheppard, and F. C. Tompkins, Proc. Intern. Symp. Reactivity Solids 5th Munich, 1964, 509 (1965).

(5) J. H. Lunsford, J. Phys. Chem. 66, 2591 (1962).

(6) L. G. Harrison, J. A. Morrison, and G. S. Rose, J. Physic. Chem. 61, 1314 (1957).

(7) J. A. Morrison and D. Patterson, Trans. Faraday Soc. 52, 764 (1956).

(8) E. R. S. Winter, J. Chem. Soc. 3, 3824 (1955).

(9) L. G. Harrison, J. A. Morrison, and R. J. Rudham, J. Phys. Chem. 61, 1314 (1957).

(10) L. G. Harrison, I. M. Hoodless, and J. A. Morrison, Disc. Faraday Soc. 28, 103 (1958).

(11) L. G. Harrison, Disc. Faraday Soc. 28, 122 (1958).

(12) M. C. R. Symons and W. T. Doyle, Quart. Rev. 14, 62 (1960).

(13) L. G. Harrison and R. J. Adams, Trans. Faraday Soc. 60, 1802 (1964).

(14) L. G. Harrison, J. Chem. Phys. 38, 3039 (1963).

(15) L. G. Harrison, R. J. Adams, and R. C. Catton, J. Chem. Phys. 45, 4023 (1966).

(16) L. G. Harrison, R. J. Adams, M. D. Baijal, and D. J. Bird, Proc. Intern. Symp. Reactivity Solids 5th Munich, 1964, 289 (1965).

(17) L. G. Harrison and R. J. Adams, Trans. Faraday Soc. 60, 1792 (1964).

(18) R. C. Catton, B. Sc. Thesis (unpublished) (1964).

(19) E. Mollwo, Ann. Physik 29, 386 and 394 (1937).

(20) H. N. Hersh, Phys. Rev. 105, 1410 (1957).

(21) R. W. Pohl, Proc. Phys. Soc. 49, 13 (1937).

(22) F. Seitz, Rev. Mod. Phys. 18, 57 (1946).

(23) D. J. Bird, B. Sc. Thesis (1963).

(24) L. G. Harrison, M. D. Baijal, and D. J. Bird, Trans. Faraday Soc. 60, 1099 (1964).

(25) J. A. Morrison, Trans. Faraday Soc. 59, 2560 (1963).

(26) F. Seitz, Rev. Mod. Phys. 26, 7 (1954).

(27) J. H. deBoer, Electron Emission and Adsorption Phenomena, (Cambridge) (1935) chapter 10 and chapter 11.

(28) D. Dutton and R. J. Maurer, Phys. Rev. 90, 126 (1953).

(29) E. E. Schneider, Photographic Sensitivity (Butterworth Scientific Publications, London) 13 (1951).

(30) N. F. Mott and R. W. Gorney, Electronic Processes in Ionic Crystals (Oxford University Press, London) 133 (1940).

(31) H. Dorendorf, Z. Physik 129, 317 (1951).

(32) R. Casler, P Pringsheim, and P. H. Yuster, J. Chem. Phys. 18, 887 and 1564 (1950).

(33) J. Alexander and E. E. Schneider, Nature 164, 653 (1949).

(34) W. Känzig, Phys. Rev. 99, 1890 (1955).

(35) W. Känzig, Phys. Rev. 109, 220 (1958).

(36) W. Känzig and T. G. Castner, J. Phys. Chem. Solids 3, 178 (1957).

(37) J. W. Wilkins and J. R. Gabriel, Phys. Rev. 132, 1950 (1963).

(38) M. H. Cohen, W. Känzig, and T. O. Woodruff, J. Phys. Chem. Solids 11, 120 (1959).

(39) W. Känzig and T. O. Woodruff, J. Phys. Chem. Solids 9, 70 (1958).

(40) J. H. O. Varley, J. Nuclear Energy 1, 130 (1954).

(41) K. Teegarden and R. J. Maurer, Z. Phys. 138, 284 (1954).

(42) W. D. Compton and J. J. Markham, Phys. Rev. 88, 1043 (1952).

(43) W. Känzig, J. Phys. Chem. Solids 17, 88 (1960).

(44) F. Seitz, Phys. Rev. 79, 529 (1950).

(45) M. H. Cohen, W. Känzig, and T. O. Woodruff, Phys. Rev. 108, 1096 (1957).

(46) J. D. Kingsley, J. Phys. Chem. Solids 23, 949 (1961).

(47) W. Känzig, Phys. Rev. Letters 4, 117 (1960).

(48) K. D. Bowers and J. Owen, Reports Prog. Phys. 18, 315 (1955).

(49) J. R. Byberg, S. J. K. Jensen, and L. T. Muus, J. Chem. Phys. 46, 131 (1967).

(50) M. H. L. Pryce, Proc. Phys. Soc A63, 25 (1950).

(51) D. J. E. Ingram, Spectroscopy at Radio and Microwave Frequencies (Butterworths, London) 305 (1955).

(52) A. Abragam and M. H. L. Pryce, Proc. Roy. Soc. A205, 135 (1951).

(53) A. Carrington and H. C. Longuet-Higgins, Mol. Phys. 5, 447 (1962).

(54) S. I. Weissman, J. Amer. Chem. Soc. 75, 2534 (1953).

(55) M. Bersohn and J. C. Baird, Electron Paramagnetic Resonance (Benjamin Inc., New York) 37,39,217 (1966).

(56) F. Fermi, Z. Phys. 60, 320 (1930).

(57) M. Tinkham, Proc. Roy. Soc. (London) A236, 549 (1956).

(58) C. P. Slichter, Principles of Magnetic Resonance (Harper and Row, New York) (1963).

(59) G. E. Pake, Paramagnetic Resonance (W. A. Benjamin Inc., New York) (1962).

(60) A. Carrington and A. D. McLachlan, Introduction to Magnetic Resonance (Harper and Row, New York) (1967) especially chapter 9.

(61) M. H. L. Pryce, Supplemento Del Nuovo Cimento, Series 10, Vol. 6, No.3, 817 (1957).

(62) T. Inui, S. Harasawa, and Y. Obata, J. Phys. Soc. Japan 11, 612 (1956).

(63) J. H. O. Varley, J. Nuclear Energy 1, 130 (1954).

(64) T. Nagamiya, J. Phys. Soc. Japan 7, 358 (1952).

(65) W. Känzig and M. H. Cohen, Phys. Rev. Letters 3, 509 (1959).

(66) W. Känzig, J. Phys. Chem. Solids 23, 479 (1962).

(67) J. H. deBoer, Reccuil Trav. Chim. Pays-Bas 56, 301 (1937).

(68) C. A. Hutchison, Phys. Rev. 75, 1769 (1949); C. A. Hutchison and G. A. Noble, Phys. Rev. 87, 1125 (1952); M. Tinkham and A. F. Kip, Phys. Rev. 83, 657 (1951); E.E. Schneider and T. S. England, Physica 17, 221 (1951).

(69) A. H. Kahn and C. Kittel, Phys. Rev. 89, 315 (1953).

(70) A. F. Kip, C. Kittel, R. A. Levy, and A. M. Portis, Phys. Rev. 91, 1066 (1953).

(71) G. Feher, Phys. Rev. 105, 1122 (1957).

(72) N. W. Lord, Phys. Rev. 105, 756 (1957).

(73) G. J. Wolga and M. W. P. Strandberg, J. Phys. Chem. Solids 9, 309 (1959).

(74) F. Seitz, Phys. Rev. 79, 529 (1950).

(75) W. Känzig, Nuovo Cimento 7, 612 (1958).

(76) C. J. Delbecq, C. J. Smaller, and P. H. Yuster, Phys. Rev. 111, 1235 (1958).

(77) C. E. Bailey, Phys. Rev. 136, 1311 (1964).

(78) W. D. Compton and C. C. Klick, Phys. Rev. 110, 349 (1958).

(79) G. Herzberg, Spectra of Diatomic Molecules (New York) 239 (1950).

(80) M. H. Cohen, Phys. Rev. 101, 1432 (1956).

(81) H. R. Pareth, Phys. Rev. 80, 708 (1950).

(82) Y. Farge, M. Lambert, and A. Guinier, J. Phys. Chem. Solids 27, 499 (1966).

(83) W. Känzig, J. Phys. Chem. Solids 17, 80 - 87 (1960).

(84) T. O. Woodruff and W. Känzig, J. Phys. Chem. Solids 5, 268 (1958).

(85) R. J. Adams and L. G. Harrison, Rev. Sci. Instr. 34, 1410 (1963).

(86) R. J. Adams, Ph. D. Thesis (University of British Columbia) (1963).

(87) L. G. Harrison, J. A. Morrison, and G. S. Rose, Proc. 2nd Int. Congress of Surf. Act., (1957).

(88) F. K. Kneubühl, J. Chem. Phys. 33, 1074 (1960).

(89) R. J. Kokes, Proc. Intern. Congr. Catalysis 3rd 1, 484 (1965).

(90) R. Lefebvre and J. Maruani, J. Chem. Phys. 42, 1480,1497 (1965).

(91) A. Smakula, Molecular Science and Molecular Engineering (John Wiley) (1959).

(92) C. L. Gardner, J. Chem. Phys. 46, 2991 (1967).

(93) A. C. Wahl and T. L. Gilbert, unpublished information for which I am indebted to Dr. D. C. Frost.

(94) L. Pauling, The Nature of the Chemical Bond (Cornell University Press, 2nd edition 1960), p. 355.

(95) C. J. Delbecq, W. Hayes, and P.H. Yuster, unpublished information quoted by Wahl and Gilbert (reference 93).

(96) T. Cole, Proc. Nat. Acad. Sci. (Washington) 46, 506 (1960).

(97) J. R. Morton, Chem. Rev. 64, 453 (1964).

(98) D. H. Wiffen, J. de Chim. Phys. 61, 1589 (1964).

(99) R. Steinheimer, Phys. Rev. 84, 244 (1953).